A SECONDARY FLOW APPROACH TO THE INLET VORTEX FLOW FIELD

by

Henri Charles Viguier

Ingénieur, Ecole Centrale des Arts et Manufactures, Paris
(1979)

SUBMITTED IN PARTIAL FULFILLMENT
OF THE REQUIREMENTS OF THE
DEGREE OF

MASTER OF SCIENCE IN
MECHANICAL ENGINEERING

at the

MASSACHUSETTS INSTITUTE OF TECHNOLOGY

November 1980
(i.e. February 1981)

© Massachusetts Institute of Technology 1980

Signature of the Author _____ Signature redacted
Department of Mechanical Engineering
November 14, 1980

Certified by _____ Signature redacted
Edward M. Greitzer
Thesis Supervisor

Accepted by _____ Signature redacted
Warren M. Rohsenow
Chairman, Departmental Graduate Committee

A SECONDARY FLOW APPROACH TO THE INLET VORTEX FLOW FIELD

by

Henri Charles Viguier

Submitted to the Department of Mechanical Engineering
on November 14, 1980, in partial fulfillment of the
requirements for the Degree of Master of Science in
Mechanical Engineering

ABSTRACT

A theoretical study is presented of the fluid mechanics of the
inlet vortex (or ground vortex) phenomenon. The vorticity field
associated with the vortex is investigated using a secondary flow
approach. In this approach the flow is assumed to be composed of an
irrotational primary flow and a weak shear flow, with the vortex
filaments associated with the latter being regarded as convected by
the former. The potential flow field induced by the inlet-ground
plane combination is computed using the panel method developed by
Hess, Mack and Stockman. Using the analysis, material lines (which
coincide with vortex lines) can be tracked between a far upstream
location, where the vorticity can be taken as known, and the engine
face location. The deformation of the material lines thus shows
directly the generation and amplification of the streamwise compo-
nent of vorticity, which is responsible for the velocity distortion
at the compressor face. Two representative flow configurations are
considered, one with headwind only and one with the flow at forty-
five degrees to the inlet axis of symmetry. Although the results
so far yield only qualitative information, they appear to provide some
insight into one mechanism associated with the inlet vortex formation.

Thesis Supervisor: Dr. Edward M. Greitzer
Associate Professor of Aeronautics and Astronautics

ACKNOWLEDGEMENTS

TABLE OF CONTENTS

TABLE OF CONTENTS (CONTINUED)

LIST OF FIGURES

LIST OF SYMBOLS

D	Inlet Diameter
H	Height of Inlet Centerline above Ground
$\dot{m}$	Inlet Mass Flow
P_T	Total Pressure
Q	Sink Strength (positive)
S	Stagnation Point
$\underline{V}$	Velocity
V_x, V_y, V_z	Velocity Components
V_i	Average Inlet Velocity ($\dot{m} = \frac{\pi}{4} D^2 V_i \rho$)
V_∞	Wind Velocity
x, y, z	Spatial Coordinates
α	Flow Angle
ϕ	Velocity Potential
ρ	Density
$\underline{\omega}$	Vorticity

CHAPTER 1

INTRODUCTION

When a gas turbine engine is operated near a ground plane at static or near static conditions a strong vortex is often observed to form between the ground and the inlet. This so-called inlet or ground vortex can be a severe problem. For example it is able to pick up loose debris from the ground, which, when drawn into the engine, can cause damage to the latter. More importantly, however, the presence of a vortex at the engine face is associated with a severe distortion of the inlet flow which can have serious consequences for engine stability. Indeed the potential for vortex induced compressor surge has risen with the advent of wide body aircraft powered by high bypass ratio turbofans since in these configurations the engines have larger diameters and are closer to the ground than in the past.

This report presents a theoretical investigation of the fluid mechanics of the ground vortex phenomenon. A secondary flow approach is used to study the vorticity field due to an inlet vortex, the purpose of this being to understand the basic fluid mechanics of the flow that give rise to such a vortex. After a review of the available literature, the secondary flow approach taken is presented. This approach requires the potential flow induced by a jet inlet close to a ground plane to be calculated. The computational method used to do this is then described. Finally the results obtained using the approach selected are presented and discussed.

CHAPTER 2

BACKGROUND

The inlet vortex has been the object of several investigations.
In 1955 Rodert and Garrett [1] conducted an experimental investigation
of the phenomenon using a full scale jet engine. They observed vortices
not only between inlet and ground but also between inlet and fuselage.
It was shown that the vortex could lift up loose material capable of
damaging the engine. The formation of the vortices was found to depend
on engine power (i.e., inlet velocity), wind speed and direction relative
to the aircraft, and engine height above the ground surface. In partic-
ular increasing the inlet velocity resulted in the broadening of the
range of wind velocities over which vortices were observed. Likewise,
tailwind conditions were found to give wider ranges than headwind
conditions.

Klein [2][3] also dealt with the problem of jet engines ingesting
debris from runways. He first tested (with no nominal ambient wind) a
small scale model consisting of an inch-diameter inlet connected to a
vacuum cleaner. The role played by the vortex formed beneath the inlet
in the pick up of loose material was again seen, without the inlet vortex
the airflow into the engine intake was found to be unable to cause
ingestion of foreign objects from the ground. Furthermore Klein deduced
from the collected data the ratio of particle terminal speed to inlet
air speed at the threshold of particle aspiration as a function of the
ratio of centerline height to engine diameter. A twenty percent scale
model was next built to investigate the influence of wind on the

threshold line previously determined. A fan added circulation to the
air approaching the inlet. Both the updraft caused by the engine and
the circulation existing in the oncoming air were found to be essential
in the ground vortex formation and increasing the strength of either
resulted in an intensification of the vortex. In addition he carried
out a significant test by simulating the ground plane by means of a
second "image" inlet. In this case the observed vortex, which ran from
one inlet to the other, was apparently similar to the one visualized
with the actual ground surface. This result implies that the thin
boundary layer developed on the ground due to the sink flow effect of
the inlet does not play a significant role in the inlet vortex formation.
(However this does not imply that, in real cases, the ground acts only
as a simple symmetry plane. According to Helmholtz's vortex laws,
circulation must be present in the aspirated air if the vortex is to
form. In the reported experiment it was generated by means of a fan.
On the other hand, in actual inlet flows, the vorticity associated with
the inlet vortex can arise from the (viscous) interaction of the
atmosphere and the ground. The length scale of these shear layers can
be much larger than the inlet diameter). This study also reported tests
of different remedies to prevent ingestion of foreign objects, none of
which were successful. Finally a forty percent scale model was used
to develop a new scheme aimed at easing the ingestion problem. This
remedy consisted of a downward directed jet which induced a local flow
below the inlet. This removed the stagnation point present in the
external flow field from the ground surface. The existence of a stagnation
point on the ground plane is often regarded as necessary for an inlet

vortex to form. The basic reasoning for this is that in an inviscid flow* the vortex filaments must either form closed loops or end on the fluid boundaries, consequently a stationary vortex can be observed only if a stagnation point exists on the ground plane where it can attach.

Glenny [4] developed scaling laws to relate model and full scale tests of ground vortex induced lifting of particles. Among the dimensionless groups he derived the following ones are to be noted: ratio of inlet velocity to wind velocity, ratio of the height of the inlet centerline to the inlet diameter and ratio of the inlet velocity to the product of wind velocity gradient and inlet diameter. The last parameter is directly related to the strength of the ambient vorticity. Increasing the first ratio or decreasing the second one (called ground clearance) was found to enhance the risk of foreign objects ingestion. Furthermore it was shown that the vortex can be blown away by sufficiently increasing the wind velocity. The so-called blowaway velocity was noted to rise when the wind direction varied from headwind to tailwind or the vorticity strength parameter (as defined above) decreased. Experimental results demonstrated the validity of these laws which can be used to predict conditions under which vortex ingestion can occur and the sizes of the particles which can be lifted from the ground.

---

*In fact viscosity effects cannot be neglected in the vicinity of the ground surface. The no-slip condition which is satisfied on this stationary surface makes vortex lines ending on the ground plane impossible: all vortex lines are either closed loops or extend to infinity.

Various methods to prevent debris ingestion were tested but none worked satisfactorily for the low values of ground clearance of current interest. Glenny proposed that to reduce the ingestion of material the ratio of inlet velocity to wind velocity be kept as low as possible while the aircraft is running on the ground. As he stated, "the worst thing is to run an engine up to full speed under quiescent conditions". This last configuration is more likely to be encountered on a stationary test rig or when the aircraft is starting its take off roll.

Using previously published observations and results of the small scale tests they ran, Colehour and Farquhar [5] postulated a model of the flow associated with an inlet vortex. The flow field was divided into two parts: on the one hand, a viscous flow limited to the vortex core and the ground plane, on the other hand, an inviscid potential flow governing the remaining of the flow field. The latter was calculated for different wind conditions by using the panel method developed by Rubbert et al. [19], the ground plane being simulated by means of a second "image" inlet. The behavior of the stagnation point whose importance has already been underlined was studied; in particular the analytical study confirmed that a sufficiently high headwind can remove the stagnation point from the ground. An irrotational vortex was next added to the flow field. In both cases the calculated velocities differed from the measured ones, so that the viscous part of the flow had to be considered. The model could be used to qualitatively explain the velocity distributions recorded in the vicinity of the stagnation region. It should be noted here that the model designed by the authors was aimed at the description of the flow field associated with the ground

vortex rather than accounting for the formation of the latter. Different vortex suppressions techniques were presented, all of them aimed at preventing the stagnation point from forming on the ground.

Motycka, Walter and Muller [6], who were concerned with the ability of the inlet vortex to distort the flow sufficiently to produce compressor surge, carried out an analytical and experimental study of the phenomenon. A three-dimensional potential flow model using a vortex panel method to represent the inlet was combined with a viscous vortex core calculation. The effects of the wind speed and direction, the ground clearance and the inlet throat velocity on these flow properties were examined. The stagnation point was assumed to coincide with the foot of the vortex and the streamline from this point was regarded as defining the vortex position. The position of these were calculated with varying wind speeds and directions. The stagnation point blowaway velocity to inlet velocity ratio was estimated as a function of the ground clearance and the wind direction. The analytical predictions compared qualitatively with experimental data. Two important results need to be noticed. Firstly the ground vortex was observed to produce a velocity and flow angle distortion at the compressor face rather than a total pressure distortion, secondly vortex size and strength were found to be proportional to the inlet diameter.

In a later paper Motycka [7] presented the results of a full scale test program conducted at Pratt & Whitney to determine the causes of the engine surges encountered during reverse operation. Comparing the inlet pressure distortion patterns and the pressure versus time traces recorded with those observed in the presence of a ground vortex resulted

in the identification of the inlet vortex as the dominant cause of these engine stalls during operation with reverser. The flow from the reverser was recognized as a major source of vorticity and was shown to produce an apparent increase in tailwind. Using the forementioned analytical study, this rise was found to cause the foot of the vortex assumed to be at the stagnation point to move further upstream and the stagnation line to shift toward the more distortion sensitive core air stream. It was also noticed that the pressure distortion patterns often indicated the existence of two vortices. This investigation was followed by the testing of a small scale model of a subsonic inlet equipped with a fan flow reverser. The results were reported by Motycka and Walter [8]. The authors studied the effects of inlet throat velocity, inlet height, aircraft ground speed, i.e., wind velocity and reverser configuration (flow and targeting) on both the ground vortex formation during reverse operation and the inlet pressure distortion induced at the compressor face. In addition a three-dimensional potential flow model similar to the one previously mentioned was employed to examine the intake flow field during reverse operation.

Bissinger and Braun [9] used a small water tunnel and the hydrogen bubble technique to visualize the flow field around an inlet with a ground vortex. The inlet vortex was shown to be part of a vortex system which also included a trailing inlet vortex, secondary vortices and ground vortices similar to the ones encountered in front of any obstacle. The role played in the ground vortex formation by the thin boundary layer developed by the ground in the sucked flow was again shown to be insignificant. In addition, the inlet vortex was observed to be unsteady and unstable, particularly its foot was noted to move

randomly on the ground plane. This feature which was also noticed
by Rodert and Garrett [1] and Colehour and Farquhar [5] was explained
by the ground vortex feeding on the widely varying ambient vorticity.
A simple potential flow model consisting of a sink and its image in
a uniform flow was used to study the number and location of the
stagnation points which were shown to play a very important role in the
formation of the whole vortex system. An explanation of the phenomenon
based on the stretching of the oncoming vortex filaments was given.
Finally Bissinger and Braun proposed measures of their own to protect
jet engines against foreign objects aspiration.

Recently Newman and Atassi [10] presented a two-dimensional free-
streamline potential flow model of the flow around an inlet close to a
ground plane. The fluid was assumed to be quiescent far from the inlet,
or in other words the wind velocity was zero. Solutions were obtained
only for ground clearance values below to a certain limit. Moreover
a physically meaningful solution was always accompanied by an alternate
spurious solution. An experimental investigation was carried out to
examine these two problems. In addition, the amplification of small
three-dimensional vortical disturbances convected by the inlet flow was
studied.

In summary, the characteristics of the ground vortex phenomenon
mentioned in the literature can be described as follows. The inlet
vortex can form only if the fluid drawn into the engine contains vorticity.
The existence of a stagnation point on the ground is believed to be
required for the phenomenon to appear. The inlet vortex which is part

of a whole vortex system may be unsteady. Further the thin boundary layer due to the inlet (sink flow) alone is not essential in the vortex formation. The following parameters are used to characterize the phenomenon: inlet throat velocity to wind velocity ratio, centerline height to inlet diameter ratio, and the ratio of the inlet velocity to the product of wind velocity gradient and inlet diameter, and wind direction. In particular increasing the first ratio or decreasing the two next ones results in the strengthening of the ground vortex.

There are thus several questions about the inlet vortex phenomenon that still remain unanswered. Up to now no satisfactory explanation of the mechanism of the ground vortex formation has been given. In particular it is still not understood why, while, for any ingested material line (i.e., vortex line), two stretched "legs" appear to connect the far upstream portion of the flow to the inlet one, only one vortex is observed. In addition, even quantitative relations between the inlet vortex parameters presented above and the engine inlet flow field are still to be found. Finally, it is highly desirable to know the engine inlet flow field induced by an inlet vortex in order to assess the sensitivity of the designed propulsion plant to the phenomenon we are concerned with. The desire to answer these questions prompted the present work.

CHAPTER 3

ANALYSIS

The goal of the current investigation is to explain the basic fluid mechanics of the inlet vortex formation and to predict the flow distortion induced by the vortex at the engine compressor face. As already emphasized, vorticity must exist in the oncoming fluid if the ground vortex is to appear. Since the shear present in the ambient flow is generally small, there must be substantial amplification of the ambient vorticity for a vortex to form. Consequently we intend to study the variations of the vorticity between far upstream and the engine compressor face.

The following assumptions can be made to investigate the structure of the flow field created by a gas turbine engine inlet close to a ground plane. First compressibility effects in the overall inlet flow are not expected to be of primary importance. While locally high Mach number regions ($\simeq 1$) exist near the engine inlet lips their influence on the phenomenon of interest is small and consequently the fluid can be assumed incompressible. In addition the fluid can also be supposed inviscid: for example the Reynolds number based on the inlet centerline height off the ground and the approach velocity is typically of the order of 10^6. This means that, though the ambient shear is created by viscosity (at some "far upstream" location), the vorticity amplification can be considered essentially inviscid. Further although there are unsteady effects observed in the presence of a ground vortex, it is not clear that these play a significant role in the inlet vortex formation. Accordingly the flow will also be taken as steady. Finally, body forces can be neglected. Thus the flow we are concerned with is incompressible,

inviscid and free of body forces. In this situation Helmholtz's
vortex theorems [11] show that the vortex filaments are always composed
of the same fluid particles, i.e., they move with the fluid. Also for
a vortex filament of fixed identity, the ratio of the vorticity to the
length of the filament remains constant as time proceeds. Thus if a
vortex filament is stretched, the vorticity associated with it increases.
The vorticity is also inversely proportional to the cross-sectional
area of the vortex filament. As a result the evolution of the vorticity
between far upstream and the engine compressor face can be deduced from
the deformation undergone by the vortex filaments in their motion toward
the engine.

To calculate the movement of vortex filaments requires the velocity
field to be determined. The flow under consideration is clearly rotational,
not only in thin shear layers, but throughout the flow domain and is
strongly three-dimensional. However, since the basic concept to be stud-
ied is the intensification of vorticity due to the stretching of the
vortex filaments as they are drawn into the inlet, a useful simplification
can be made by viewing the problem as a small shear, large-disturbance
flow, as described by Hawthorne in Reference 12. In this approximation
which is currently utilized to explain the appearance of secondary flows,
the flow is assumed to be composed of an irrotational primary flow and
a weak shear flow. The vortex filaments associated with this shear are
regarded as being deformed by this primary flow only. In other words
the additional influence of the so-called "secondary"—velocities on the
convection of vortex filaments is neglected. The primary flow can be
determined using potential flow theory and, in particular, advantage can

be taken of the fact that numerous numerical methods exist to compute
potential flows.

The following approach can be used to study the variations of the
vorticity in the flows we are interested in. First a flow geometry is
selected. The previously introduced overall parameters describing
the inlet vortex formation are given typical values: it is to be
emphasized that our intention is not to perform a parametric study of
the ground vortex phenomenon but rather to investigate flow situations
which are known to present an inlet vortex. Secondly the potential flow
about this geometry is determined. Thirdly material lines are picked
far upstream and tracked as they move toward the inlet. These lines
once coinciding with vortex lines will coincide with them for all time.
Consequently by examining the stretching and tipping they undergo it is
possible to predict the vorticity pattern induced at the compressor
face by a given far upstream vorticity distribution. A further step
(not taken in the present report) would consist of computing the secondary
flow produced at this location by the calculated vorticity distribution.

The far upstream vorticity can be resolved into three components
respectively: 1) streamwise, 2) normal to the ground surface (vertical)
and 3) transverse to the flow stream direction and parallel to the ground
plane (horizontal). The evolution of the streamwise component can be
predicted very simply. Let us consider a flow that has, at a far up-
stream location, streamwise vorticity only. For a constant density
inviscid flow, if the vorticity at this location is streamwise, then the
vorticity everywhere will also be in the streamwise direction, i.e., the

flow is a Beltrami flow*. Streamlines and vortex tubes thus coincide,
Since the streamtube area is inversely proportional to the local
velocity (from continuity), the strength of the streamwise vorticity
at any location will thus be directly proportional to the velocity.
Therefore if the flow in the inlet is taken as uniform the ratio of the
streamwise (or Beltrami) vorticity at the engine face location to that
far upstream is equal to the area contraction ratio of any streamtube
between far upstream and the compressor face. As the fluid is in-
compressible, this last ratio equals the inlet throat velocity to wind
velocity ratio. The flow situations we are concerned with are
characterized by large values of this parameter, say minimum 10 or
greater. Hence this Beltrami vorticity can be expected to increase by
an order of magnitude or more between far upstream and the compressor
face.

---

* This can be seen by examining the circulation about a small closed
material contour which is aligned with the stream far upstream. The
circulation at this location, and thus anywhere downstream is zero.
Since the contour remains aligned with the streamlines. This implies
that all the vorticities is in the streamwise direction. Alternately
one can use the expressions developed by Hawthorne for changes in the
normal and streamwise components of vorticity. If, there is just
streamwise vorticity $\underline{v} \times \underline{\omega} = \nabla P_T = 0$, so the total pressure is constant
and since this remains true there can be no vorticity arising which
is not parallel to the velocity.

In spite of this, it is felt that this process is not the primary cause of the ground vortex formation for several reasons. One of these is that the inlet vortex formation described in the literature appears to depend on the angle of yaw of the inlet; whereas the mechanism just described is independent of it. In addition experiments have been carried out at MIT in which the shear was generated by a honeycomb so there was no component of Beltrami vorticity far upstream and a vortex formed. Further the situation that one would generally expect to find in an engine test is some sort of ambient shear layer associated with a ground boundary layer, i.e., region of total pressure defect. Such a flow consists of normal vorticity only at the far upstream location. Finally the stretching of filaments that one can get due to the non-Beltrami component can be considerably larger than that due to the one-dimensional effects. Thus, and as will be shown below, attention should be focussed on the components of vorticity which are normal to the streamlines at the far upstream loacation.

Although the amplification of the Beltrami component can be found by basically one-dimensional considerations, the evolution of the two remaining vorticity components is an inherently three-dimensional phenomenon and has to be studied using the procedure previously described. In particular material lines are picked which are, far upstream, normal to the ground surface or both transverse to the flow stream direction and parallel to the ground plane. The selection of those lines that are most useful to follow can be greatly helped by a preliminary investigation of the primary flow field.

The approach which we intend to follow was first applied by
Lighthill [13] to the prediction of secondary flows and uses the
"drift" or total displacement of fluid particles as the quantity
that is studied. In steady flow streamlines and pathlines coincide and
in such a case the trajectory of any particle can be readily deduced
from an integration along the streamlines. Further the way a given
particle describes its trajectory can be determined using the drift
time concept. The drift time of a particle between two points is the
time this particle needs to go from one point to the other. In a
steady flow this quantity depends only on the extremity points which,
of course, must lie on a same streamline. With the help of this
concept it is possible to follow material lines and surfaces as they
are convected by the flow. In particular the deformations of vortex
lines can be easily studied. In order to study the drift of fluid
particles, i.e., to track fluid particles, a computer program has been
written which, from the initial position of a particle, calculates the
trajectory the latter follows in a given time. This code can also
easily be used to trace flow streamlines and thus obtain further insight
into the flow structure. A general description and a listing of this
program can be found in Appendix A.

The three-dimensional flow field created by a jet engine inlet
close to a ground plane is quite complex. A qualitative appreciation
of this flow field can be obtained using a simple model consisting of
a sink and its image in a uniform flow. The results of this investi-
gation are reported in Appendix B. As emphasized there, the description
of the potential primary flow near the inlet given by this model is too

approximate for any quantitative prediction of the vorticity variations to be expected and a more complex model has to be used. In the next sections such a model is described and the results obtained using it are discussed.

CHAPTER 4

FLOW MODEL DESCRIPTION

4.1 Flow Geometry

The flow geometry that is investigated can be seen in Figure 1.
It consists of a cylindrical inlet and its image which is introduced
to simulate the ground plane. The inlets are set at an angle of in-
cidence (denoted α) in a uniform freestream whose direction is parallel
to the plane of symmetry (between the inlet and its image) and whose
magnitude is V_∞. Further for the cases investigated the inlet center-
line height off the ground to inlet diameter ratio $\frac{H}{D}$ is taken equal to
1.25, which is a value representative of a modern, high bypass ratio
engine configuration. Under the approximations listed in the previous
section the operating condition for the given inlet is defined by two
non-dimensional parameters: the ratio of freestream velocity to
average inlet velocity, $\frac{V_\infty}{V_i}$ and the flow angle α. (Note that this
implies kinematical similarity only, rather than full dynamic similarity).
The inlet geometry is shown in Figure 2. Notice that the selected
inlet has no centerbody: the internal machinery which controls the
amount of fluid entering the inlet is assumed to be far enough from the
inlet lip for its effect to be lumped into a single parameter, mass
flow through the inlet, and its geometry to be neglected. Additionally
in order to minimize the influence of the fluid exiting the engine on
the flow near and upstream the forward part of the inlet, the inlet
walls have to be extended as far as possible downstream. As will be
seen below, this is also required for good accuracy in the numerical
calculation of the potential flow about the inlet.

4.2 Potential Flow Calculation

4.2.1 General Discussion of Panel Methods

The approach taken requires the potential flow about the geometry described above to be computed. Different methods exist to calculate potential flow about three-dimensional bodies. It is not the purpose of this report to describe them in detail and a complete coverage of these matters can be found in the abundant literature, for example [14][18][19][22]. However a brief description of the computational method used to solve the present flow will be given.

Let us consider the irrotational flow of an inviscid incompressible fluid around a body of arbitrary shape. The fluid velocity $\underline{V}$ at any field point can be expressed as the sum of two velocities.

$$\underline{V} = \underline{V}_\infty + \underline{v} \tag{1}$$

The velocity $\underline{V}$ is called the onset flow and represents the irrotational velocity field that would exist in the absence of the body. The velocity $\underline{v}$ is denoted the disturbance velocity and can be derived from a potential function φ

$$\underline{v} = - \underline{\nabla} \varphi \tag{2}$$

The velocity $\underline{V}_\infty$ is supposed known while the disturbance velocity potential φ has to be determined.

The methods we intend to discuss are all based on Green's theorem

which states that the velocity potential φ at any point in the flow field can be expressed in terms of the induced effects of source and doublet sheets distributed on a surface S which contains the body contour and can extend into the flow as on a wake. The problem is thus to determine the source and doublet distribution which induce a flow field satisfying the boundary conditions. These latter are of the Neumann type (specification of the normal velocity): in particular, on the body contour they express the absence of through flow. If the disturbance velocity potential at a field point p is given by

$$\varphi(p) = \iint_S \sigma(q)\left(\frac{-1}{4\pi r}\right)\, dS + \iint_S \mu(q)\, \frac{\delta}{\delta n_q}\left(\frac{1}{4\pi r}\right)\, dS \tag{3}$$

where r = distance between p and the surface point q

n_q = direction normal to S at q

σ = source strength

μ = doublet strength

dS = surface element

application of the boundary conditions results in the derivation of the following integral equation, where the left side is known:

$$\frac{\delta\varphi}{\delta n_p} = \iint_S \sigma(q)\, \frac{\delta}{\delta n_p}\left(\frac{-1}{4\pi r}\right)\, dS + \iint_S \mu(q)\, \frac{\delta}{\delta n_p}\left[\frac{\delta}{\delta n_p}\left(\frac{1}{4\pi r}\right)\right]dS \tag{4}$$

The left hand side is, with p being a point of the body contour,

$$\frac{\delta\varphi}{\delta n_p} = \underline{V}_\infty \cdot \underline{n}_p \qquad\qquad (5)$$

The problem amounts to solving the above integral equation for the source and doublet strengths: once these are known, the velocity field can be determined using Equations (1) and (2). Note that there are different singularity distributions that produce identical flow fields outside the body contour. Consequently one must decide what types of singularity are to be used to solve the particular boundary value problem and insure the existence of a unique solution. The approach generally taken is to cover any part of the surface S with only a single type of singularity. Some investigators limit themselves to one type of singularity for the whole surface, thereby restricting the field of application of the methods they develop. For example methods using sources [14][15] can compute the flows only over arbitrary non-lifting configurations while the doublet or surface vorticity methods [16] can handle problems involving lift. The most widely used methods are those developed by Hess et al. [14][17][18] and by Rubbert et al. [19][20][21] which all employ source and doublet distributions. One major difference between these methods is that in the latter doublet sheets are used both to generate circulation and to describe bodies while in the former they are utilized only to introduce circulation around bodies or wake elements, when necessary.

Once the positioning of sigularity sheets on the body contour and, if necessary, in the flow (wakes) is completed, the problem is reduced

to numerically solving the integral equation expressing the boundary
conditions for the distribution of strength of these singularities.
Note that the flow field we intend to study is truly three-dimensional,
consequently the numerical procedure selected to be used to compute
the singularity distributions must be capable of handling arbitrary
three-dimensional bodies (even if advantage can be taken of the geometry
described above presenting two planes of symmetry). This requirement
eliminates the methods that are restricted to axisymmetric bodies
[16][22] .

In the procedures capable of dealing with arbitrary bodies, the
boundary surface S is approximated by a large number of small quadri-
lateral panels, on each of which the singularity strength is assumed
constant (Typical values of the number of panels are between 250 and
1000). In this way the singularity distribution depends on a finite
number N of parameters and the discretization associated with any
numerical procedure is performed. In principle if the number of panels
is made large enough, the solution obtained will converge to the exact
one. Two remarks are in order at this point. First in the methods
developed by Rubbert et al., doublet sheets, when meeting a closed
surface represented by sources, are extended inside this surface in
order to avoid large source strength gradients. These internal doublets
sheets are also divided in small panels but the relative strengths of
the latter are specified as linear functions of the strengths of the
adjoining external panels, so that these internal sheets do not introduce
additional unknowns. Secondly using flat surface elements and singularity
densities that are constant on each element is the simplest way of

implementing finite strength surface singularity distribution methods.
The code used in the present investigation was of this type. It was
developed by Hess, Stockman and Mack [23] and is based on the methods
developed by Hess and co-workers over the past two decades. The
present formulation was in fact designed to be used on inlet type
geometries. It can be noted, however, that accuracy can be increased
and computing time can be decreased by utilizing so-called higher-order
methods [15][22], which employ curved surface elements and a singularity
density that varies over each element.

The numerical determination of the N singularity strengths which
describe the whole singularity distribution proceeds as follows. N points
called control points are selected where the boundary conditions are
imposed. A control point is located at the centroid of each source panel
and exterior doublet panel if any. Further for lifting surfaces a suitable
representation of the Kutta condition must also be implemented [17][18].
As the velocity at any point of the flow field can be expressed as a
linear combination of the N singularity strengths, the coefficients of
which are deduced from the geometric relationship of this point and
the panels, application of the boundary conditions at all control points
yields a set of N linear equations for the N unknown singularity strengths.
If $\underline{V}_{ij}$ is the velocity induced at the control point of the ith panel
by a unit value of the singularity density on the jth panel and if $\underline{n}_i$
is the unit normal vector to i^{th} panel, the set of linear equations
obtained is as follows

$$\sum_{j=1}^{N} A_{ij}\, \sigma_j = -\underline{n}_i \cdot \underline{V}_\infty + V_{ni} \tag{6}$$

where $A_{ij} = -\underline{V}_{ij} \cdot \underline{n}_i$

σ_j denotes the singularity density on the jth panel.

V_{ni} denotes the imposed normal velocity at the control point of the ith panel ($V_{ni} = 0$ on body contour)

The above matrix equation which approximates the integral Equation (4) is solved numerically. The linearity of this equation is a very attractive property which is used to save computing time and to handle special applications of interest (lifting flows, inlets at prescribed mass flow). In particular once the time-consuming computation of the matrix $\{A_{ij}\}$ is completed, the determination of the flow for various onset flows requires only the linear Equation (6) to be solved. Further solutions can be superposed to yield solutions to more complex flows. Moreover use can be made of symmetries in the flow geometry to save computing time: since the relationships between singularity strengths on symmetrical panels can be used, the number of unknowns can be decreased, thus reducing the computational task associated with the solution of the Equation (6). On the other hand no gain can be made in the evaluation of the matrix $\{A_{ij}\}$ since the velocities induced at a random point by two symmetrical panels must be computed separately. Finally in the basic formulation mentioned above the Kutta condition is taken to be of the Neumann type, i.e., to consist of specifying the direction of the velocity at the trailing edge; however References 17 and 18 describe how to

circumvent this restriction and use more physically meaningful expressions of the Kutta condition.

Although the concepts may appear straightforward there are computational problems encountered in the implementation of the so-called panel methods. As already mentioned large source strength gradients can be observed at the meeting of a closed source surface and a doublet sheet if the latter ends at this location: such gradients can induce significant numerical errors in the computation of the tangential surface velocity component and, accordingly, are unacceptable. Some methods circumvent the above numerical difficulty by placing the doublet sheet inside the closed surface (Rubbert et al.) while others, which use only doublet sheets to produce circulation containing onset flows, extend the doublet sheets so that they cover the body surface [17][18]. The latter procedure appears to give better results than the former (based on results in the open literature). It must be noted that the source strength gradients do not affect the far-field influence of the source panels: more important from this point of view are the numerical errors associated with the normal velocity component boundary condition. In addition the no through flow condition is satisfied only at the body contour control points, away from these points the body walls can "leak". This computational problem, which can be severe in three-dimensional configurations, can be alleviated by increasing the source panel density in regions of high curvature*, using doublet panels which

----

*The calculated source strengths on curved surfaces are shown to be accurate only to first order in the angle subtended by the panel because of the planar panel approximation.

are an order of magnitude more tolerant of surface curvature or
implementing previously mentioned higher-order methods.

4.2.2 Potential Flow about an Inlet at Prescribed Mass Flow

In the cases studied the time-saving technique of super-
position of fundamental solutions can be used to obtain solutions at
various flow conditions. The inlet operating condition is defined in
general by four parameters: angle of attack, angle of yaw, freestream
velocity and mass flow through the inlet. Consequently, since the ·
governing equation and boundary conditions are linear (Laplace's
equation), the solution for arbitrary values of these parameters can be
obtained by linearly combining four independendent basic solutions. The
problem is reduced to defining these four fundamental solutions. Whatever
the onset flow may be, good accuracy in the potential flow calculation
near the inlet mouth may require the inlet to have a long afterbody
especially for cases of high $\frac{V_i}{V_\infty}$. The choice of the first three fundamental
solutions to the flow around the inlet is straightforward: they consist ·
of the flows due to unit value uniform onset flows at 1) 0° angle of
attack and yaw, 2) 90° angle of attack with 0° angle of yaw, 3) 90° angle
of yaw with 0° angle of attack. A forward position (called control station)
is chosen where the mass flows for these flows are evaluated: flows 2) and
3) give mass flows which are near zero. These three fundamental solutions
can be linearly combined to give the flow about the inlet at any angle
of attack, any angle of yaw and any freestream velocity, however one
does not have freedom to choose the mass flow through the inlet.
Consequently a fourth fundamental flow is required to control the amount
of fluid entering the inelt. Different approaches can be taken. In one

early approach the so-called closed-duct method, [24][25], the inlet is extended with a long afterbody which is closed at the rear by a wall normal to the centerline, and the flow induced by a unit value uniform onset flow at 0° angle of attack and yaw about the so-defined body is used as fourth fundamental flow. In this case although the flow may vary locally near the closing wall it is well behaved near the lips. Further the distance between the control station and the closing wall has to be quite large for the accuracy of the results to be good: this requirement is often very expensive (computing time, storage) to meet in three-dimensional configurations due to the large number of panels needed. Thus another possibility is to use as fourth basic flow that for the inlet in static condition, in which the flow velocity is zero at infinity while a finite amount of fluid enters the inlet. This flow can be obtained in the following two ways. First a singularity sheet is placed across the inlet duct far from the mouth and a non zero normal velocity is prescribed on this "suction" surface. The flow in the vicinity of this surface is inaccurate (for the same reasons as before), however it is well-behaved at the control station where the evaluated mass flow is again different from the specified one due to "leakage". This procedure gives good results inside the inlet and near the lip but inaccuracies appear in the exterior region [22] (region in which we are, in our application, very interested). These arise from the fluid feeling the the influence of the suction surface through the inlet wall. In particular a "spurious" stagnation point appears on the exterior surface, which makes this way of generating the static solution inacceptable for our purpose (particularly if it is noticed that due to the large value of the average inlet velocity to wind velocity ratio, the static

solution is the main component of the global solution in the vicinity of the inlet). Another way of producing the static solution is to use as onset flow the flow induced by a vorticity distribution on the shroud surface. This approach yields a more accurate solution for the static operation. In particular it can be shown that the solution obtained by means of this method is the correct solution if the afterbody length is infinite (even with finite dimension elements) [22]. Further the velocity on the exterior surface decreases as the distance from the lip increases and it is always in the right direction. All this makes the solution obtained in the latter way the most attractive fourth basic solution.

4.2.3 Potential Flow Computation of Hess, Mack and Stockman

The computational method selected to calculate the potential flow about the configuration of interest can now be outlined. The core of this procedure is the constant source strength panel method developed by Hess [14] to solve flow about arbitrary non lifting bodies. Most of the development effort arises from adapting this standard procedure to the peculiar case of arbitrary three-dimensional inlets. In particular the previously described technique of superposition is used to obtain the flow about the inlet at various operating conditions. The fundamental solutions consist of the flows induced by unit value onset flows parallel to the coordinate axes and the flow associated with the inlet in static operation. The latter flow, whose importance in the situation we are concerned with has already been emphasized, is produced by a distribution of unit vortices on the shroud surface (actually a dipole distribution

is employed: use is made of the relationship between a dipole sheet and a vortex sheet given in Reference 18). These vortices are placed in such a way that they form vortex rings, which, for an axisymmetric inlet, are oriented exactly on the circular cross sections.

Advantage was taken of the availability of a computer program implementing the above method. A description of this program, as well as a more thorough presentation of the method, can be found in Reference 23. In the configuration of current interest the flow geometries associated with the above described fundamental flows present two planes of symmetry. Advantage can be taken of the possibility of predicting the relationships between the singularity strengths on symmetry related panels to reduce both the computing time and the required storage. The available code was able to allow for only one plane of symmetry and, consequently, had to be modified to bring in the two-plane of symmetry capability. Even with the introduction of this feature solving the flow about the inlet (i.e., computing the source strengths associated with the fundamental flows) remains a fairly lengthy task. Particularly, the amount of storage required is enough to limit the number of panels used to approximate the inlet. The next section describes the results obtained using this computational method.

CHAPTER 5

RESULTS

5.1 Potential Flow Calculation

As has been already discussed, the computational method used requires
a large amount of storage, and this puts a limitation on the number of
panels which can be utilized to describe the inlet. The present calcu-
lation was conducted using 240 panels on each half inlet. The panels
which are planar quadrilateral elements are input by means of coordinates
of their vertices. The latter which lie on the inlet surface are orga-
nized in so called N-lines [23] which traverse the inlet in the axial
direction at a given circumferential location*. In our case all N-lines
are similar and lie in planes containing the inlet centerline.

Initial numerical experiments revealed that the number and circum-
ferential positioning of these lines strongly affect the results (leakage,
streamline pattern in the vicinity of the inlet). Based on these initial
calculations the configuration used was chosen to be eleven equally spaced
N-lines on each half inlet. In this case the limitation on the number
of panels and the necessity of using elements whose largest dimension
is small compared to inlet diameter lead to the distribution shown in
Figure 3b (front view) and Figure 4 (exterior side view). The locations
of the panel vertices on any N-line are given in Figure 3a. It must be

---

*An N-line starts at the most aft location of the inlet, proceeds forward
along the interior surface, around the lip and then along the exterior
surface up to the end of the inlet.

noticed that the inlet investigated is not extended as far downstream as desirable: the input surface is only 1.3 diameter long. However with such a configuration the leakage (defined as the relative variation of the volume flux) between two axial locations at respectively 0.05 D and 1.25 D from the lip is equal to 6.7% for the static operation fundamental flow and 1.2% for the 0° angle of attack and yaw fundamental flow. These acceptable results indicate that the selected panel density is adequate at least for the internal flow. Further it was found that extending the inlet downstream as desirable requires a considerably larger number of panels to be used since simply enlarging the panels gave poorer results.

Once the fundamental solutions are determined, the potential primary flow about the inlet at any operating condition can be studied. We choose to investigate the following configurations:

$$\text{Case 1:} \quad \frac{V_i}{V_\infty} = 30 \, , \quad \alpha = 0°$$

$$\text{Case 2:} \quad \frac{V_i}{V_\infty} = 45 \, , \quad \alpha = 45°$$

The cross flow configuration $\frac{V_i}{V_\infty} = 30$, $\alpha = 45°$, was not used because of the absence of a stagnation point in front of the lip on the ground plane: in this case the wind velocity is large enough with respect to the inlet velocity for the stagnation point to be blown away.

5.2 Streamlines

We will first examine the streamlines of the potential flow field in the neighborhood of the inlet, using the calculation for fluid particle trajectories described in Appendix A. Since the flow is three-dimensional, it is important to note at the outset that the results are presented as projections of these streamlines on the coordinate planes or as plots of the streamlines in these planes.

<u>Case 1</u> : $\dfrac{V_i}{V_\infty} = 30$, $\alpha = 0°$

The streamlines for this case are shown in Figures 6 through 9. The first two of these, Figures 5 and 6, show streamlines lying in the x, z plane (the symmetry plane of the inlet). Figure 5 shows the over-all flow field, while Figure 6 shows a smaller region but presents more detail. Some of the general features of the flow can be seen in these figures, although many aspects are shown more clearly in subsequent figures. However from these two figures one can infer that there are three locations of stagnation points or lines. The first is a stagnation point on the ground plane in front of the inlet and is denoted S_1 in Figures 5 and 6. The stagnation streamline is shown by a dash-dot line in Figure 5. The second is also a stagnation point and forms on the ground at the rear of the inlet: it is denoted S_2 in Figure 6. This point is really an artifice of the calculation and

would not be present in the actual situation*. The third location is a line around the inlet which meets the symmetry plane of the inlet at S. This again is, to some extent, a product of the calculation. In the "real" flow it is to be expected that this stagnation line should be on the outer surface of the inlet, however the strong recirculation connected with the use of the present code in near static operation shifts this line off the inlet. In a sense, then, this gives us an inlet configuration which has an "effective" shape with a much thicker lip and a somewhat different external geometry. (In fact since the space between the inlet and the ground is entirely filled with recirculating flow, the inlet external surface is seen by the oncoming flow as extending to the ground plane). Because of this recirculation some aspects of the flow field cannot be described adequately using the present computational method, although others can be seen clearly. This distinction between what can and cannot be resolved with an analysis of the present type will be made in more detail in what follows.

Figure 7 gives the streamlines in the x, y plane (the ground plane) and presents a different view of the overall features seen in Figures 5 and 6, namely the two stagnation points and the stagnation line. Only half the flow is shown because of the symmetry. The next Figure, 8, shows the streamlines in the vicinity of the inlet projected on a plane

---

*It can also be pointed out that the first stagnation point would not exist in a real (viscous) flow either since particles on the ground plane would separate before reaching the stagnation point.

normal to the axis of the inlet. Projections of these streamlines
on the ground plane can be seen in Figure 9. For convenience the
streamlines are numbered and the same type of lines (i.e., dash-dot,
solid etc ..) are used in both figures. The traces shown are, of
course, only parts of the streamlines (which can extend to infinity);
in view of the time taken for each calculation, the particles have been
tracked only in the regions of interest. The stagnation line and, to a
smaller extent, the first stagnation point can be seen in these figures.
Figure 10 shows, together with a front view of the inlet, the arch
shaped stagnation line about the latter and a cross section of the
capture surface* four inlet heights** upstream of the inlet. As seen
in Figure 11 which gives the traces of the capture surface on both
the ground plane and the symmetry plane this distance is sufficiently
upstream to be regarded as "far upstream". Finally, Figure 12 gives
a perspective view of the three stagnation locations described
above.

The recirculation of part of the flow exiting the engine plays a
very significant role in the formation of the stagnation points or

---

*The capture surface is defined here as the surface separating the portion
of the flow which enters the inlet for the first time from the portion of
the flow which does not enter or re-enters the inlet (recirculation).
**The inlet height, centerline to ground is the relevant length scale
to characterize this flow.

lines observed. As has been already indicated, this shifts the stagnation line which would be expected to form on the inlet off the surface of the latter. Further the second stagnation point S_2 arises also from the fact that the fluid particles leaving the engine turn sharply instead of moving straight aft. The first stagnation point should occur where fluid particles which come from ahead of and below the inlet meet. However in the potential flow calculation, the particles that proceed from under the inlet are in fact exiting the engine instead of coming directly from far upstream. It follows that for the present calculation the stagnation streamline associated with S_1 lies on the capture surface. As will appear more clearly in section 4 of this chapter (Figure 36), the portion of the inlet cross section that is filled with non recirculating flow is almost circular. Its axis is only slightly above the inlet centerline while its diameter, which can be regarded as the effective inlet inside diameter, is estimated to be equal to 0.8 D. Consequently the actual value of the ratio $\frac{H}{D}$ is roughly 1.6, whilst the ratio $\frac{V_i}{V_\infty}$ equals 30 as desired. This may partially explain why the flow field above the plane which is parallel to the ground plane and contains the inlet centerline appears not to be strongly affected by the presence of the ground in the sense that the streamlines lie in planes including the inlet centerline as in the case of the inlet alone.

Case 2 : $\dfrac{V_i}{V_\infty} = 45$, $\alpha = 45°$

The features described above are also observed in the 45° cross flow case, namely stagnation point S_1 near the front of the inlet,

spurious stagnation point S_2 on the ground plane at the rear of the inlet, arch shaped stagnation line about the engine, recirculating flow. These aspects of the flow field can be seen in Figure 13 which shows streamlines lying in the ground plane. The effect of the yaw introduced by the cross wind appears clearly. The first stagnation point has moved off the inlet symmetry plane in the direction of the cross flow while the second stagnation point proceeds in the opposite direction. The points where the stagnation line meets the ground plane can also be seen in this figure (they are denoted L and L'). This line is no longer roughly normal to the inlet axis and is determined by the combined effects of the wind and the recirculating flow. The latter fills, as previously, the space between the inlet and the ground. As will be confirmed by results presented in section 4 of this chapter, this flow is stronger on the leeward side than on the windward side of the inlet. Figure 14 shows the projections, on a plane normal to the inlet axis, of streamlines near the stagnation streamline associated with S_1. The latter is shown by a dashed line. In Figure 15 are given the projections on the ground plane of the same streamlines (which, for convenience, are numbered in both Figures 14 and 15). The flow coming from ahead of and below the inlet appears clearly to be associated with the formation of the first stagnation point while the stagnation stream-line is again found to lie on the capture surface. In Figure 16 is shown the projection of this line on the inlet symmetry plane. Figure 17 shows a perspective view of the three stagnation locations observed. Finally in Figure 18 the trace of the capture surface on the ground plane is given. This surface is found, as previously, to end farther forward

than expected. Further the closeness of the forward stagnation streamline and the capture surface must be noted and kept in mind when studying the deformation of vortex lines. In summary one can say that the features of the flow field can be explained by combining the effects of the yaw with the features recognized in case 1.

In both case 1 and case 2 the flow field is found to contain several expected features, namely forward stagnation point on the ground plane, stagnation line about the inlet and capture surface whose cross-section varies rapidly in the neighborhood of the inlet. However the quantitative nature of these features is affected by the existence of a large re-circulating flow. For example the capture surface is observed to end farther forward than expected, instead of forming on the inlet the stagnation line appears off the latter and the forward stagnation streamline is found to lie on the capture surface. Further the flow existing actually below the inlet cannot be determined using the present model and numerous questions which the simple model investigation reported in Appendix B raises about the nature of the flow under the inlet at the closing of the capture surface remain unanswered. In the present calculation the capture surface is smaller than expected and the flow it bounds is only a part of the flow which is actually sucked by the inlet. However this part of the flow does seem to be adequately predicted, as seen for example in the forward stagnation streamline. The shortcomings of the present model lie rather in the inability to describe certain regions of the flow. Proceeding through the next steps of the approach described in Chapter 3 will reveal whether the present model, in spite of its limitations, can be used to explain the inlet vortex formation.

At the same time it will be possible to find out how the model can be improved to achieve a more precise description of the flow field. Note that the strong recirculation which is the cause of all the difficulties encountered results from the very nature of the model rather than numerical inaccuracies. In the current model the total pressure is assumed to be the same everywhere (potential flow). Consequently, due to the large velocity difference between points in the internal stream and the external stream, the streamlines must turn sharply when exiting the inlet. In the actual case the internal and external streams have different total presssures and the fluid particles leaving the engine move nearly straight aft in a jet with the static pressure being essentially constant across the jet while the velocities outside and inside the latter differ largely. Additionally it must be noticed that due to the high value of the ratio $\frac{V_i}{V_\infty}$ the flow very close to the inlet is not very different from that about the inlet in <u>static operation</u>. This static solution is (partially) induced by vortex rings (dipoles) and this accounts for the tendency of the flow to fan out downstream of the engine. Using a very long afterbody can ease, to some extent, the difficulties discussed above but this turns out to be difficult to implement in the present situation.

5.3 Material Lines

In addition to the streamlines we have examined the behavior of selected material lines as well. As stated previously, since the flow considered is incompressible, inviscid and without body forces, if these lines coincide at some time with vortex lines they do so always. Thus within the approximation considered here the tracking of

the material lines shows directly the convection and amplification of the vortex filaments.

As discussed in Chapter 3, we resolve the far upstream vorticity into three components. These are the streamwise (or Beltrami) component, the component perpendicular to the ground plane (vertical) and the component parallel to the ground plane (horizontal) and perpendicular to the mean flow direction far upstream. The last is the only component that would exist in a two-dimensional boundary layer flow over the ground. The material lines that are studied represent the second and third of these components since, as described before, the amplification of the Beltrami vorticity between two locations can be seen directly from the ratio of velocities. As in the case of the streamlines we will look at the two cases separately.

Case 1

In the absence of cross flow one does not need to track material lines which are horizontal far upstream, since, within the context of the present description of the flow, vortex filaments which lie on these material lines can only give rise to a vorticity distribution at the engine face location which is symmetric with respect to the inlet plane of symmetry. Consequently, even if parts of these material lines near the stagnation streamline connecting S_1 to the inlet, as sketched in Figure 19, and the corresponding vortex stretching is large, no single vortex appears because the associated streamwise components are equal and opposite. In other words, in this case there is no way that these filaments can give rise to a single "vortex" rather than two symmetrically placed counter rotating vorticity distributions. Therefore we have only investigated the deformation of material lines which are vertical far

upstream.

Figure 20 shows the shapes into which a vortex line which is vertical at a location four centerline heights upstream of the inlet face is deformed. The material lines shown are in the x, z plane, i.e., the plane of symmetry of the inlet. It can be seen that the fluid line undergoes substantial stretching as it enters the inlet. However, perhaps somewhat surprisingly, this stretching appears to be relatively symmetric in spite of the fact that there is a stagnation streamline (shown as a dash-dot line) on one side of the inlet only. The capture surface is also shown in the figure (as a dashed line) to give an idea of the extent of the recirculation region (which is almost symmetrical about the inlet centerline). Figures 21 and 22 show two different views of a vortex line which is vertical far upstream and 0.60 inlet heights (0.75 inlet diameters) from the x, z plane. Figure 21 shows the projections on the x, z plane with the numbers corresponding to different times. The situation appears quite similar to that occuring on the x, z plane as regards top and bottom symmetry. Figure 22 shows the projections on a plane normal to the inlet axis (the y, z plane). Figure 23 shows the projections on the same plane of the positions of a vortex line that is initially 1.6 inlet heights (2.0 inlet diameters) from the x, z plane, i.e., near the capture surface. Note that since vortex lines cannot end in the flow the lines tracked must extend to infinity. However those portions of the material lines outside the capture surface, which do not enter the inlet, are not shown. Note also that both the head (top) and the foot (bottom) of the parts of the material lines that are shown will lag behind the middle part since

particles which are on the ground plane will stay there, while particles on the capture surface will approach the stagnation line as described in the previous section. The velocity differential means that the particles near the center of the fluid line will exit the engine while those at the foot and head remain near the stagnation regions*. Once a vortex line enters the inlet, we can no longer track it entirely and only parts of the legs extending from the stagnation regions to the inlet can be traced. These legs are both strongly stretched and, consequently, have high vorticity levels, although a quantitative appreciation for their stretching is difficult from just the tracking of material lines since the deformation increases rapidly for fluid particles closer and closer to the ground plane or the capture surface. The next section presents an attempt to evaluate the vorticity levels of both legs.

The study of the deformations of material lines initially off the x, z plane gives a clue to the possible inlet vortex formation mechanism. The existence of two stretched legs and the observation of a single vortex seem difficult to reconcile. However the locations of these legs must also be examined. While the foot of any vortex line approaches the stagnation point S_1 and the associated leg nears the corresponding

---

* By the definition of a stagnation point, the closer to such a point the streamline followed by a fluid particle is, the longer time it takes to this particle to reach a position downstream of the stagnation point.

stagnation streamline, the location reached by the upper leg which

extends from the inlet up to the vortex line head (defined as the top

of that part of the vortex line which is on the "inside" of the

capture surface) depends on the vortex line initial position. Knowing

the location of the vortex line head far upstream is sufficient to

determine the location reached by the latter after an infinitely long

time. To a close approximation the streamline followed by the fluid

particle which coincides with the vortex line head lies in a plane

containing the inlet centerline. Further since it is on the capture

surface this particle cannot ever pass the arch-shaped stagnation line.

Eventually using these two pieces of information it is possible to

determine the ultimate position of the vortex line head. Figure 24

thus shows the suggested deformations of vertical material lines. A

far upstream uniform distribution of vertical vortex lines evolves

into a configuration in which the upper legs of the lines are "fanned out"

over the upper part of the inlet while the lower legs are squeezed around

the stagnation streamline associated with S_1. (Although the stagnation

regions are never reached in the actual flow, these trends remain valid).

The predicted squeezing goes with an increase of the associated circula-

tion per unit area, the problem remains to compare this rise with that due to

vorticity amplification in the upper legs. Note that if the existence

of stagnation points is admitted (i.e., separation effects are neglected)

as in the current model, the stretching of both legs is infinite. The

difference lies in the spatial distribution of the associated vorticity

amplification as can be seen in Figure 23 where fluid particles close to

the foot and head of the vortex line are tracked. Note that the trend

discussed above would be expected to be even more pronounced, if the computation did not include the recirculation region, since the arch-shaped stagnation line would then be on the inlet external surface.

Case 2

Similar conclusions can be reached in this case for the vertical material lines. Figures 25 and 26 show a vortex line which is vertical far upstream. The initial position is marked by the small cross in Figure 27. Figure 25 gives the projections on the x, z plane of the shapes into which this line is deformed while Figure 26 shows the projections on a plane normal to the inlet axis. The configuration into which a far upstream uniform distribution of vertical vortex lines evolves is no longer symmetrical with respect to the inlet plane of symmetry. However the basic features are similar to those identified in the previous case: the upper legs of the vortex lines tracked are finally "fanned" over the upper part of the inlet while the lower legs are squeezed around the stagnation streamline associated with S_1 in a manner that is qualitatively the same as in case 1. Due to the position of the forward stagnation streamline the vorticity concentration at the engine face location is located to the left of the symmetry plane of the inlet when looking downstream into the latter.

As already emphasized, the flow in the present case is not symmetrical with respect to the inlet plane of symmetry. Accordingly it is desirable to study the deformations of far upstream horizontal vortex lines. This is done in Figures 28 through 33. The material lines tracked are far upstream respectively 0.8, 0.4 and 0.16 inlet heights

(1.0, 0.5 and 0.2 inlet diameters) from the ground plane. In addition they initially have the same projection on the ground plane: the latter is shown in Figure 27. Figures 28, 30 and 32 show projections on the ground plane for the three material line locations while Figures 29, 31, 33 give projections on a plane normal to the inlet axis. As in the previous case the deformations of only those portions of the material lines inside the capture surface are investigated. The fluid particles close to this surface are found to lag behind due to the presence of stagnation locations in the near vicinity of the inlet while those in the middle of the portion of material line tracked enter the engine much sooner. The first fluid particles to be drawn into the inlet appear to enter that half of the latter which does not contain the forward stagnation streamline. However when very large drift times are considered, i.e., particles very close to the capture surface are tracked, the corresponding legs are observed, again somewhat surprisingly, to be rather symmetrically placed: this appears clearly in Figures 30 and 31. Thus both legs of the far upstream horizontal material lines are found to be strongly stretched and no clear indication of the formation of a definite vortex can be seen from the material lines. It is thus desirable to study more thoroughly the stretching undergone by these lines.

5.4 Quantitative Calculation of Vorticity Amplification

Our purpose in the present section is to attempt to obtain a quantitative appreciation for the stretching undergone by material lines as they are drawn into the engine and thus to study more thoroughly the

amplification of a far upstream vorticity distribution. In particular we intend to compare the sizes of the regions of high vorticity which were indicated by the examination of material lines. We will first describe the calculation procedure used and then discuss the results obtained in the two flow configurations currently investigated.

The location at which we want to determine the vorticity distribution due to a far upstream shear flow is in the vicinity of the engine face. In our model this is in the portion of the inlet where the streamlines are straight and parallel, say 0.75 D downstream of the inlet lip. In the (semi-infinite) inlet model chosen the streamlines downstream of this section would be essentially straight lines. Further if the streamlines at an inlet section are parallel straight lines the velocity over this section is uniform and, by definition, equals V_i. Consequently we can extend the computed streamlines downstream of the inlet section of interest as straight lines with the velocity equal to V_i. Once the above assumptions are made, it is possible to determine the stretching undergone by a small fluid line connecting two neighbouring particles at a "far upstream" location. To do this it is only necessary to calculate the drift times of these particles between this location and the inlet. Let t_1 and t_2 be the drift times between a "far upstream" location and the selected inlet section of two particles initially at respectively P_1 and P_2. For purposes of discussion assume t_1 to be larger than t_2. In this case when the particle initially at P_1 attains the cross section of interest, at P_1' , the particle initially at P_2 has moved a distance $V_i(t_1 - t_2)$ downstream of this section, to P_2' (see Figure 34). To a good

approximation the small straight fluid line which initially connects

the particles P_1 and P_2 can be regarded as being deformed into the

straight material line $P_1' \, P_2'$. The stretching undergone by this line

is then given by $\dfrac{P_1' \, P_2'}{P_1 \, P_2}$ (this approximation of course improves as the

initial distance $P_1 \, P_2$ decreases).

The flow situations we are concerned with are characterized by

the strong contraction of the streamtubes between far upstream and

the inlet. It follows that for the values of the distance $P_1 \, P_2$

usually used (less than 0.20 H), the distance $P_1' \, P_2'$ is nearly equal to

$V_i(t_1 - t_2)$ and the fluid line tracked is finally almost parallel to the

inlet axis. In such a case the vorticity at P_1' due to a vortex line

initially aligned with $P_1 \, P_2$ is almost streamwise, with its orientation

depending on the direction of the vorticity along the vortex line as

shown in Figure 34. If we carry out this process for a number of such

lines the vorticity distribution induced at the inlet section of interest

by a far upstream shear flow can be found. To do this one can compute

the drift times of fluid particles which far upstream are at the nodes

of a regular grid describing the flow field interior to the capture

surface in such a way that one of its two directions is initially

parallel to the vorticity. It remains then to associate those neigh-

bouring particles that define far upstream fluid lines in the direction

of the initial vorticity (horizontal or vertical). One remark is now

in order. The vorticity value determined with the help of the procedure

described above, which is actually an average over the small vortex line

tracked, is taken to exist at the location where the streamline followed

by the fluid particle with the larger drift time meets the selected inlet

section. It follows from this convention that among the few particles of a given material line which are tracked the particle with the smallest drift time attains the inlet section of interest at a point which cannot be given a value of vorticity. This explains the existence. in our results of points without associated vorticity level. We next discuss the results yielded by the above approach for the two flow configurations currently considered.

Case 1: $\dfrac{V_i}{V_\infty} = 30$, $\alpha = 0°$

Because of the symmetry of the flow with respect to the x, z plane, the grid defined by the particles to be tracked has to cover only half the cross section of the capture surface. This grid is initially in a plane which is normal to the inlet axis and located 4.8 inlet heights (6 inlet diameters) upstream of the inlet lip. Figure 35 shows a view of this plane. The description of the cross section of the capture surface is seen to be quite complete: indeed the latter is everywhere less than a quarter of a diameter from the grid. It follows that due to the high streamtube contraction which characterizes this flow, the streamlines followed by the grid peripheral fluid particles can be expected to be close to the recirculating flow boundary. Further since fluid particles initially near the ground plane enter the inlet in the vicinity of the forward stagnation streamline, it has been found useful to increase the grid resolution near the ground plane: the lowest particles in the grid are only 0.008 H far from the ground surface.

The points where these streamlines meet the inlet section of interest are shown in Figure 36 (S denotes the trace of the forward

stagnation streamline in this section). Since the streamlines are assumed to extend downstream as straight parallel lines, Figure 36 can also be regarded as giving the projection on a plane normal to the inlet axis of the shape into which the upstream particle grid is deformed. Using this figure it is possible to obtain an appreciation for the shape of the portion of the inlet cross section that is filled with recirculating flow. This region appears to be quite circular, its axis being only slightly above the inlet centerline, and fills about 40 per cent of the inlet section. Accordingly it must be noticed that roughly half of the flow field surrounding the forward stagnation streamline cannot be described using the present calculation procedure since that portion of the flow field which is between the stagnation streamline and the inlet wall is filled with recirculating particles. Although this could be qualitatively expected in view of the results of the flow field investigation presented in the second section of this chapter the quantitative extent of the inability of the present computation to predict the whole flow around the stagnation streamline is only now apparent.

As has been already discussed, only the stretching of far upstream vertical vortex lines need be studied for this case. Figure 37 shows the vorticity distribution at the inlet section of interest due to a far upstream distribution of vertical vorticity (in fact the stretching levels undergone by fluid lines linking neighbouring particles are given). The numbers are all referenced to unity, i.e., to a uniform shear flow, however it should be emphasized that they are

relative quantities and can be directly applied to any vorticity
distribution. Figure 38 shows an enlarged view of the stagnation
streamline region. Precise values of the vorticity levels are
in fact illusory and overall trends are more important. Therefore
the results are presented using the key given in Table 1. The
presence of a minus sign means that the vorticity vector has the
magnitude indicated and is pointing upstream. Positive values denote
vorticity vectors pointing downstream. High values of stretching
(say more than 100) are observed in two regions of small extent
close to the recirculating flow boundary, namely a thin ring in the
top of the inlet section and a more compact zone near the stagnation
streamline. It is to be emphasized that if the former presents
lower stretching values than the latter, this is only due to the
difference in grid resolution and distance of the peripheral fluid
particles from the capture surface. In fact since in the present
calculation separation effects are neglected the stretching increases
without bound when the fluid particles tracked get closer to the capture
surface or the ground plane since the particles that are in these
surfaces ultimately get "stuck" in the stagnation line or point.
Comparing precisely the shapes of these zones of high vorticity is
difficult because of their small extents and in spite of the existence
of these regions no vorticity distribution pattern is observed which
indicates clearly the formation of a vortex. It appears that this is
due to the fact that in the present calculation the high vorticity
level zones are all found close to the recirculating flow boundary
(i.e., near the capture surface) while the high stretching region

associated with the forward stagnation point would be expected to be found inside the flow that enters the inlet from upstream. Accordingly due to the inability of the present calculation to predict the whole flow around the forward stagnation streamline, no quantitative conclusion can be reached about the magnitude of the vorticity amplification at this point. An understanding of the latter definitely requires the suppression or at least the reduction of the recirculating flow, especially below the inlet and this is recommended as a high priority item in the extension of this work.

Case 2: $\quad \dfrac{V_i}{V_\infty} = 45, \quad \alpha = 45°$

Similar conclusions can be drawn from the results of the 45° cross flow case. As previously the grid defined by the fluid particles tracked is initially in a plane normal to both the ground plane and the free stream direction. Figure 39 shows the trace of this plane in the ground while in Figure 40 is given a front view of the initial shape of the grid. We see that here again the description of the capture surface cross section is quite complete. Further, as before, the grid resolution is increased in the vicinity of the ground plane in order to study more thoroughly the part of the flow near the stagnation streamline which the model can describe: the lowest particles are initially 0.008 H, 0.016 H or 0.08 H far from the ground plane. Figure 41 shows the projection on the inlet section of interest of the "final" shape (i.e., the shape where the streamlines are parallel) into which the grid considered is distorted. The trace of the stagnation streamline

is again denoted S. The effect of the yaw appears clearly in the highly asymmetric deformation of the grid. The recirculating flow is observed to be stronger on the leeward side than on the windward side of the inlet. Thus the portion of the inlet cross section which is filled with non-recirculating flow is not circular. Further it now covers slightly less than half the inlet section: this is believed to be due to the use of a higher value of $\frac{V_i}{V_\infty}$. Finally as in the previous case roughly only half the flow surrounding the stagnation streamline can be predicted.

In contrast to the first case far upstream vertical and horizontal vorticity components must both be considered. Figures 42 and 43 show the vorticity distribution induced over the inlet section of interest by a far upstream uniform vertical vorticity distribution (the key to be used to read this figure can also be found in Table 1). As previously, high vorticity levels are only observed in local regions close to the recirculating flow boundary. However, even if the accuracy of the results given by the present model for the highest particles in the grid can be questioned, higher stretching values are found for particles entering the inlet to the left of the stagnation streamline. This can be explained by the closeness of the capture surface and the stagnation streamline and the associated combination of the effects of the stagnation point S_1 and the stagnation line. However again we cannot obtain the required quantitative information relative to the formation of the ground vortex due to the region of greatest interest, namely the stagnation streamline vicinity, being at the edge of the zone which the calculation describes correctly.

The attempt to examine a far upstream horizontal uniform shear also

encounters this problem. Figures 44 and 45 show the vorticity distribution induced by such a shear. The only conclusion that can be made is that the vorticity levels found are generally lower than for an initially vertical shear. Further the contours of equal vorticity coincide with the projections of those grid lines that are far upstream vertical, the higher vorticity values being obtained, as expected, for fluid particles close to the capture surface. In addition the vorticity level found does not vary significantly when particles closer and closer to the ground plane are tracked.

CHAPTER 6

SUMMARY AND CONCLUSIONS

The vorticity field associated with an inlet vortex (or ground vortex) has been investigated using a secondary flow approach. In this method the three-dimensional rotational flows that characterize this phenomenon are taken to be composed of an irrotational primary flow and a weak shear flow, with the vortex filaments associated with this shear being regarded as convected by the primary flow only. A computer program was developed to track specified material lines, which coincide with the vortex lines in this flow, between far upstream, where the vorticity can be regarded as known, and the engine face location. The primary flow was computed using an existing code, which was adapted to take advantage of the symmetries present in the geometries studied.

Two flow configurations were investigated in detail, both with high values of inlet velocity to far upstream (ambient) velocity ratio: one with the ambient velocity parallel to the inlet axis of symmetry and one with the ambient velocity at forty-five degrees to this direction. Both streamlines and material lines were tracked. Vertical (normal to the ground plane) and horizontal (parallel to the ground plane) material lines were used so that the behavior of each of the different components of the far upstream vorticity could be seen. In addition the vorticity distributions which occurred at the compressor face due to the amplification (stretching) of the far upstream vorticity distributions were evaluated.

The results of this work can be summarized as follows. The flow
is found to contain several expected features, namely a stagnation
point on the ground plane near the front of the inlet, a stagnation
line about the inlet and a capture surface whose cross-section varies
rapidly in the neighborhood of the inlet. However the quantitative
nature of these features is affected by the existence of a strong
recirculating flow, which is due to the nature of the calculation
procedure. Because of this, only that part of the flow which is
bounded by the computed capture surface seems to be adequately pre-
dicted by the model developed. In addition the capture surface found
is smaller than the one that would be expected to exist in the real flow.
It follows that only a portion of the flow sucked into the inlet is
correctly described by the model selected. In particular the flow around
the (very important) forward stagnation streamline cannot be studied in
its entirety since this streamline lies on the computed capture surface.
In spite of these limitations, the qualitative investigation of the
deformations of vortex lines initially normal to the free stream
direction shows, in both cases, the vorticity in both legs of these
filaments to be strongly amplified. Further the vorticity distributions
at the engine compressor face due to horizontal and vertical uniform
shear flows are found to contain very local zones of high vorticity
close to the recirculation region, although no pattern is observed which
quantitatively indicates the formation of a vortex. (It is felt that,
again, this arises partially from the inability of the computation to
describe the details of the flow around the forward stagnation stream-
line.) This result notwithstanding, the present work still provides

useful information about the inlet vortex formation mechanism. In particular, the tracking of vortex lines which are initially <u>vertical</u> shows the salient features of the generation of streamwise vorticity between far upstream and the engine face location. Vertical vortex lines that are uniformly distributed far upstream are seen to evolve into a configuration in which the upper legs of the lines are fanned over the upper part of the inlet, while the lower legs are squeezed around the forward stagnation streamline. This implies the occurrence of locally higher levels of circulation per unit area in this latter location, i.e., the formation at the engine face plane of two regions of opposite circulation and different spatial extents. One of these is small and appears around the stagnation streamline while the other is larger and fills the upper part of the inlet; the former strongly suggests the occurrence of an inlet vortex. Finally while the study of the deformations of <u>horizontal</u> vortex lines shows the strong stretching undergone by both legs of such lines, no pronounced asymmetry was observed in the cases studied which might be clearly identified with the formation of a definite single vortex.

CHAPTER 7

RECOMMENDATIONS FOR FUTURE WORK

It is clear that the inability to draw more specific conclusions
about the inlet vortex formation mechanism arises from the recirculation
flow introduced by the computational method implemented. Therefore
the next logical step is to improve the computational procedure used to
compute the potential flow field so as to suppress this recirculation
of fluid particles. In particular it is necessary that the forward
stagnation streamline be inside the portion of the flow adequately
described. The value of any modification can be assessed by examining
the extent of the recirculation in the flow between the inlet and the
ground, since this part of the flow seems to be the most sensitive
location to the artifical phenomenon observed. The following remarks
and suggestions may make the selection and design of a new computational
method easier. First it must be noticed that in the flow situations
we are concerned with the value of the inlet velocity to wind velocity
ratio is so high that the flow very close to the inlet is not very
different from that about the inlet in static operation. The code used
is not suitable to compute flow configurations in which the inlet is
nearly in static operation unless a huge amount of storage is available.
This is believed to arise from the fact that the onset flow used to obtain
the static solution (which is one of the four fundamental solutions to
be linearly combined) is dominant in the cases of interest—and the
vortex rings used to induce this flow cause the streamlines to turn
sharply downstream of the engine. While lengthening the inlet can ease

the problem, the feasible improvement is believed to be limited. Note also that increasing the number of panels would increase the time taken by the tracking of material lines (which is already large). It is preferable to modify the onset flow used to obtain the static solution. This flow must give a solution which is independent of the first three basic solutions and vanishes far upstream. In view of the difficulties encountered in the present study, it appears that the fourth onset flow must be parallel to the inlet axis (or at the most slightly diverging) downstream of the inlet. A possible choice consists of the following. Inside the inlet surface and slightly behind the inlet lip is placed an axisymmetric intake of smaller thickness which extends farther downstream than the inlet studied and the axis of which coincides with the inlet centerline. The flow about this intake in static operation is axisymmetric and can be computed using appropriate codes. In particular advantage can be taken of the fact that the intake surface can be represented in a much more detailed manner than in a three-dimensional flow, for example it can be as long as desirable while higher-order methods can be used. The fourth onset flow is obtained by superposing two axisymmetric flows: one for the added intake in static solution, one for its image also in static operation. This flow induces a static solution and, as desired, diverges only slightly downstream of the inlet studied. Since a complete understanding of the inlet vortex formation requires the potential flow calculation to be improved, the testing of the above modification is recommended in the extension of the present work.

Furthermore, in the current approach, the vorticity amplification
is found to increase without bound when the portions of vortex lines
tracked get closer and closer to the capture surface or the ground
plane. However in the real flow viscous diffusion will limit the
vorticity intensification in regions of high stretching. Therefore,
it is also suggested that future studies should examine the influence
of viscous effects, although it should be emphasized that it is expected
that this can be done in an approximate manner since we are seeking
the overall effects rather than the details of the velocity distribution
within the viscous core.

Once an accurate quantitative appreciation for the vorticity
amplification is obtained, it will be possible to calculate the vorticity
distribution induced by any far upstream shear distribution at the
engine face location. Up to now only uniform shear flows have been
considered and the use of more realistic shear profiles (boundary layer-
like for example) is, however, highly desirable. The final step would
then consist of computing the (secondary) velocities produced at the
compressor face by the calculated vorticity distribution.

APPENDIX   A

FLUID PARTICLE TRACKING COMPUTER PROGRAM

Since the mean flow is assumed to be steady, the fluid particle
trajectories coincide with the flow streamlines, hence, their equations
are by definition:

$$\frac{dx}{V_x} = \frac{dy}{V_y} = \frac{dz}{V_z}$$

where V_x, V_y, V_z are the components of the primary flow velocity field
in respectively the i, j, k directions.   These functions which are
determined by the potential flow field calculation procedure are inputs
to the program.

Streamlines are curves and, consequently, can be described by means
of a single parameter, which may be one of the space coordinates.   If,
for instance, the x-coordinate can be utilized as independent variable,
the above equations can be rewritten as follows:

$$\frac{dy}{dx} = \frac{V_y}{V_x} = f(x,y,z)$$

$$\frac{dz}{dx} = \frac{V_z}{V_x} = g(x,y,z)$$

Looking at this system of two first order ordinary differential
equations reveals that the velocity component V_x has to be non-zero
for the x-coordinate to be a useful parameter.   Therefore a convenient

way of describing a streamline is to use as parameter the space

coordinate associated with the locally largest velocity component.

In this case, the streamline equations can always be rewritten as a

system of two ordinary differential equations, whose exact form

depends on which coordinate is the actual parameter. Consequently

calculating the trajectory of a particle amounts to solving successively

different systems of first order ordinary differential equations. Each

system is subject to initial conditions which express the continuity

of the solution at the boundary separating two regions of different

parametric representations or, for the first system considered when

tracking a fluid particle, the necessity for the solution to start at

the given initial point.

The progression along any trajectory is controlled in two ways.

First with the aim of monitoring the description of the followed

streamline, the flow velocity components at each calculated point are

compared to see whether, starting from this point, a different space

coordinate has to be used as parameter. Secondly the time elapsed from

the instant when a particle leaves the given initial point to the

instant when the same particle reaches the last calculated point is

evaluated every three points or when crossing the boundary separating two

regions of different parametric representations and compared with the

given travel time so as to establish whether it is necessary to keep

on calculating the streamline. If not the position reached by the

tracked particle is determined by interpolation. Thus fluid particle

tracking involves two calculations which are carried out simultaneously,

namely streamline computation and drift time evaluation. Let us now consider them separately.

A predictor-corrector method developed by Hamming [26] is utilized to solve the previously mentioned systems of first order ordinary differential equations and thus calculate the streamlines. This non self-starting fourth order method uses four preceding points to compute a new one. Further it has the following advantages over one-step methods of comparable accuracy, such as Runge-Kutta methods. The local truncation error can be easily estimated and corrected for. Moreover, if the system of first order ordinary differential equations of interest is of the form

$$\frac{dY}{dX} = F(X,Y)$$

where   X is a real variable

         Y is a n-dimensional vector

    and F is a vector valued function

as few as two evaluations of the derivative function F are required per step against four in the often used fourth-order Runge-Kutta methods. The latter consideration is particularly important when the derivative function is complicated and each evaluation needs substantial computing time. In our case evaluating the function F amounts to calculating the velocity components at a point of the flow field. This can be quite time-consuming if a panel method is utilized to determine

the latter since then the lengthy computation of the influence coefficients of all the panels has to be carried out for each point where the velocity is searched for. A fourth order Runge-Kutta method proposed by Ralston [27] is employed to start the calculation at the very beginning and restart it after adjusting the stepsize or changing the way the streamline is described.

As previously indicated, the streamlines are divided into parts whose parametric descriptions differ. Let P and P' be two points in such a part of an arbitrary trajectory. The time a particle needs to travel from P to P' is given by

$$t_{PP'} = \int_P^{P'} \frac{d\beta}{V_\beta}$$

where β is x, y or z depending on which coordinate is actually used in the region of interest. Consequently, if the streamline segment connecting two points cannot be wholly described by the same space coordinate, the evaluation of the time it takes to a particle to move from one of these points to the other involves computing and adding up different integrals. The latter are estimated as follows. The appropriate quantity $\frac{1}{V_x}$, $\frac{1}{V_y}$, or $\frac{1}{V_z}$ is evaluated at each calculated trajectory point. The obtained values are interpolated by means of a succession of cubic spline functions and/or parabolae which are then integrated between adequate limits to yield the value of the integral searched for. Generally every cubic spline function is associated with four consecutive points of the followed streamline, sharing the extremity points with contiguous functions. However when the role of

independent variable shifts from one space coordinate to another, only one or two points may have been calculated since the last drift time evaluation. Three points can still define a cubic spline function while two points can be interpolated by means of a parabola providing that the slope of the preceding interpolating function at the first point is used as additional boundary condition. The position reached by the tracked particle in a given time is found in the following way: firstly the independent variable value is determined using the last derived interpolating function, secondly the corresponding dependent variable values are computed with the help of the forementioned fourth order Runge-Kutta method.

Some comments are now in order. The accuracy and computational speed of the solution of any first-order ordinary differential equation is currently controlled by halving the independent variable step size when the local truncation error is above a certain limit and doubling it when the same error is below another limit. Nevertheless in our case it has been found necessary to bound the possible increase in step size. If the step size when reaching highly curved segments of the followed streamline is too large, the necessity for changing the way the trajectory is described is recognized only at a point where the velocity component associated with the new describing coordinate greatly exceeds the velocity component associated with the old describing coordinate. This can result in inaccuracies in the calculation (in the sense that the computed points do not lie on the same streamline). Further the program has been observed to run into difficulties in the vicinity of stagnation points.

The drift time evaluation has proven to be much more sensitive to the step size than the streamline calculation. This can be explained by the inability of the spline functions and parabolae to interpolate correctly the locally high-valued and rapidly varying quantities $\frac{1}{V_x}$, $\frac{1}{V_y}$, $\frac{1}{V_z}$. A reduction in step size can ease the problem, nevertheless a limit exists beyond which it is no longer economically possible to perform the intended tracking. Varying the step size and comparing the obtained final positions has been found a reliable way of assessing the value of the results.

Note: for reasons which appear clearly in Section 5.4, a version of the above program has been developed in which the tracking of a particle is stopped when the latter reaches a given plane $x = x_{plane}$ while the independent variable is the x-coordinate. This additional feature is denoted "plane cutoff" in the following listing. When this alternative is selected, the input drift time is a dummy parameter and the actual drift time is found by interpolation.

```
C******************************************************************************
C                    FLUID PARTICLE TRACKING PROGRAM
C******************************************************************************
C
C          THE VELOCITY FIELD IS GIVEN BY VX,VY,VZ FUNCTIONS OF X,Y,Z
C          THESE QUANTITIES ARE COMPUTED BY SUBROUTINE VXVYVZ(X,Y,Z,VX,VY,VZ)
C
C
           DIMENSION Y(2),YS(2,4),FS(2,3),STI(4,4),F(2),YSS(2),
     &               E(2),YF(2),YFS(2),AUX(3,3)
           DIMENSION NLINE1(10), NLINEN(10), NFILE(4),
     &               XC(1100), YC(1100), ZC(1100),
     &               XN(1100), YN(1100), ZN(1100),
     &               SIGMAS(1100),SIGMA1(1100),SIGMA2(1100),SIGMA3(1100),
     &               FLUXX(4), FLUXY(4), FLUXZ(4), FLUX(4),
     &               AREA(1100)
C
           LOGICAL    IL1,IL2,IL3,TYPEA,TYPEB,TYPEC,TYPED
C
           EQUIVALENCE ( XC(1) , XN(1) , SIGMA1(1) , AREA(1) )
           EQUIVALENCE ( YC(1) , YN(1) , SIGMA2(1) )
           EQUIVALENCE ( ZC(1) , ZN(1) , SIGMA3(1) )
C
           CHARACTER CH*1(3),RUNID*4
C
           COMMON / G       / MT,A,B,C,J,T,TM,MTP
           COMMON / SUPP1    / NEXT,NSTORE
           COMMON / SUPP2    / JJ,SLP
           COMMON / SUPP3    / IAST(3,3)
           COMMON / SUPP4    / IOPT,XPLANE
C
           COMMON / HEIGHT / HGRO,ZMIN
           COMMON / INFOV  / BB(50),SIGMAS,SIGMA1,SIGMA2,SIGMA3,
     &                       CC(4),KFLOW
           COMMON / ONSETF / ONSETX(53),ONSETY(53),ONSETZ(53)
           COMMON / ANGLE  / IATACK, ALPHAX(3), ALPHAY(3), ALPHAZ(3)
           COMMON / BDINFO / KOUNT(50), NLINE(50), NTYPE(50), NLT(500),
     &                       ISECT
           COMMON / CONFLG / TITLE(18), CASE, LIFSEC, LIST, NOFF, MPR,
     &                       IOUT, IWIDTH, LASWAK, NSYM, KONTRL, IPERS,
     &                       IPRINT, SF
           COMMON / INFORM / NSORCE(10), NWAKE(10), NSTRIP(10),
     &                       WIDTH(50,10), WIDXTR(2,10)
           COMMON / RANGES / RHO1SQ, RHO2SQ
           COMMON / IMPORT / NON, NFLOW, NHALF, NCOUNT
           COMMON / NORMAL / XNT(1), YNT(1), ZNT(1)
C
           DATA NFILE / 4,22,27,29 /
C
C          READ RUN IDENTIFICATION
           READ(7,2007) RUNID
C
C          STORAGE WANTED ?
           READ(7,2008) NSTORE
C
           IF ( NSTORE.EQ.0 ) GO TO 500
           OPEN ( 35 , ACCESS="DIRECT" )
           NEXT=1
C
C          DRIFT TIME OR XPLANE CUTOFF ?
```

```
500        READ(7,2014) IOPT,XPLANE
C
C          READ CALCULATION PARAMATERS
           READ(7,2006)
           READ(7,2013) NMUL,XLIM,EMAX2
C
C------------------------------------------------------------------------
C          PREPARATION FOR SUBROUTINE VXVYVZ
C          - - - - - - - - - - - - - - - -
C          THE FOLLOWING STATEMENTS ARE SPECIFIC TO
C          THE FLOW FIELD CONSIDERED
C
           DO 600 I=1,4
           OPEN ( NFILE(I) , MODE = "IN" )
600        CONTINUE
C
           KUNIT = 29
           REWIND 4
           REWIND 29
C
           READ ( KUNIT ) TITLE, CASE, LIFSEC, LIST, NOFF, MPR, IOUT,
     &                    IWIDTH, LASWAK, NSYM, KONTRL
           READ ( KUNIT ) IATACK, ALPHAX, ALPHAY, ALPHAZ, AREA, NLINE1,
     &                    NLINEN, RHO1SQ, RHO2SQ, TYPEA, TYPEB, TYPEC,
     &                    TYPED
           READ ( KUNIT ) XC, YC, ZC
           READ ( KUNIT ) NSORCE, NWAKE, NSTRIP, WIDTH, WIDXTR, BB, IB
           READ ( KUNIT ) XN, YN, ZN
           READ ( KUNIT ) NOFSAV, NFLUX, NSETS, NV, NSETV, NCSAVE, IUNIT,
     &                    NON, NFLOW, NHALF, NCOUNT
           READ ( KUNIT ) KOUNT, NLINE, NTYPE, NLT, ISECT, SF
           HGRO = 0.
           ZMIN = 0.
           IF ( NSYM .NE. 2 ) GO TO 2400
           READ ( KUNIT ) HGRO, ZMIN
2400       CONTINUE
           READ ( KUNIT ) DIAM, ARFP
           REWIND KUNIT
           REWIND NSETS
           REWIND NFLUX
C
           WRITE(38,2003) (TITLE(I),I=1,17),CASE,HGRO,DIAM
C
           N2 = 0
           DO 2500 JS=1,LIFSEC
2500       N2 = N2 + NSTRIP ( JS )
           ONSETX (N2+1) = 1.
           ONSETY (N2+1) = 0.
           ONSETZ (N2+1) = 0.
           ONSETX (N2+2) = 0.
           ONSETY (N2+2) = 0.
           ONSETZ (N2+2) = 1.
           ONSETX (N2+3) = 0.
           ONSETY (N2+3) = 1.
           ONSETZ (N2+3) = 0.
           KFLOW = NFLOW - 3
C
           CALL READ1(NSETS,SIGMAS,KONTRL)
           CALL READ1(NSETS,SIGMA1,KONTRL)
           CALL READ1(NSETS,SIGMA2,KONTRL)
```

```
        CALL READ1(NSETS,SIGMA3,KONTRL)
C       NOTE: SUBROUTINE READ1 IS SPECIFIC TO THE FLOW CONFIGURATION
C             CONSIDERED AND ,THEREFORE, IS NOT GIVEN
        XNT(1) = 0.
        YNT(1) = 0.
        ZNT(1) = 0.
C
C       READ FLOW DATA
        READ(7,2006)
        READ(7,2013)ALPHA,VINF,VC
        READ(7,2006)
C
        ALPHAR = ALPHA * 3.14159265 / 180.
        CC(2) = VINF*COS(ALPHAR)
        CC(3) = 0.
        CC(4) = VINF*SIN(ALPHAR)
        READ ( NFLUX ) JP
        READ ( NFLUX ) (FLUXX(K),FLUXY(K),FLUXZ(K),FLUX(K),K=1,4)
        CC(1) = ( VC*ARFP-CC(2)*FLUX(2)-CC(3)*FLUX(3)-CC(4)*FLUX(4) ) /
     &          FLUX(1)
C
C       WRITE FLOW DATA
        WRITE(38,2004) ALPHA,VINF,VC
C
C       END PREPARATION FOR SUBROUTINE VXVYVZ
C------------------------------------------------------------------------
C
C       WRITE CALCULATION PARAMETERS
        WRITE(38,2010) NMUL,XLIM,EMAX2
C
C       NUMBER OF CALCULATED STREAMLINES
        NPC=0
C
C       STORE GENERAL DATA
        IF ( NSTORE.EQ.0 ) GO TO 210
        WRITE(35'NEXT) RUNID,CASE,HGRO
        NEXT=NEXT+1
        WRITE(35'NEXT) DIAM,ALPHA,VINF
        NEXT=NEXT+1
        WRITE(35'NEXT) VC,NMUL,XLIM
        NEXT=NEXT+1
        WRITE(35'NEXT) EMAX2
        NEXT=NEXT+1
        WRITE(35'NEXT) NPC
        NEXT=NEXT+1
C
210     CH(1)='X'
        CH(2)='Y'
        CH(3)='Z'
C
250     NPC=NPC+1
C
C       READ STARTING POINT DATA
        READ(7,2013)X0,Y0,Z0,KP,KPP,H,TM,IP,EMAX,EMIN
C
C       WRITE STARTING POINT DATA
        WRITE(38,2000)X0,Y0,Z0,H,TM,EMAX,EMIN,KP
C
C       INITIALIZATIONS
        HI    = H
```

```
                      HSUP = NMUL * H
                      T    = 0.
                      J    = 2
                      IC   = 1
                      IJUMP = 0
                      IFIRST = 1
      C
      C               STORE STARTING POINT DATA
                      IF ( NSTORE.EQ.0 ) GO TO 220
                      WRITE(35'NEXT) X0,Y0,Z0
                      NEXT=NEXT+1
                      WRITE(35'NEXT) H,TM,EMAX
                      NEXT=NEXT+1
                      WRITE(35'NEXT) EMIN,KP
                      NEXT=NEXT+1
                      NRNPTS = NEXT
                      WRITE(35'NEXT) IC
                      NEXT=NEXT+1
      C
      C               STARTING TESTS
      220             CALL VXVYVZ(X0,Y0,Z0,A,B,C)
                      XLIM1 = XLIM + 3*NMUL*H*(KP-1)
                      CALL SPHERE (ISP,KP,A,B,C,X0,XLIM1,EMAX2)
                      IF ( KP .NE. 0 ) GO TO 1100
                      IF ( ISP .NE. 0 ) GO TO 1110
                      IJUMP = 1
                      GO TO 1120
      1110            HSUP = NMUL * HSUP
                      H    = NMUL * H
                      GO TO 1120
      1100            IF ( ISP .EQ. -1 ) GO TO 1120
                      HSUP = NMUL * HSUP
                      H    = NMUL * H
                      IJUMP = 1
      1120            CONTINUE
                      CALL FVMAX(A,B,C,RV,IW)
                      IF(RV)1,1,2
      1               H=(2*KP-1)*H
                      GO TO (100,200,300),IW
      2               H=(1-2*KP)*H
                      GO TO (100,200,300),IW
      C
      C               START TRACKING
      C               - - - - - - -
      C
      100             MT=1
                      GO TO 400
      200             MT=2
                      GO TO 400
      300             MT=3
      C
      400             X   =IAST(1,MT)*X0+IAST(2,MT)*Y0+IAST(3,MT)*Z0
                      Y(1)=IAST(3,MT)*X0+IAST(1,MT)*Y0+IAST(2,MT)*Z0
                      Y(2)=IAST(2,MT)*X0+IAST(3,MT)*Y0+IAST(1,MT)*Z0
                      YS(1,1)=Y(1)
                      YS(2,1)=Y(2)
                      WRITE(38,2001)CH(MT),IC,X0,Y0,Z0,A,B,C,H
      C
      C               STORE STARTING POINT
                      IF(IFIRST.EQ.0) GO TO 230
```

```
              CALL WRPLOT(X0,Y0,Z0)
              IFIRST = 0
C
C             DRIFT TIME CALCULATION IN TRANSITION FIELD
230           IF(J.EQ.2) GO TO 6
              GO TO (3,4),J-2
3             CALL SPLINE2(STI,KK,XS,YSS)
              GO TO 5
4             CALL SPLINE3(STI,KK,XS,YSS)
5             IF(KK.EQ.1) GO TO 900
              J=J+1
6             STI(1,1)=X
              STI(2,1)=1./(IAST(1,MT)*A+IAST(2,MT)*B+
     &                 IAST(3,MT)*C)
              STI(3,1)=Y(1)
              STI(4,1)=Y(2)
C
C             FIND FOUR STARTING POINTS
              H=H+H
              MR=1
              GO TO 50
7             DO 13 I=1,3
              X     = AUX(1,I)
              Y(1) = AUX(2,I)
              Y(2) = AUX(3,I)
              IC=IC+1
              YS(1,I+1)=Y(1)
              YS(2,I+1)=Y(2)
              CALL TRANS(X,Y(1),Y(2),XP,YP,ZP)
              CALL WPPLOT(XP,YP,ZP)
              IF(MOD(IC,IP).NE.0) GO TO 10
              WRITE(38,2002)IC,XP,YP,ZP
10            CALL EQUAT(X,Y,F)
              FS(1,I)=F(1)
              FS(2,I)=F(2)
              STI(1,J)=X
              STI(2,J)=1./(IAST(1,MT)*A+IAST(2,MT)*B+
     &                 IAST(3,MT)*C)
              STI(3,J)=Y(1)
              STI(4,J)=Y(2)
              IF(J.NE.4) GO TO 11
              CALL SPLINE4(STI,KK,XS,YSS)
              IF(KK.EQ.1) GO TO 900
11            J=J+1
13            CONTINUE
C
C             FOUR STARTING POINTS HAVE BEEN FOUND
C             START HAMMING ALGORITHM
12            I=3
14            CALL HAMMING(YS,FS,I,H,E,X)
C
              HP = H
              CALL TRANS(X,YS(1,4),YS(2,4),XP,YP,ZP)
              IF ( IJUMP . EQ. 1 ) GO TO 75
              CALL SPHERE (ISP,KP,A,B,C,XP,XLIM,EMAX2)
              IF ( ISP) 75,71,72
71            IJUMP = 1
              H = 2 * SIGN ( HI , H )
              IL1 = .TRUE.
              IL2 = .FALSE.
```

```
          GO TO 21
72        IJUMP = 1
          HSUP = NMUL * HSUP
C
75        GTEST = ( ABS(E(1)) + ABS(E(2)) )*6.7222222
          IL1= GTEST.GT.EMAX
          IL2=(GTEST.LT.EMIN).AND.(ABS(H).LT.HSUP)
          IL3=IL1.OR.IL2
          IF(IL3) GO TO 21
C
C     1.  ERROR ACCEPTABLE
          IC=IC+1
          CALL WRPLOT(XP,YP,ZP)
          IF(MOD(IC,IP).NE.0) GO TO 15
          WRITE(38,2002)IC,XP,YP,ZP
15        STI(1,J)=X
          STI(2,J)=1./(IAST(1,MT)*A+IAST(2,MT)*B+
     &              IAST(3,MT)*C)
          STI(3,J)=YS(1,4)
          STI(4,J)=YS(2,4)
          IF(J.NE.4) GO TO 16
          CALL SPLINE4(STI,KK,XS,YSS)
          IF(KK.EQ.1) GO TO 900
16        J=J+1
C
C         CHANGE OF PARAMETER ?
          CALL FVMAX(A,B,C,RV,IW)
          IF(IW.NE.MT) GO TO 18
          I=I+1
          GO TO 14
18        XO=XP
          YO=YP
          ZO=ZP
          MTP=MT
          IF(RV) 19,19,20
19        H=(2*KP-1)*ABS(H)
          GO TO (100,200,300),IW
20        H=(1-2*KP)*ABS(H)
          GO TO (100,200,300),IW
C
C     2.  ERROR UNACCEPTABLE
21        X=X-HP
          YS(1,1)=YS(1,3)
          YS(2,1)=YS(2,3)
          Y(1)=YS(1,3)
          Y(2)=YS(2,3)
          MR=2
          IF(IL1) GO TO 50
          H=2*H
C
C         FIND  FOUR STARTING POINTS
54        DO 70 II=1,3
C
          IF(.NOT.IL2) GO TO 1130
          CALL RUNGE(X,Y,H)
          GO TO 1140
1130      X    = AUX(1,II)
          Y(1) = AUX(2,II)
          Y(2) = AUX(3,II)
1140      CONTINUE
```

```
C
            CALL TRANS(X,Y(1),Y(2),XP,YP,ZP)
            CALL EQUAT(X,Y,F)
C
            IF ( IJUMP .EQ. 1 ) GO TO 80
            XLIM1 = XLIM + 3*HI*(KP-1)
            CALL SPHERE (ISP,KP,A,B,C,XP,XLIM1,EMAX2)
            IF ( ISP .NE. 0 ) GO TO 80
            IJUMP = 1
            X     = STI(1,J-1)
            Y(1) = STI(3,J-1)
            Y(2) = STI(4,J-1)
            CALL TRANS(X,Y(1),Y(2),XU,YO,ZO)
            H = SIGN(HI,H)
            MTP = MT
            GO TO (100,200,300),MT
C
80          IC=IC+1
            YS(1,II+1)=Y(1)
            YS(2,II+1)=Y(2)
            CALL WRPLOT(XP,YP,ZP)
            IF(MOD(IC,IP).NE.0) GO TO 24
            WRITE(38,2002)IC,XP,YP,ZP
24          FS(1,II)=F(1)
            FS(2,II)=F(2)
            STI(1,J)=X
            STI(2,J)=1./(IAST(1,MT)*A+IAST(2,MT)*B+
     &               IAST(3,MT)*C)
            STI(3,J)=Y(1)
            STI(4,J)=Y(2)
            IF(J.NE.4) GO TO 25
            CALL SPLINE4(STI,KK,XS,YSS)
            IF(KK.EQ.1) GO TO 900
25          J=J+1
C
C           CHANGE OF PARAMETER ?
            CALL FVMAX(A,B,C,RV,IW)
            IF(IW.NE.MT) GO TO 18
C
70          CONTINUE
C           GO BACK TO HAMMING ALGORITHM
            GO TO 12
C
C           FIND STEPSIZE TO BE USED IN RUNGE-KUTTA CALCULATION
50          YFS(1) =Y(1)
            YFS(2) =Y(2)
            ICOUNT = 0
51          YF(1)  =YFS(1)
            YF(2)  =YFS(2)
            Y(1)   =YFS(1)
            Y(2)   =YFS(2)
            X1=X
            H=H/2.
            ICOUNT = ICOUNT + 1
            H2=H+H
            CALL RUNGE(X1,Y,H)
            AUX(1,1) = X1
            AUX(2,1) = Y(1)
            AUX(3,1) = Y(2)
            CALL RUNGE(X1,Y,H)
```

```
            X1=X
            CALL RUNGE(X1,YF,H2)
            ERR1=ABS((Y(1)-YF(1))/30.)
            ERR2=ABS((Y(2)-YF(2))/30.)
            IL1=(ERR1.LE.EMAX).AND.(ERR2.LE.EMAX)
            IF(IL1) GO TO 1150
            IF(ICOUNT.GT.40) STOP ' MORE THAN 40 BISECTIONS IN RUNGE #1 '
            GO TO 51
1150        X1    = AUX(1,1)
            YF(1)= AUX(2,1)
            YF(2)= AUX(3,1)
            ICOUNT = 0
            GO TO 53
52          YF(1)=YFS(1)
            YF(2)=YFS(2)
            X1=X
            CALL RUNGE(X1,YF,H)
            AUX(1,1) = X1
            AUX(2,1) = YF(1)
            AUX(3,1) = YF(2)
53          Y(1)=YF(1)
            Y(2)=YF(2)
            CALL RUNGE(X1,Y,H)
            AUX(1,2) = X1
            AUX(2,2) = Y(1)
            AUX(3,2) = Y(2)
            CALL RUNGE(X1,Y,H)
            AUX(1,3) = X1
            AUX(2,3) = Y(1)
            AUX(3,3) = Y(2)
            H2=H+H
            X1=X1-H2
            CALL RUNGE(X1,YF,H2)
            ERR1=ABS((Y(1)-YF(1))/30.)
            ERR2=ABS((Y(2)-YF(2))/30.)
            IL1=(ERR1.LE.EMAX).AND.(ERR2.LE.EMAX)
            IF(IL1) GO TO (7,54),MR
            H=H/2.
            ICOUNT = ICOUNT + 1
            IF(ICOUNT.GT.40) STOP ' MORE THAN 40 BISECTIONS IN RUNGE #2 '
            GO TO 52
C
C
C
C           WRITE RESULTS
C           -------------
900         WRITE(38,2005)T,IC,XS,YSS(1),YSS(2)
C
            IF ( NSTORE.EQ.0 ) GO TO 360
            LPJ = J+JJ
            IF ( MOD(LPJ,60).NE.0 ) GO TO 1160
            NPTS=IC
            NEXT=NEXT-1
            GO TO 1170
1160        IF( LPJ.NE.40 ) GO TO 1180
            NPTS=IC-2
            NEXT=NEXT-3
            GO TO 1170
1180        CONTINUE
            NPTS=IC-1
            NEXT=NEXT-2
```

```
1170        CONTINUE
            WRITE(35'NEXT) XS,YSS(1),YSS(2)
            NEXT=NEXT+1
            NINT=NEXT
            NEXT=NRNPTS
            WRITE(35'NEXT) NPTS
            NEXT=NEXT+1
            NEXT=NINT
C
360         IF(KPP.EQ.0) GO TO 250
C
            DO 700 I=1,4
            CLOSE ( NFILE(I) )
700         CONTINUE
C
            IF ( NSTORE.EQ.0 ) GO TO 800
            NEXT=5
            WRITE(35'NEXT) NPC
            NEXT=NEXT+1
            CLOSE ( 35 )
800         CONTINUE
C
C
2000        FORMAT(//' STARTING POINT: X=',E12.5,'  Y=',E12.5,'  Z=',
     &      E12.5,/,' STEPSIZE=',E12.5,/,' DRIFT TIME=',E12.5,/,
     &      ' MAXIMUM ERROR=',E12.5,'       MINIMUM ERROR=',E12.5,/,
     &      ' KP =',I2,' (KP=1 IF COUNTERFLOW , KP=0 IF PARALLEL FLOW)',/)
2001        FORMAT(/,' * ',A1,' IS PARAMETER: POINT',I6,/,3X,'X= ',
     &              E12.5,3X,'Y= ',E12.5,3X,'Z= ',E12.5,/,3X,'VX=',
     &              E12.5,3X,'VY=',E12.5,3X,'VZ=',E12.5,/,3X,'H =',
     &              E12.5,/)
2002        FORMAT(' POINT ',I6,' : X=',E12.5,' Y=',E12.5,' Z=',E12.
     &              5)
2003        FORMAT(/,1X,17A4,/,' CASE ID = ',A4,/,' HEIGHT ABOVE GROUND = ',
     &              E12.5,/,' INLET DIAMETER = ',E12.5,/,79(1H-),/)
2004        FORMAT(' ALPHA = ',F6.2,' DEGREES',' / VINFINITY = ',E12.5,
     &              ' / AVERAGE V = ',E12.5,/,
     &              ' ( VOLUME FLOW = AVERAGE V * CROSS-SECTIONAL AREA )',
     &              /,79(1H-))
2005        FORMAT(/,' RESULTS:',/,'    DRIFT TIME=',E14.7,'    (',
     &      I6,')',/,'        X=',E12.5,/,'        Y=',E12.5,/,'        Z=',
     &      E12.5)
2006        FORMAT(/,1HA,/)
2007        FORMAT(///,A4)
2008        FORMAT(/,I1)
2010        FORMAT(/,' HSUP=',I3,' * H  /',' XLIM= ',E12.5,
     &              ' / EMAX ( FAR FIELD TEST ) =',E12.5)
2013        FORMAT(V)
2014        FORMAT(/,I1,3X,F10.4)
C
            STOP
            END
C
            BLOCK DATA
            COMMON / SUPP3 / IAST(3,3)
            DATA IAST /1,0,0,0,1,0,0,0,1/
            END
C
C
C
```

```
C           SUBROUTINES
C           * * * * * *
C
C
C           -------------------------------------
C           SUBROUTINE VXVYVZ ( X,Y,Z,VX,VY,VZ)
C           -------------------------------------
C
            SUBROUTINE TRANS(U,V,W,XP,YP,ZP)
C
            COMMON/G/MT,A,B,C,J,T,TM,MTP
            COMMON/SUPP3/IAST(3,3)
C
            XP=IAST(1,MT)*U+IAST(3,MT)*V+IAST(2,MT)*W
            YP=IAST(2,MT)*U+IAST(1,MT)*V+IAST(3,MT)*W
            ZP=IAST(3,MT)*U+IAST(2,MT)*V+IAST(1,MT)*W
            RETURN
            END
C
C
            SUBROUTINE EQUAT(X,Y,F)
C
            DIMENSION Y(2),F(2)
            COMMON/G/MT,A,B,C,J,T,TM,MTP
C
            GO TO (1,2,6),MT
C           Z IS PARAMETER
6           XC=Y(1)
            YC=Y(2)
            ZC=X
            GO TO 3
C           X IS PARAMETER
1           XC=X
            YC=Y(1)
            ZC=Y(2)
            GO TO 3
C           Y IS PARAMETER
2           XC=Y(2)
            YC=X
            ZC=Y(1)
3           CALL VXVYVZ(XC,YC,ZC,VX,VY,VZ)
            A=VX
            B=VY
            C=VZ
            GO TO (4,5,7),MT
7           F(1)=VX/VZ
            F(2)=VY/VZ
            RETURN
4           F(1)=VY/VX
            F(2)=VZ/VX
            RETURN
5           F(1)=VZ/VY
            F(2)=VX/VY
            RETURN
            END
C
C
            SUBROUTINE RUNGE(X,Y,H)
C
            DIMENSION Y(2),F(2),Y9(2),PHI(2),SK1(2),SK2(2)
            COMMON/G/MT,A,B,C,J,T,TM,MTP
```

```
C
                CALL EQUAT(X,Y,F)
                DO 1 I=1,2
                YB(I)=Y(I)
                PHI(I)=0.17476028*F(I)
                Y(I)=YB(I)+0.4*F(I)*H
1               SK1(I)=F(I)
                XT=X+0.4*H
                CALL EQUAT(XT,Y,F)
                DO 2 I=1,2
                PHI(I)=PHI(I)-0.55148066*F(I)
                Y(I)=YB(I)+0.29697761*SK1(I)*H+0.15875964*F(I)*H
2               SK2(I)=F(I)
                XT=X+0.45573725*H
                CALL EQUAT(XT,Y,F)
                DO 3 I=1,2
                PHI(I)=PHI(I)+1.20553560*F(I)
3               Y(I)=YB(I)+(0.21810040*SK1(I)-3.05096516*SK2(I)+3.832864
     &          76*F(I))*H
                X=X+H
                CALL EQUAT(X,Y,F)
                DO 4 I=1,2
                PHI(I)=PHI(I)+0.17118478*F(I)
4               Y(I)=YB(I)+PHI(I)*H
                RETURN
                END
C
C

                SUBROUTINE HAMMING(YS,FS,I,H,E,X)
C
                DIMENSION YS(2,4),FS(2,3),YT1(2),YT2(2),F(2),E(2)
                COMMON/G/MT,A,B,C,J,T,TM,MTP
C
C               PREDICTOR
                X=X+H
                YT1(1)=YS(1,1)+(2*FS(1,3)-FS(1,2)+2*FS(1,1))*H*4/3.
                YT1(2)=YS(2,1)+(2*FS(2,3)-FS(2,2)+2*FS(2,1))*H*4/3.
                IF(I-3)2,1,2
2               YT2(1)=YT1(1)+E(1)*112/9.
                YT2(2)=YT1(2)+E(2)*112/9.
                GO TO 3
1               YT2(1)=YT1(1)
                YT2(2)=YT1(2)
3               CALL EQUAT(X,YT2,F)
C
C               CORRECTOR
                YT2(1)=(9*YS(1,4)-YS(1,2)+3*H*(F(1)+2*FS(1,3)-FS(1,2)))/
     &          8.
                YT2(2)=(9*YS(2,4)-YS(2,2)+3*H*(F(2)+2*FS(2,3)-FS(2,2)))/
     &          8.
                E(1)=(YT2(1)-YT1(1))*9/121.
                E(2)=(YT2(2)-YT1(2))*9/121.
                YT2(1)=YT2(1)-E(1)
                YT2(2)=YT2(2)-E(2)
                DO 4 IJ=1,2
                DO 5 IS=1,3
5               YS(IJ,IS)=YS(IJ,IS+1)
                DO 4 ISS=1,2
4               FS(IJ,ISS)=FS(IJ,ISS+1)
                YS(1,4)=YT2(1)
```

```
        YS(2,4)=YT2(2)
        CALL EQUAT(X,YT2,F)
        FS(1,3)=F(1)
        FS(2,3)=F(2)
        RETURN
        END
C
C

        SUBROUTINE FVMAX(A,B,C,RV,IW)
C

        DA=ABS(A)
        DB=ABS(B)
        DC=ABS(C)
        IF(DA-DB)1,2,2
1       IF(DB-DC)3,4,4
4       IW=2
        RV=B
        RETURN
3       IW=3
        RV=C
        RETURN
2       IF(DA-DC)5,6,6
5       IW=3
        RV=C
        RETURN
6       IW=1
        RV=A
        RETURN
        END
C
C
C
C       SPLINE SUBROUTINES
C       - - - - - - - - -
C

        SUBROUTINE SPLINE2(STI,KK,XS,YSS)
C

        DIMENSION STI(4,4),YSS(2),Y(2)
        COMMON/G/MT,A,B,C,J,T,TM,MTP
        COMMON/SUPP2/JJ,SLP
        COMMON/SUPP3/IAST(3,3)
        COMMON/SUPP4/IOPT,XPLANE
C

        IV=0
        X1=STI(1,1)
        X2=STI(1,2)
        X1F=X1
        PA=SLP*(X2-X1)+STI(2,1)-STI(2,2)
        PA=-PA/(X1-X2)**2
        PB=SLP-2*PA*X1
        PC=STI(2,1)-(PA*X1+PB)*X1
C

        TP=T
        IF ( IOPT.EQ.0 ) GO TO 300
        XCOORD = IAST(1,MTP)*STI(1,2)+IAST(3,MTP)*STI(3,2)+
     &           IAST(2,MTP)*STI(4,2)
        IF ( XCOORD.GE.XPLANE ) GO TO 200
        IV=1
300     XR=X2
        LABEL=2
        GO TO 2
```

```
C
1            XR=(X1+X2)/2
C
2            X INT=PA*(XR**3-X1F**3)/3+(PB*(XR+X1F)/2+PC)*(XR-X1F)
             T=TP+XINT
             IF ( IV.EQ.1 ) GO TO 10
             IF ( IOPT.EQ.1 ) RETURN
             DIFFO=ABS(T)-TM
             DIFF=DIFFO/TM
             IF(ABS(DIFF)-0.00001) 6,3,3
3            IF(DIFFO) 4,4,5
4            X1=XR
             GO TO (1,10),LABEL
5            X2=XR
             LABEL=1
             GO TO 1
C
6            IF(LABEL.NE.2) GO TO 200
             X=STI(1,2)
             Y(1)=STI(3,2)
             Y(2)=STI(4,2)
             GO TO 210
200          IF ( IOPT.EQ.1 ) XR=XPLANE
             HH=XR-STI(1,1)
             X=STI(1,1)
             Y(1)=STI(3,1)
             Y(2)=STI(4,1)
             MT=MTP
             CALL RUNGE(X,Y,HH)
210          CONTINUE
C
             KK=1
             J=20
             JJ=3
             GO TO (7,8,9) MTP
7            XS=X
             YSS(1)=Y(1)
             YSS(2)=Y(2)
             IF ( IOPT.EQ.0 ) GO TO 11
             GO TO 2
11           RETURN
8            XS=Y(2)
             YSS(1)=X
             YSS(2)=Y(1)
             RETURN
9            XS=Y(1)
             YSS(1)=Y(2)
             YSS(2)=X
             RETURN
10           KK=0
             J=1
             RETURN
             END
C
C
             SUBROUTINE SPLINE3(STI,KK,XS,YSS)
C
             DIMENSION STI(4,4),YSS(2),Y(2),H(2),SIG(2)
             REAL*4 M(3)
             COMMON/G/MT,A,B,C,J,T,TM,MTP
```

```
      COMMON/SUPP2/JJ,SLP
      COMMON/SUPP3/IAST(3,3)
      COMMON/SUPP4/IOPT,XPLANE
C
      H(1)=STI(1,2)-STI(1,1)
      H(2)=STI(1,3)-STI(1,2)
      XLB=H(2)/(H(1)+H(2))
      XMU=1-XLB
      SIG(1)=(STI(2,2)-STI(2,1))/H(1)
      SIG(2)=(STI(2,3)-STI(2,2))/H(2)
      D1=6*(SIG(2)-SIG(1))/(H(1)+H(2))
      M(1)=0.
      M(3)=0.
      M(2)=D1/2
C
      JJ=0
1     JJ=JJ+1
      TP=T
      IF ( IOPT.EQ.0 ) GO TO 40
      XCOORD = IAST(1,MTP)*STI(1,JJ+1)+IAST(3,MTP)*STI(3,JJ+1)+
     &         IAST(2,MTP)*STI(4,JJ+1)
      IF ( XCOORD.GE.XPLANE ) GO TO 12
40    XINT=(STI(2,JJ)+STI(2,JJ+1))*H(JJ)/2-(M(JJ)+M(JJ+1))*
     &     (H(JJ)**3)/24.
      T=T+XINT
      IF ( IOPT.EQ.1 ) GO TO 2
      IF(ABS(T)-TM) 2,3,4
2     IF(JJ-2) 1,5,5
5     SLP=H(2)*M(2)/6+(STI(2,3)-STI(2,2))/H(2)
      J=1
      KK=0
      RETURN
3     KK=1
      J=30
      GO TO (20,21,22),MT
20    XS=STI(1,JJ+1)
      YSS(1)=STI(3,JJ+1)
      YSS(2)=STI(4,JJ+1)
      RETURN
21    XS=STI(4,JJ+1)
      YSS(1)=STI(1,JJ+1)
      YSS(2)=STI(3,JJ+1)
      RETURN
22    XS=STI(3,JJ+1)
      YSS(1)=STI(4,JJ+1)
      YSS(2)=STI(1,JJ+1)
      RETURN
4     KK=1
      J=30
      X1=STI(1,JJ)
      X2=STI(1,JJ+1)
11    XR=(X1+X2)/2
41    XIX=-M(JJ)*(XR-STI(1,JJ+1))**4/(24*H(JJ))+M(JJ+1)*(XR-ST
     &  I(1,JJ))**4/(24*H(JJ))+(M(JJ)*H(JJ)**2-6*STI(2,JJ))*(XR-
     &  STI(1,JJ+1))**2/(12*H(JJ))+(6*STI(2,JJ+1)-M(JJ+1)*H(JJ)*
     &  *2)*(XR-STI(1,JJ))**2/(12*H(JJ))+(M(JJ)*H(JJ)**3)/24.+(6
     &  *STI(2,JJ)-M(JJ)*H(JJ)**2)*H(JJ)/12.
      T=TP+XIX
      IF ( IOPT.EQ.1 ) RETURN
      DIFFO=ABS(T)-TM
```

```
         DIFF=DIFFO/TM
         IF(ABS(DIFF)-0.00001) 12,25,25
25       IF(DIFFO) 26,26,27
26       X1=XR
         GO TO 11
27       X2=XR
         GO TO 11
12       IF ( IOPT.EQ.1 ) XR=XPLANE
         HH=XR-STI(1,JJ)
         X=STI(1,JJ)
         Y(1)=STI(3,JJ)
         Y(2)=STI(4,JJ)
         MT=MTP
         CALL RUNGE(X,Y,HH)
         GO TO (15,16,17) MTP
15       XS=X
         YSS(1)=Y(1)
         YSS(2)=Y(2)
         IF ( IOPT.EQ.0 ) GO TO 18
         KK=1
         J=30
         GO TO 41
18       RETURN
16       XS=Y(2)
         YSS(1)=X
         YSS(2)=Y(1)
         RETURN
17       XS=Y(1)
         YSS(1)=Y(2)
         YSS(2)=X
         RETURN
         END
C
C
         SUBROUTINE SPLINE4(STI,KK,XS,YSS)
C
         REAL*4 M(4)
         DIMENSION STI(4,4),H(3),XLB(2),XMU(2),SIG(3),D(2),
     &             YSS(2),Y(2)
         COMMON/G/MT,A,B,C,J,T,TM,MTP
         COMMON/SUPP2/JJ,SLP
         COMMON/SUPP3/IAST(3,3)
         COMMON/SUPP4/IOPT,XPLANE
C
         DO 1 I=1,3
1        H(I)=STI(1,I+1)-STI(1,I)
         XLB(1)=H(2)/(H(1)+H(2))
         XLB(2)=H(3)/(H(2)+H(3))
         XMU(1)=1-XLB(1)
         XMU(2)=1-XLB(2)
         DO 2 I=1,3
2        SIG(I)=(STI(2,I+1)-STI(2,I))/H(I)
         DO 3 I=1,2
3        D(I)=6*(SIG(I+1)-SIG(I))/(H(I)+H(I+1))
         M(1)=0.
         M(4)=0.
         DELTA=XLB(1)+XMU(2)-4.
         M(2)=(XLB(1)*D(2)-2*D(1))/DELTA
         M(3)=(XMU(2)*D(1)-2*D(2))/DELTA
         JJ=0
```

```
7          JJ=JJ+1
           TP=T
           IF ( IOPT.EQ.0 ) GO TO 40
           XCOORD = IAST(1,MT)*STI(1,JJ+1)+IAST(3,MT)*STI(3,JJ+1)+
      &           IAST(2,MT)*STI(4,JJ+1)
           IF ( XCOORD.GE.XPLANE ) GO TO 12
40         XINT=(STI(2,JJ)+STI(2,JJ+1))*H(JJ)/2-(M(JJ)+M(JJ+1))*(H(
      &         JJ)**3)/24.
           T=T+XINT
           IF ( IOPT.EQ.1 ) GO TO 4
           IF(ABS(T)-TM) 4,5,6
4          IF(JJ-3) 7,8,8
8          SLP=H(3)*M(3)/6 + (STI(2,4)-STI(2,3))/H(3)
           DO 9 I=1,4
9          STI(I,1)=STI(I,4)
           J=1
           KK=0
           RETURN
5          KK=1
           J=40
           GO TO (20,21,22),MT
20         XS=STI(1,JJ+1)
           YSS(1)=STI(3,JJ+1)
           YSS(2)=STI(4,JJ+1)
           RETURN
21         XS=STI(4,JJ+1)
           YSS(1)=STI(1,JJ+1)
           YSS(2)=STI(3,JJ+1)
           RETURN
22         XS=STI(3,JJ+1)
           YSS(1)=STI(4,JJ+1)
           YSS(2)=STI(1,JJ+1)
           RETURN
6          KK=1
           J=40
           X1=STI(1,JJ)
           X2=STI(1,JJ+1)
11         XR=(X1+X2)/2.
41         XIX=-M(JJ)*(XR-STI(1,JJ+1))**4/(24*H(JJ))+M(JJ+1)*(XR-ST
      &    I(1,JJ))**4/(24*H(JJ))+(M(JJ)*H(JJ)**2-6*STI(2,JJ))*(XR-
      &    STI(1,JJ+1))**2/(12*H(JJ))+(6*STI(2,JJ+1)-M(JJ+1)*H(JJ)*
      &    *2)*(XR-STI(1,JJ))**2/(12*H(JJ))+(M(JJ)*H(JJ)**3)/24.+(6
      &    *STI(2,JJ)-M(JJ)*H(JJ)**2)*H(JJ)/12.
           T=TP+XIX
           IF ( IOPT.EQ.1 ) RETURN
           DIFFO=ABS(T)-TM
           DIFF=DIFFO/TM
           IF(ABS(DIFF)-0.00001) 12,25,25
25         IF(DIFFO) 26,26,27
26         X1=XR
           GO TO 11
27         X2=XR
           GO TO 11
12         IF ( IOPT.EQ.1 ) XR=XPLANE
           HH=XR-STI(1,JJ)
           X=STI(1,JJ)
           Y(1)=STI(3,JJ)
           Y(2)=STI(4,JJ)
           CALL RUNGE(X,Y,HH)
           GO TO (15,16,17),MT
```

```
15          XS=X
            YSS(1)=Y(1)
            YSS(2)=Y(2)
            IF ( IOPT.EQ.0 ) GO TO 18
            KK=1
            J=40
            GO TO 41
18          RETURN
16          XS=Y(2)
            YSS(1)=X
            YSS(2)=Y(1)
            RETURN
17          XS=Y(1)
            YSS(1)=Y(2)
            YSS(2)=X
            RETURN
            END
C
C
C

            SUBROUTINE SPHERE (ISP,KP,VX,VY,VZ,XO,XLIM,EMAX)

C
C           THIS SUBROUTINE DETERMINES WHETHER THE CALCULATED POINT IS
C           IN THE FAR FIELD OR IN THE NEAR FIELD
C           IF THE POINT IS IN THE FAR FIELD , THEN
C           HSUP = ( NMUL ** 2 ) * HI
C           IF THE POINT IS IN THE NEAR FIELD , THEN
C           HSUP = NMUL * HI
C           WHERE :
C           HSUP IS THE LARGEST VALUE THE STEP SIZE ABSOLUTE VALUE CAN TAKE
C           HI   IS THE STEP SIZE INITIAL VALUE ( INPUT )
C           NMUL IS INPUT
C
            COMMON / INFOV   / BB(50),SIGMAS(1100),SIGMA1(1100),
        &                     SIGMA2(1100),SIGMA3(1100),CC(4),KFLOW
C
            IF ( XO .GT. XLIM ) GO TO 10
            IF ( CC(2) .NE. 0 ) GO TO 1
            DELTVX = ABS ( VX )
            GO TO 2
1           DELTVX = ABS ( ( VX - CC(2) ) / CC(2) )
2           CONTINUE
            IF ( CC(4) .NE. 0 ) GO TO 3
            DELTVY = ABS ( VY )
            GO TO 4
3           DELTVY = ABS ( ( VY - CC(4) ) / CC(4) )
4           CONTINUE
            IF (( DELTVX.GT.EMAX ).OR.( DELTVY.GT.EMAX )) GO TO 10
C           FAR FIELD
            ISP = 3.* KP - 2
            RETURN
C           NEAR FIELD
10          ISP = -KP
            RETURN
            END
C
C

            SUBROUTINE WRPLOT(X,Y,Z)
C
C           THIS SUBROUTINE STORES THE CALCULATED POINT IN FILE35
```

```
C
       COMMON/SUPP1/NEXT,NSTORE
C
       IF ( NSTORE.EQ.0 ) GO TO 10
       WRITE(35'NEXT) X,Y,Z
       NEXT=NEXT+1
10     RETURN
       END
```

APPENDIX B

QUALITATIVE INVESTIGATION OF THE FLOW USING

A SIMPLE TWO-SINK MODEL

B-1 Model Description

The most basic model of the flow to be studied consists of a sink
and its image in a uniform free stream. In the configuration shown in
Figure B.1 the flow far away from the sinks is uniform and parallel to
the x-axis, its magnitude is V_∞. The two sinks, which have the same
strength Q (positive), are located on the z-axis at respectively
$z = H$ and $z = -H$.

The velocity potential is given by

$$\phi(x,y,z) = V_\infty x + \frac{Q}{4\pi}\left(\frac{1}{r_+} + \frac{1}{r_-}\right)$$

where

$$r_+ = \sqrt{x^2 + y^2 + (z - H)^2}$$

$$r_- = \sqrt{x^2 + y^2 + (z + H)^2}$$

Therefore the components of the flow velocity at a point M(x,y,z) are

$$V_x = \frac{\delta\phi}{\delta x} = V_\infty - \frac{Q x}{4\pi}\left(r_+^{-3} + r_-^{-3}\right)$$

$$V_y = \frac{\delta \phi}{\delta y} = -\frac{Qy}{4\pi} \left(\pi_+^{-3} + \pi_-^{-3} \right)$$

$$V_z = \frac{\delta \phi}{\delta z} = -\frac{Q}{4\pi} \left(\frac{z-H}{\pi_+^3} + \frac{z+H}{\pi_-^3} \right)$$

The velocity potential can be rewritten in the following nondimensional form:

$$\tilde{\phi} = \frac{\phi}{V_\infty H} = \frac{x}{H} + \frac{\frac{Q}{V_\infty H^2}}{4\pi} \left(\frac{1}{\frac{\pi_+}{H}} + \frac{1}{\frac{\pi_-}{H}} \right)$$

The nondimensional velocity is then given by

$$\tilde{\underline{V}} = \frac{\underline{V}}{V_\infty} = \tilde{\underline{\nabla}} \, \tilde{\phi}$$

where the operator $\tilde{\underline{\nabla}}$ is equal to

$$\tilde{\underline{\nabla}} = \underline{i} \frac{\delta}{\delta \frac{x}{H}} + \underline{j} \frac{\delta}{\delta \frac{y}{H}} + \underline{k} \frac{\delta}{\delta \frac{z}{H}} = \underline{i} \frac{\delta}{\delta \tilde{x}} + \underline{j} \frac{\delta}{\delta \tilde{y}} + \underline{k} \frac{\delta}{\delta \tilde{z}}$$

Examining the above equations results in the recognition of the ratio $\frac{Q}{V_\infty H^2}$ as the dimensionless group quantifying the relative influence of sink strength, sink height from plane of symmetry and wind velocity. Its value can be chosen by following the below reasoning.

If a sink of strength Q is used to modelize a jet engine, then we have

$$Q = \frac{\pi}{4} D^2 \cdot V_i$$

where D and V_i are respectively the inlet diameter and the inlet throat velocity.

If γ and η are equal to respectively the inlet velocity to wind velocity ratio $\dfrac{V_i}{V_\infty}$ and the inlet centerline height to inlet diameter ratio $\dfrac{H}{D}$, then the above equation can be rewritten as follows

$$Q = \frac{\pi}{4} \times \frac{\gamma}{\eta^2} \times H^2 V_\infty$$

$$\frac{Q}{V_\infty H^2} = \frac{\pi}{4} \times \frac{\gamma}{\eta^2}$$

Substituting for γ and η representative values of 50 and 1.5 gives

$$\frac{Q}{V_\infty H^2} = 17.45$$

The results discussed in the next section correspond to

$$\frac{Q}{V_\infty H^2} = 20$$

As previously mentioned the flow situations we are concerned with are characterized by high values of the ratio $\dfrac{V_i}{V_\infty}$. One can also say that they are characterized by high values of the ratio $\dfrac{A_\infty}{\frac{\pi D^2}{4}}$, where A_∞ is the far upstream cross-sectional area of the jet engine

capture surface*, for, if the flow is assumed to be incompressible, this ratio is equal by continuity to $\frac{V_i}{V_\infty}$. In the simple two-sink model, the inlet diameter D is not relevant, however, the altitude of the sink above ground, i.e., plane of symmetry, can be utilized to evaluate the capture surface size. If the latter is supposed to have far upstream a half-circular cross-section of radius r_∞ , we have

$$\frac{r_\infty}{H} = \frac{D}{H} \times \sqrt{\frac{V_i}{2 V_\infty}}$$

$$\frac{r_\infty}{H} = \frac{\sqrt{\frac{\gamma}{2}}}{\eta}$$

Substituting again for γ and η typical values of 50 and 1.5 yields

$$\frac{r_\infty}{H} \simeq 3.3$$

This result, which does not depend on the inlet model used, gives an indication of the dimension of the capture surface at infinity.

---

*The capture surface of a sink-type device (i.e., inlet) is defined as the surface separating the portion of the flow which enters the sink (inlet) from the portion of the flow which does not enter.

B-2 Results

Using the simple model previously described it is possible to obtain a qualitative appreciation for the three-dimensional flow induced by a jet engine inlet close to a ground plane. To do this, some judiciously chosen particles are followed with the help of the fluid particle tracking program. The results to be shown consist of projections of these streamlines on the coordinate planes.

The x, z and x, y planes are both plane of symmetry of the flow field. The peculiar role played by the x, z plane was recognized early. Figures B.2 and B.3 show some of the streamlines running in this plane. For the particular value of the dimensionless sink strength used the flow above or in the ground plane is observed to contain three stagnation points, lying all on the x, z plane. The first one S_1 is formed inside the capture surface on the ground plane and is associated with a converging flow as can be seen in Figures B.2 and B.4. Figure B.4 shows the projections on the x, y plane (ground plane) of streamlines in "wrap around" the streamline connecting S_1 to the sink. The second stagnation point S_2 lies on both the ground plane and the capture surface. Note that the fluid particles only appear to leave this point either to go inside the capture surface and be finally sucked into the sink or to move downstream, as is shown in Figures B.3 and B.5. This feature can be explained by streamlines close to the capture surface and the x, y plane meeting the x, z plane tangentially

(i.e., in a cusp*), thus providing the flow leaving S_2 in the

x, z plane with fluid particles. In other words the flow observed

about S_2 in the x, z plane may be regarded as arising from fluid

particles moving along the capture surface near or in the x, y plane

impinging on the x, z plane. Figure B.4 also indicates this feature.

The third stagnation point S_3 is formed off the ground plane and is

associated with the meeting of particles coming from far upstream,

which either proceed downstream or are aspirated by the sink, and

particles leaving the second stagnation point.

The features described above are peculiar to the flow in the x, z

plane. None of the flow patterns observed about S_2 is present in the

flow off this plane. Off the x, z plane the fluid particles either

flow past the capture surface or are sucked by one of the sinks, in

this case, describing trajectories which are wrapped about the so-called

stagnation streamline connecting S_1 to the sink. A global view of the

flow is sketched in Figure B.6.

Difficulties are encountered when trying to understand the

structure of the flow, especially about S_2. These are basically due

to the use of the point sink. Although the sink is suitable for an

investigation of the far field, where the engine is perceived only as a

---

*A cusp is the only manner in which a streamline off the x, z plane can

meet the latter since the velocity at any point of a plane of symmetry

is parallel to this plane.

sucking device, in the present study we are concerned with the flow field near the engine as well. The inlet vortex, when present, is observed to "attach" to the ground within a distance of one or two inlet diameters from the inlet lip; thus, as the intake height from the ground to intake diameter ratio is typically equal to 1-2, the length scales in the problem are all of order of the inlet diameter. Therefore a geometrical representation of the inlet which is adequate on this scale is required. There are other drawbacks to the simple sink model. Firstly the direction of the wind relative to the engine cannot be introduced. Secondly the first stagnation point, where the inlet vortex, if present, seems to attach, is always found on the positive part of the x-axis (see Figure B.1), i.e., after the sink projection when marching along the x-axis in the free stream direction: this is not consistent with the experimental results reported in the literature. (The first limitation will obviously vanish if the engine geometry is taken into account, since then the suction in the absence of wind will no longer be axisymmetric.) It is therefore seen that a more exact description of the potential flow near the inlet is needed. However the use of the simple sink model was able to yield some qualitative appreciation for the three-dimensional flow as well as enable us to define some of the requirements an acceptable model must meet. A further use of the sink model was to give, as a test case for the fluid particle tracking program, some valuable results about the behavior of this program.

TABLE 1: KEY TO FIGURES 37,38,42,43,44,45

Amplitude between	key
0 and 5	1
5 - 10	2
10 - 15	3
15 - 20	4
20 - 25	5
25 - 30	6
30 - 40	7
40 - 50	8
50 - 60	9
60 - 70	10
.	
.	
100 - 110	14
.	
.	
350 - 360	39
.	
.	
500 - 510	54
.	
.	

For amplitude values larger than 30, the key equals x if the amplitude is between 10x - 40 and 10x - 30.
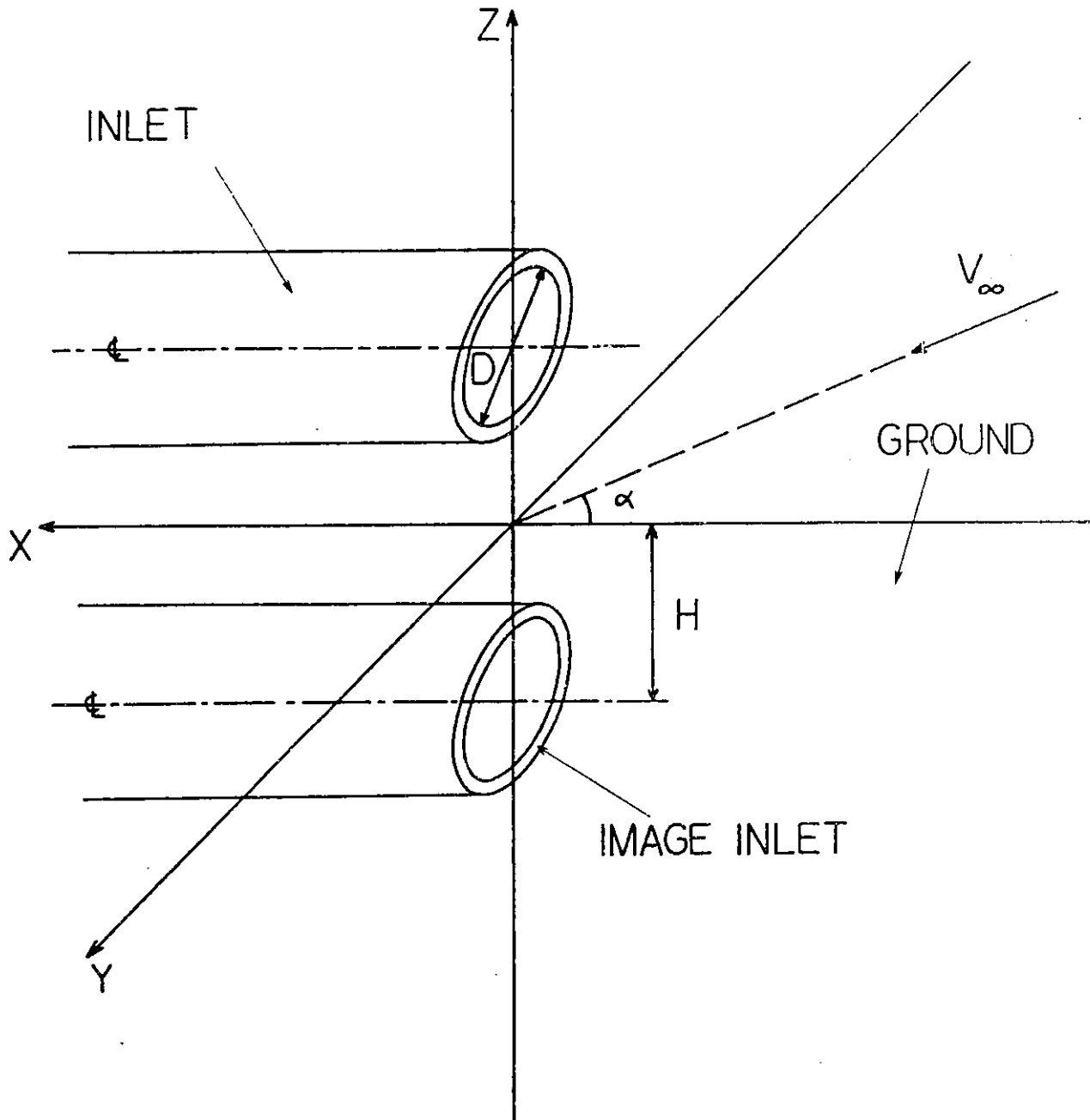
FIGURE 1: Flow Geometry
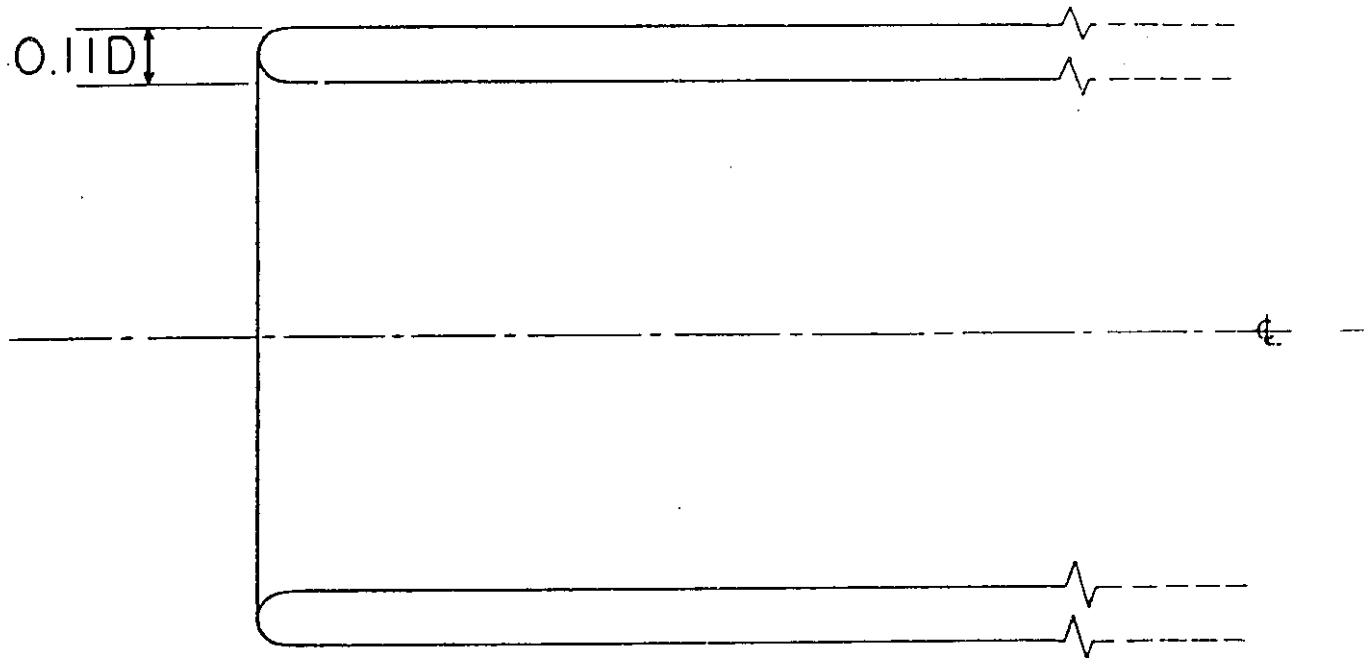
FIGURE 2: Inlet Geometry
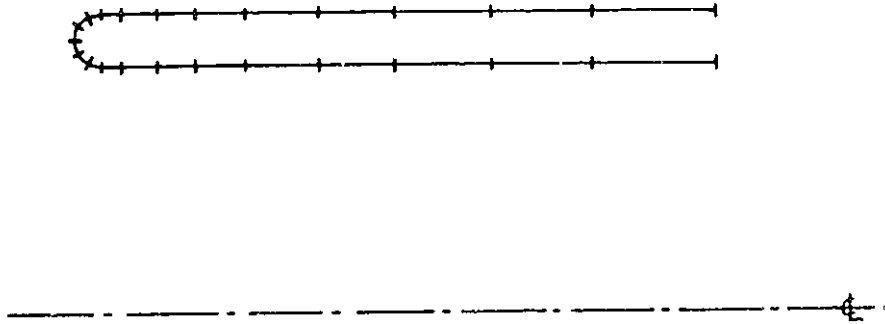
FIGURE 3a: N-line and Panel Vertices
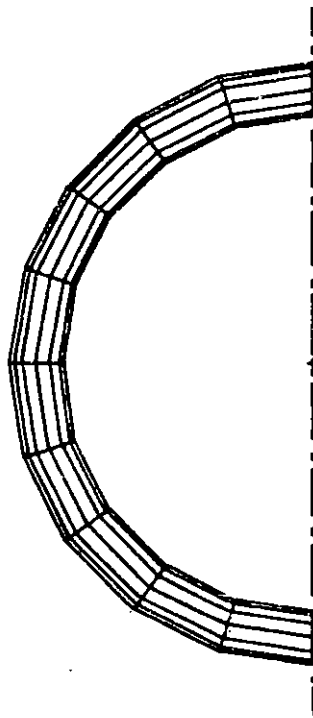
FIGURE 3b: Front View (because of Symmetry, only Half the Inlet is Shown)

FIGURE 3:   Inlet Panel Representation
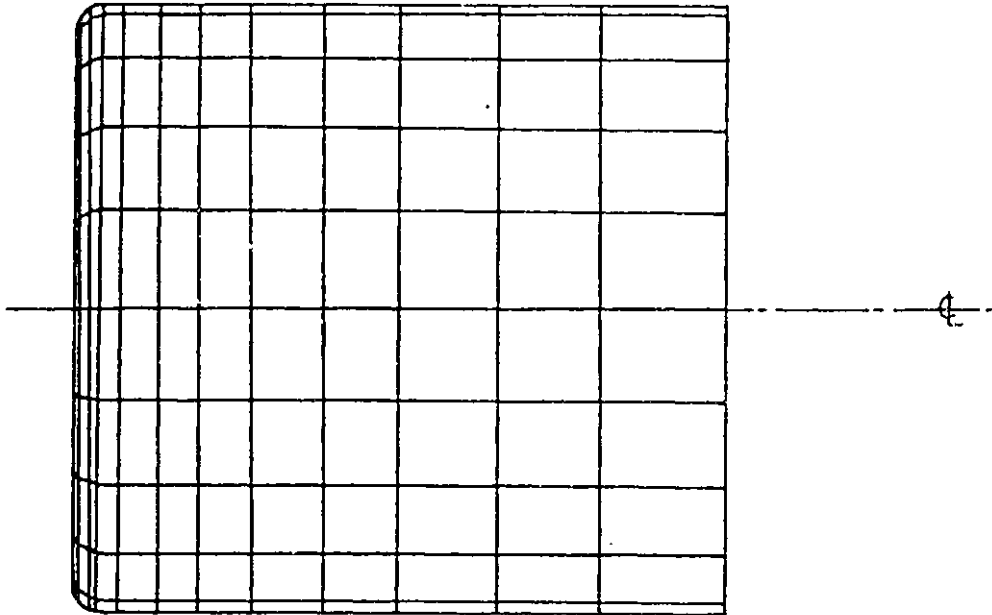
FIGURE 4: Side View of Inlet Panel Representation

.S

INLET

⊄

Stagnation
Streamline

Z

GROUND

X

S₁
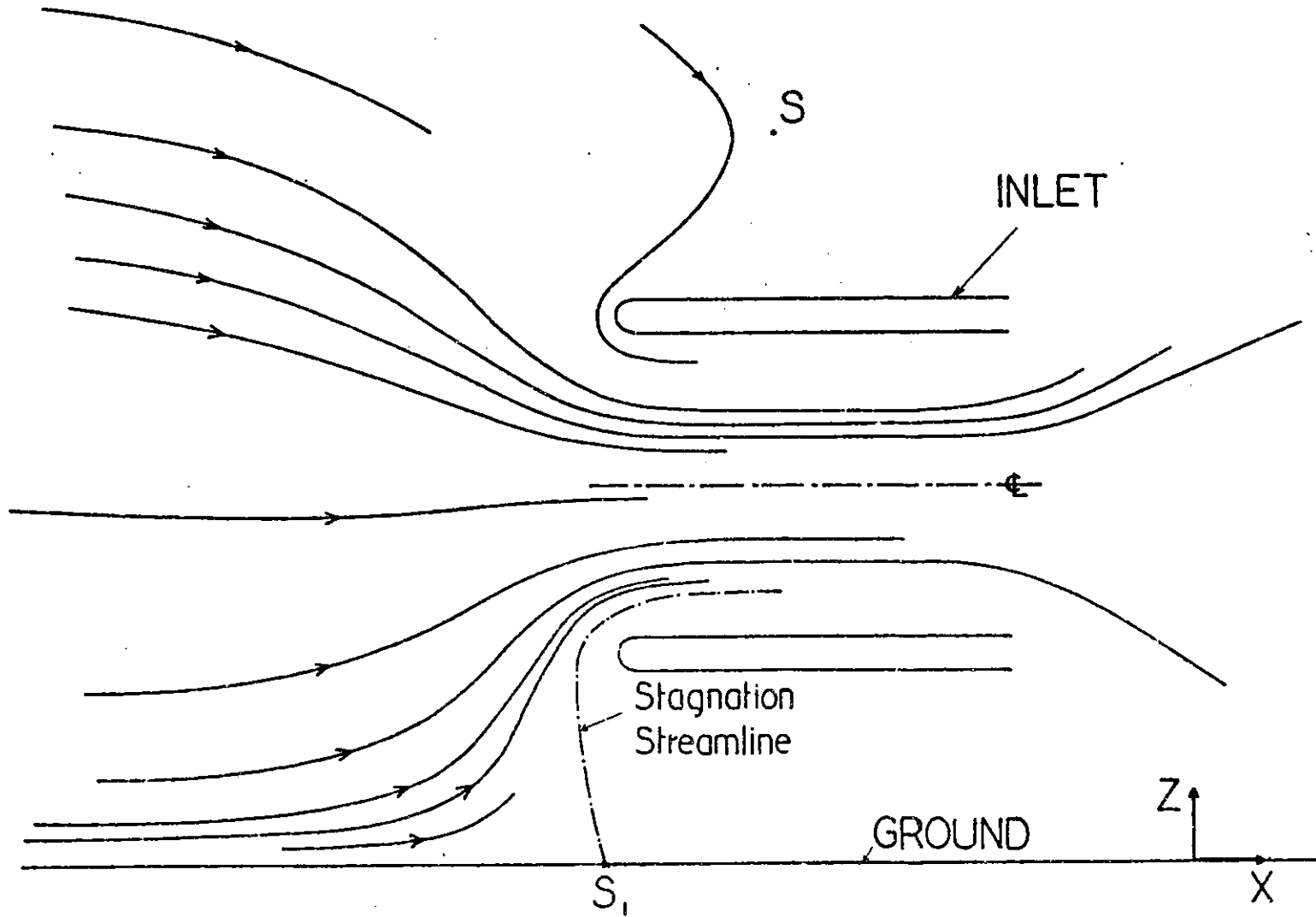
FIGURE 5: Streamlines in the x, z Plane, Case 1

S

INLET

₡

Z

X   S₁   GROUND   S₂
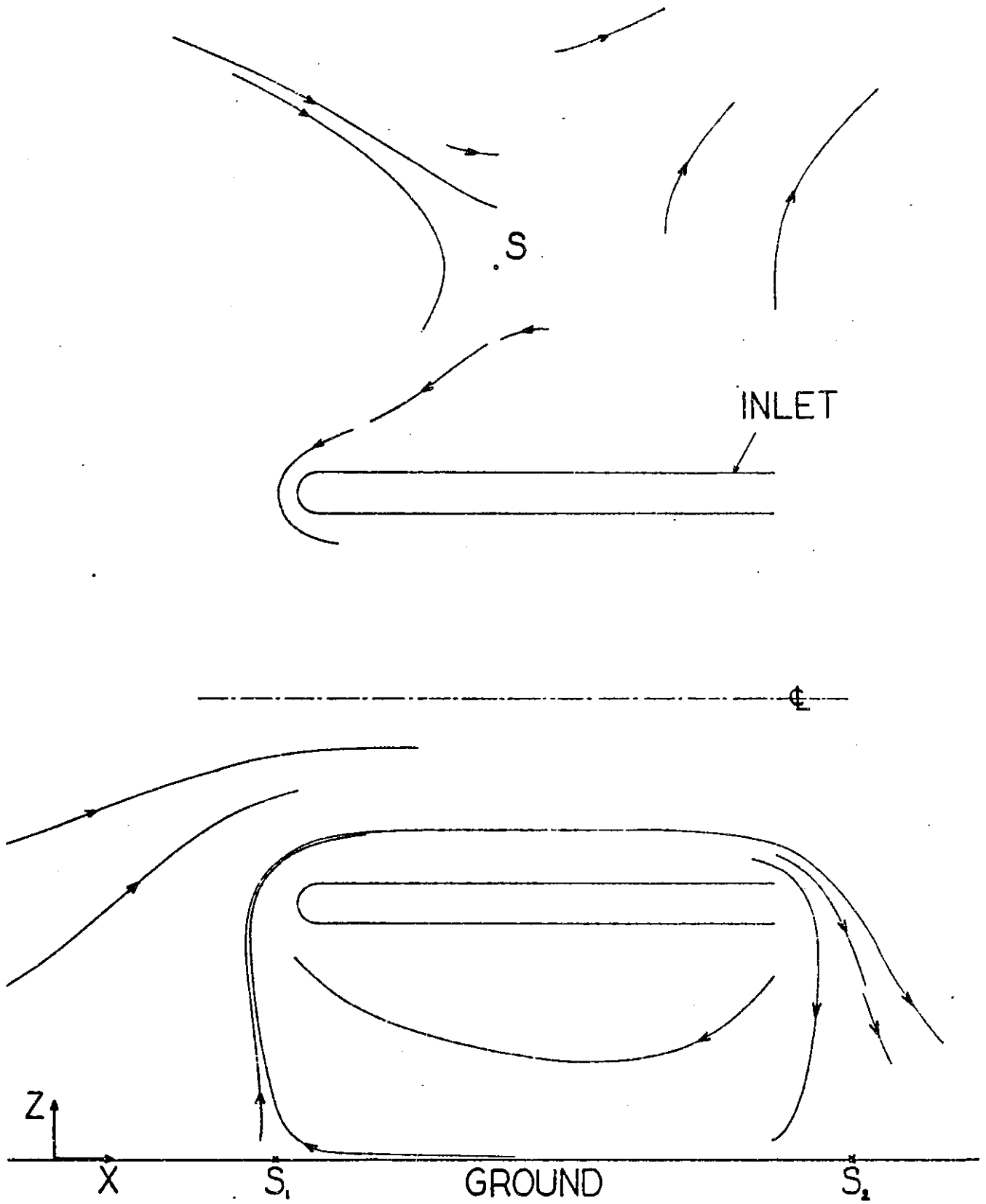
FIGURE 6:   Streamlines in the x, z Plane, Case 1
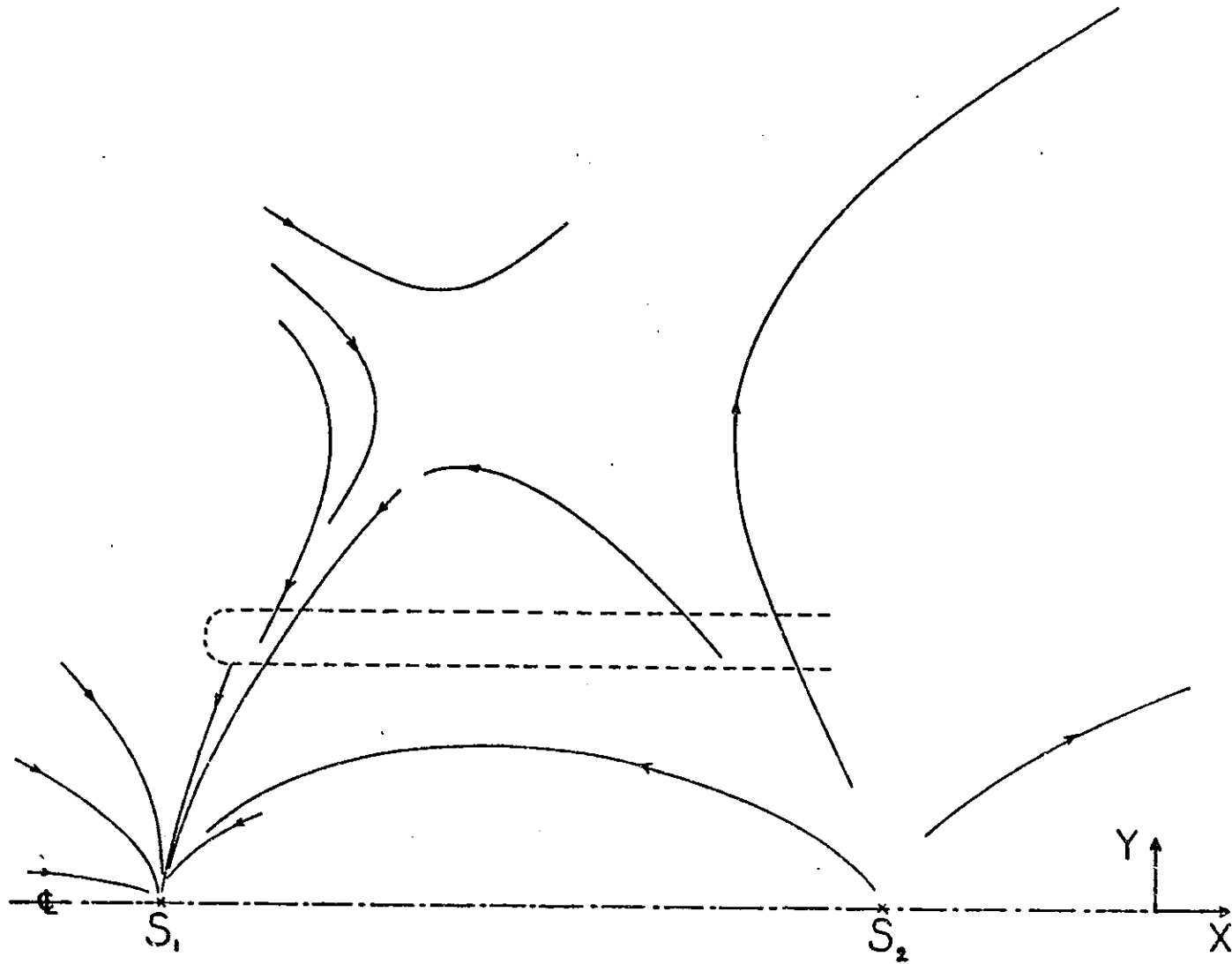
FIGURE 7:   Streamlines in the x, y Plane, Case 1
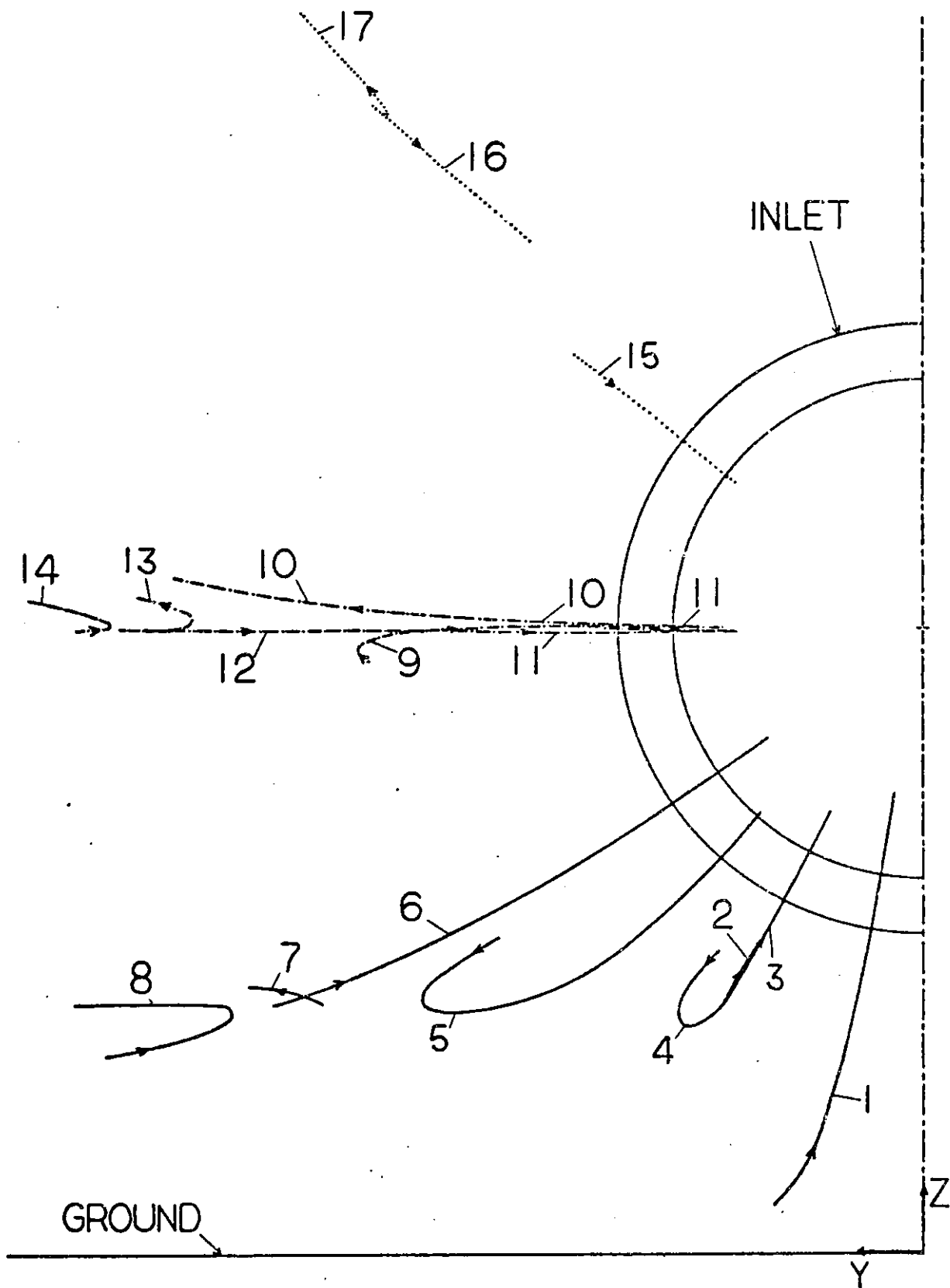
FIGURE 8: Projections of Streamlines on the y, z Plane, Case 1
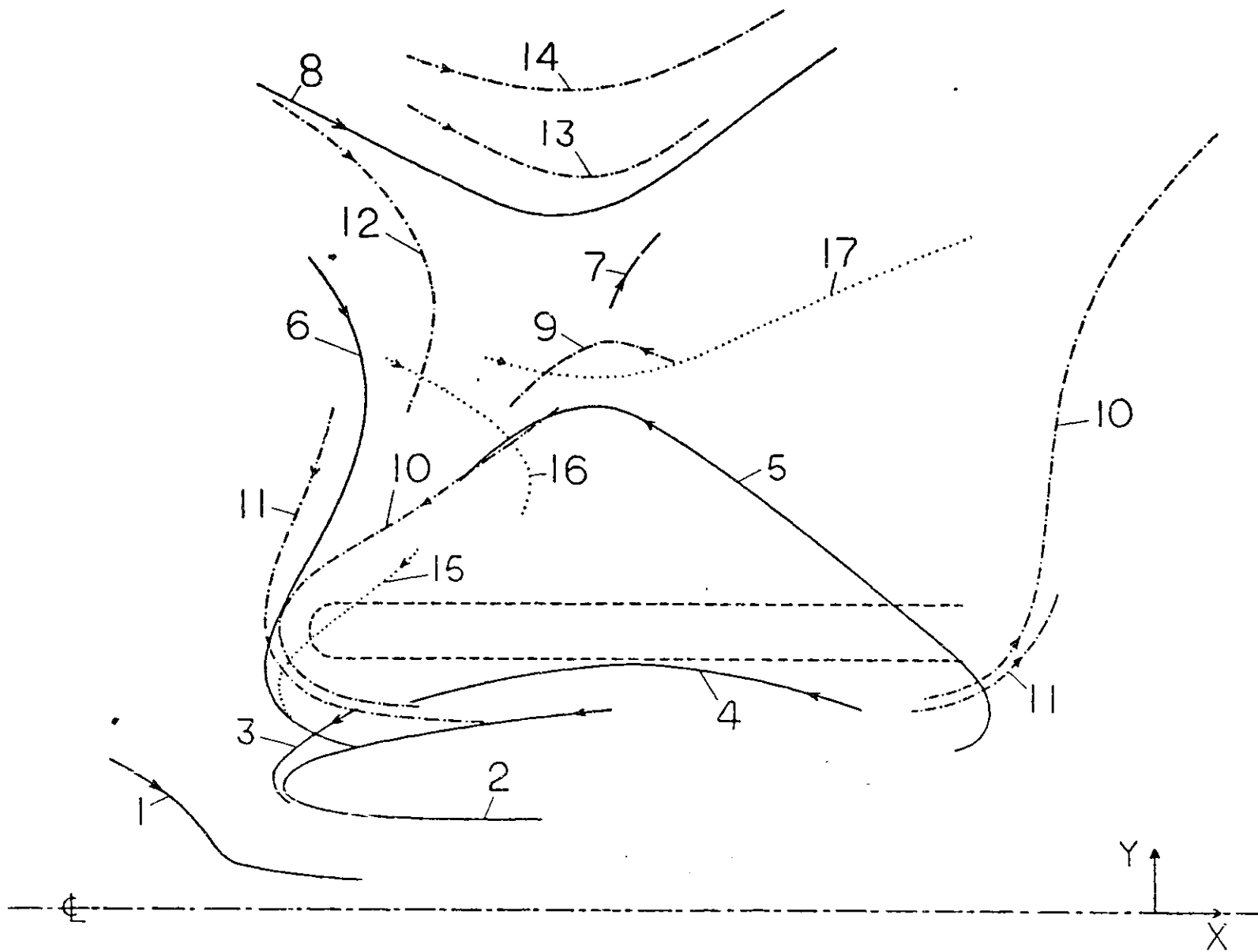
FIGURE 9: Projections of the Streamlines Shown in Figure 8 on the x, y Plane, Case 1

CAPTURE SURFACE

STAGNATION
LINE

INLET

GROUND
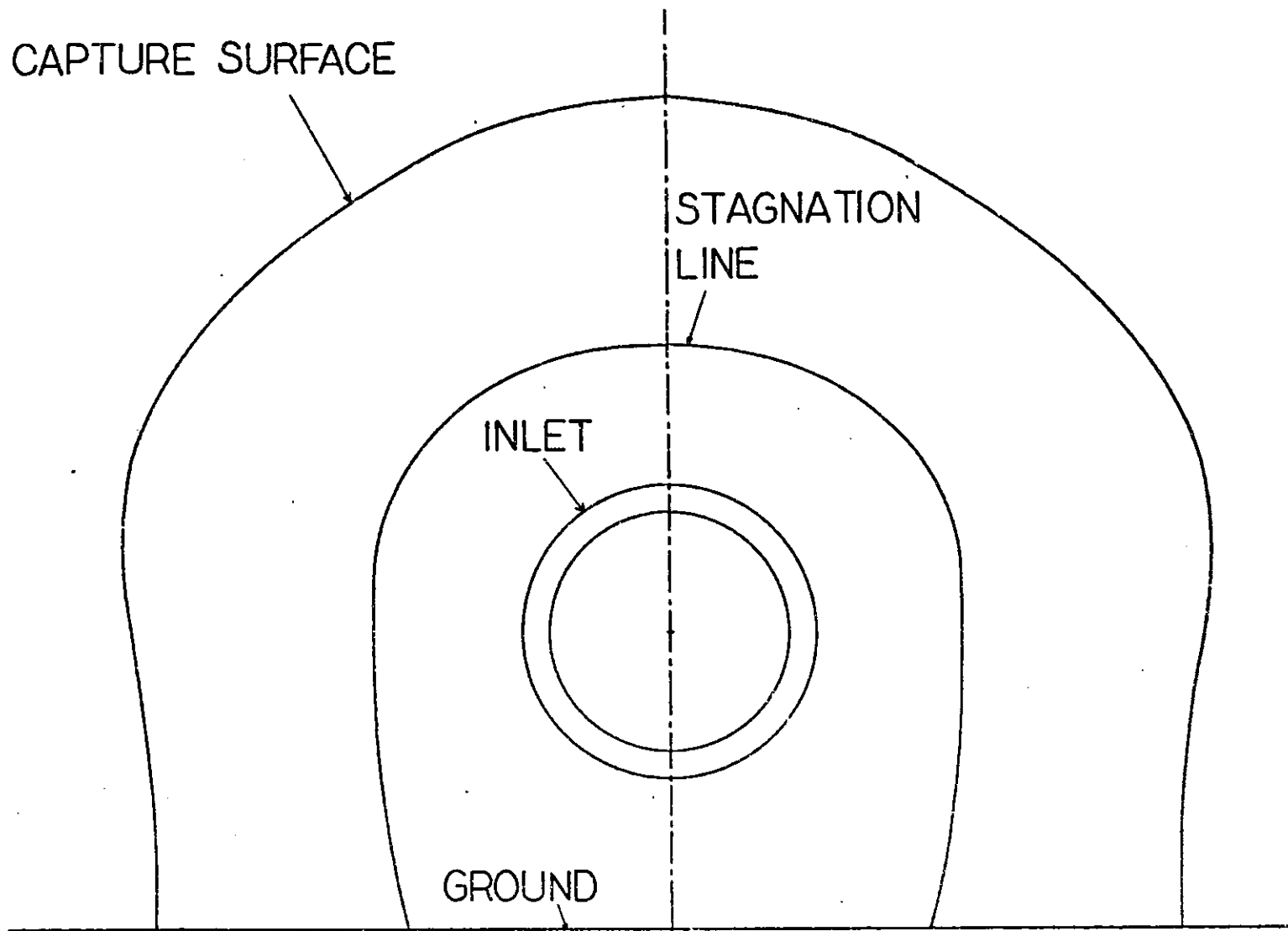
FIGURE 10: Cross Section of the Capture Surface, Four Inlet Heights Upstream of the Inlet,
Front View of the Stagnation Line, Case 1

110

CAPTURE SURFACE

INLET

GROUND

Z

S₁

X
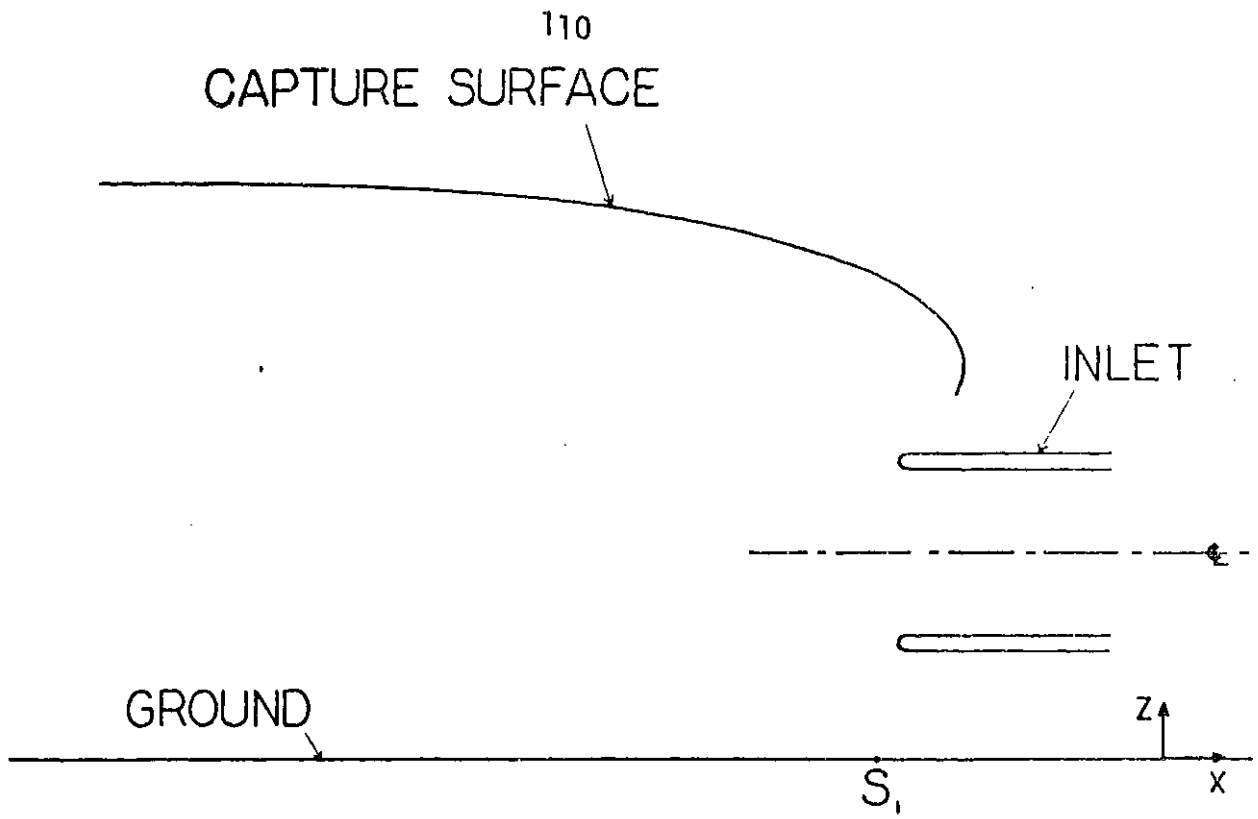
FIGURE 11a: Trace on the x, z Plane

CAPTURE SURFACE

INLET

y

x

S₁
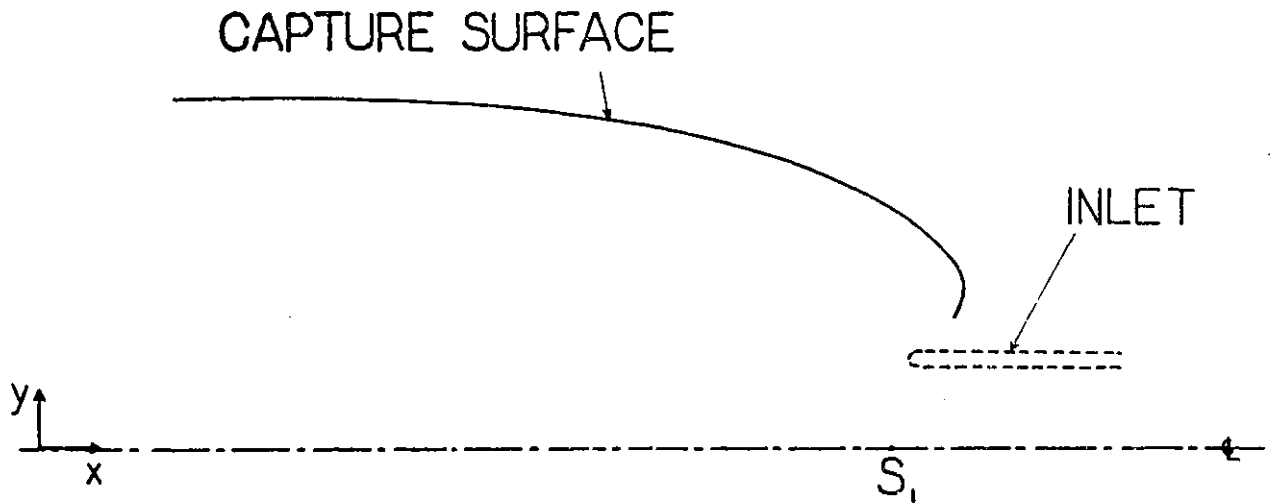
FIGURE 11b: Trace on the x, y Plane

FIGURE 11: Capture Surface, Case 1
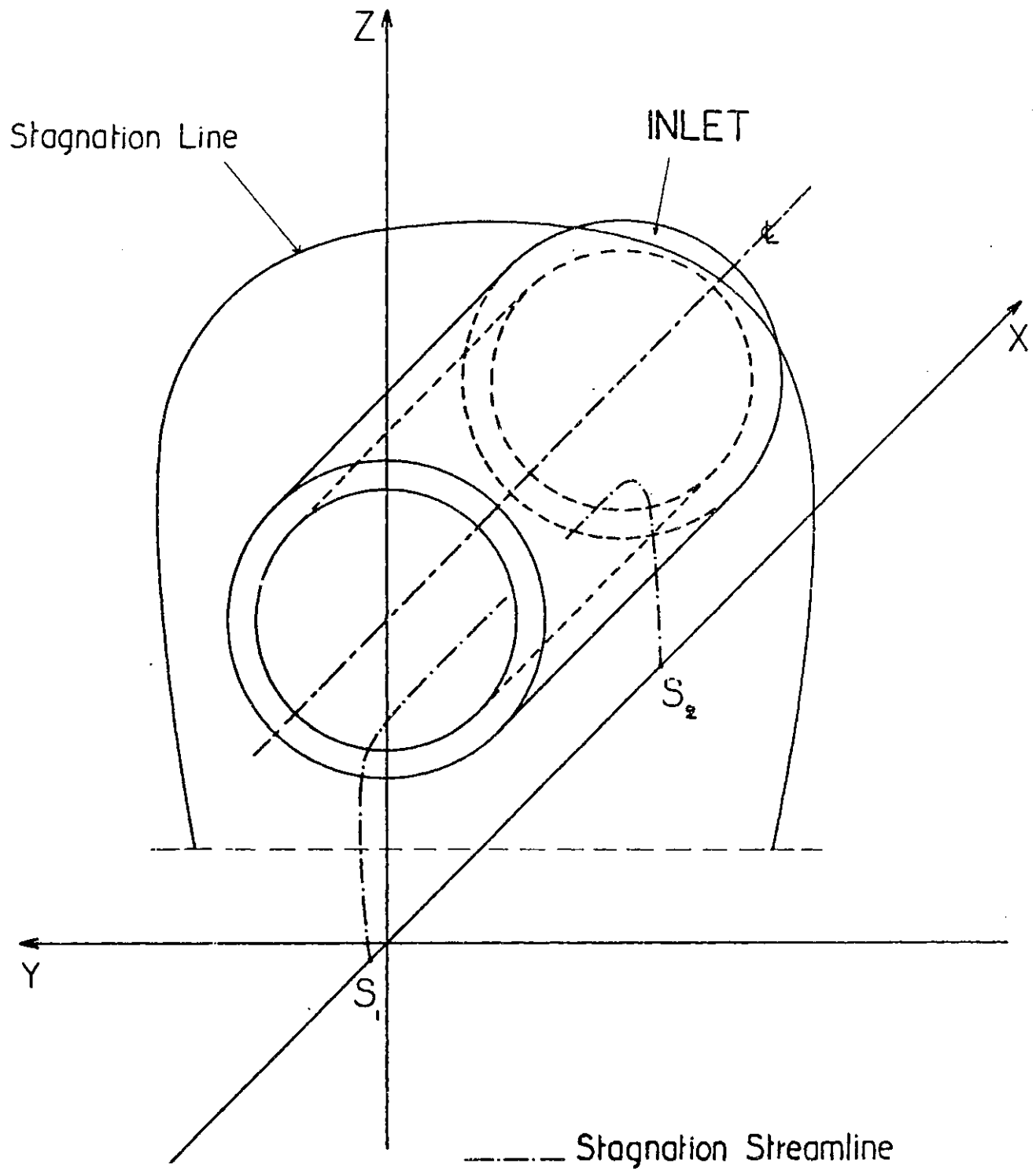
FIGURE 12: Perspective View of Stagnation Locations, Case 1
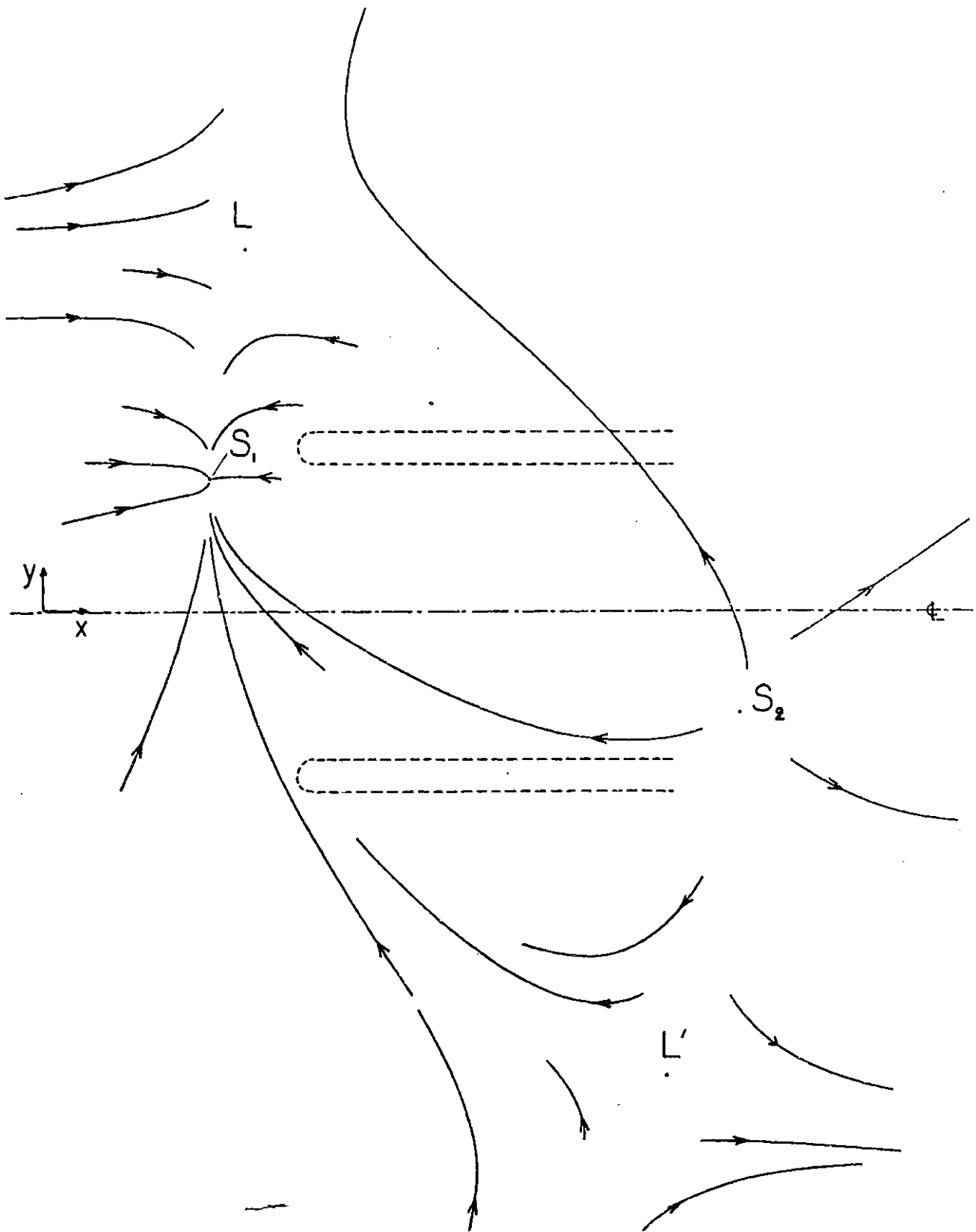
FIGURE 13: Streamlines in the x, y Plane, Case 2
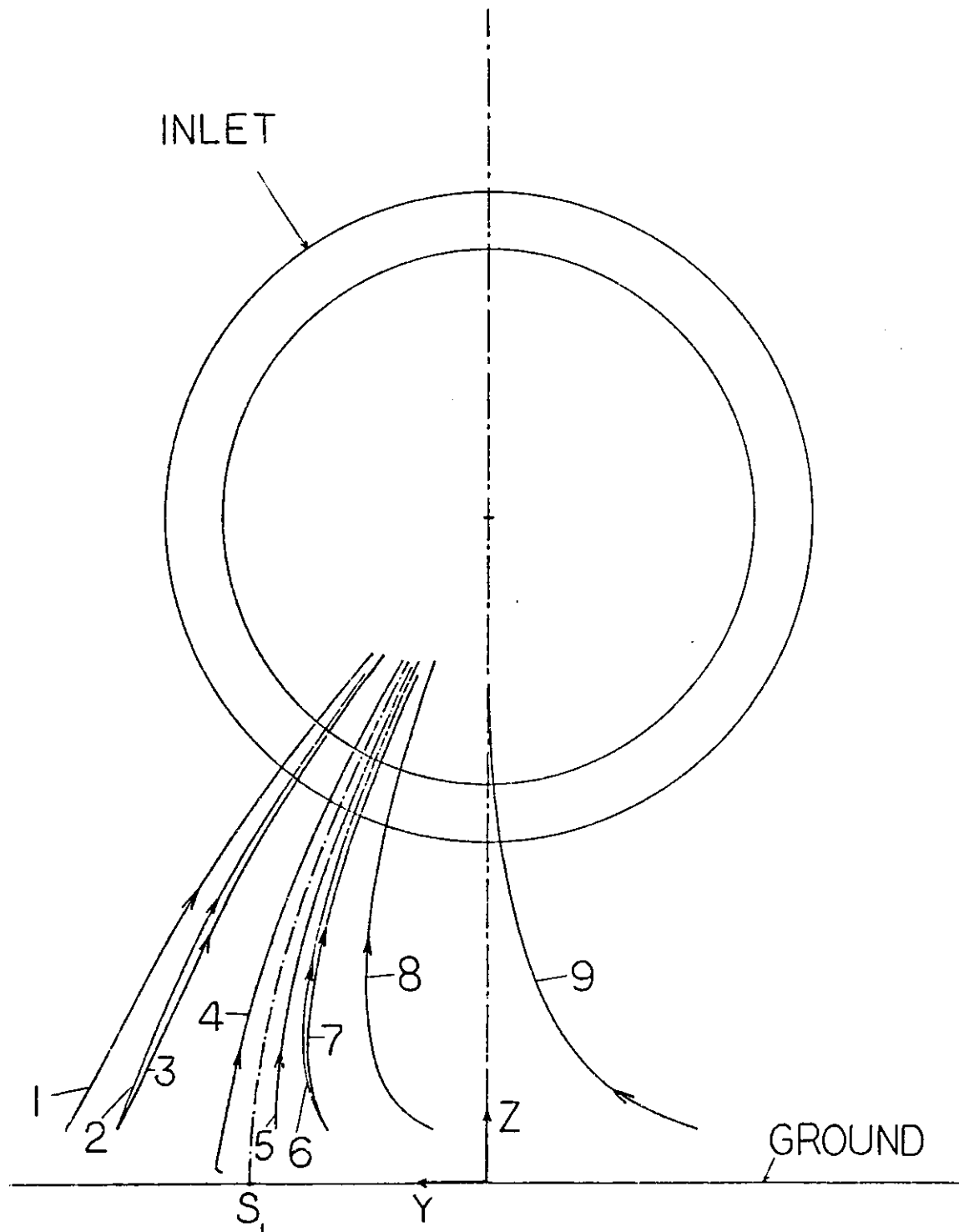
FIGURE 14: Projections of Streamlines on the y, z Plane, Case 2
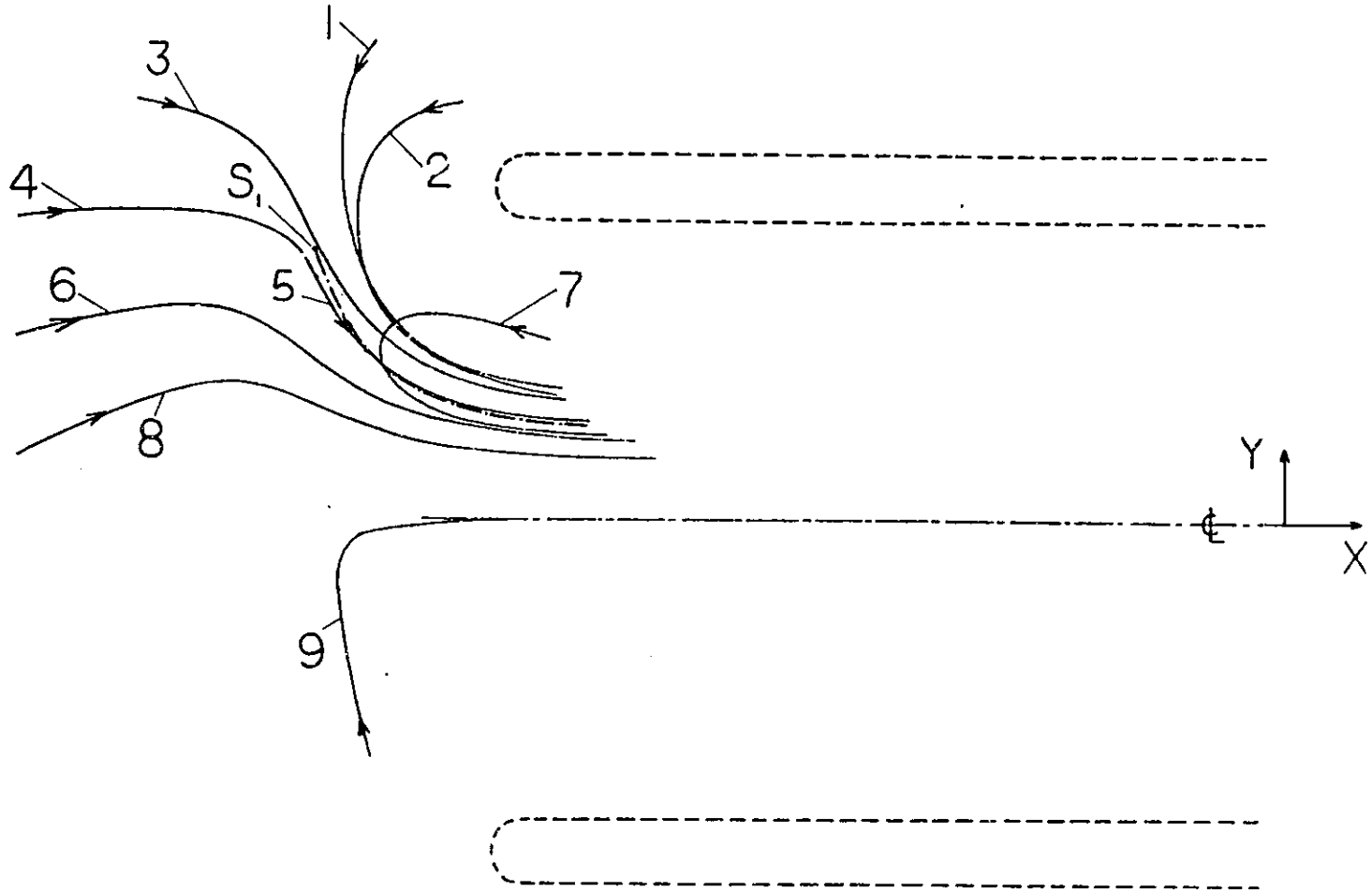
FIGURE 15: Projections of the Streamlines Shown in Figure 14 on the x, y Plane, Case 2
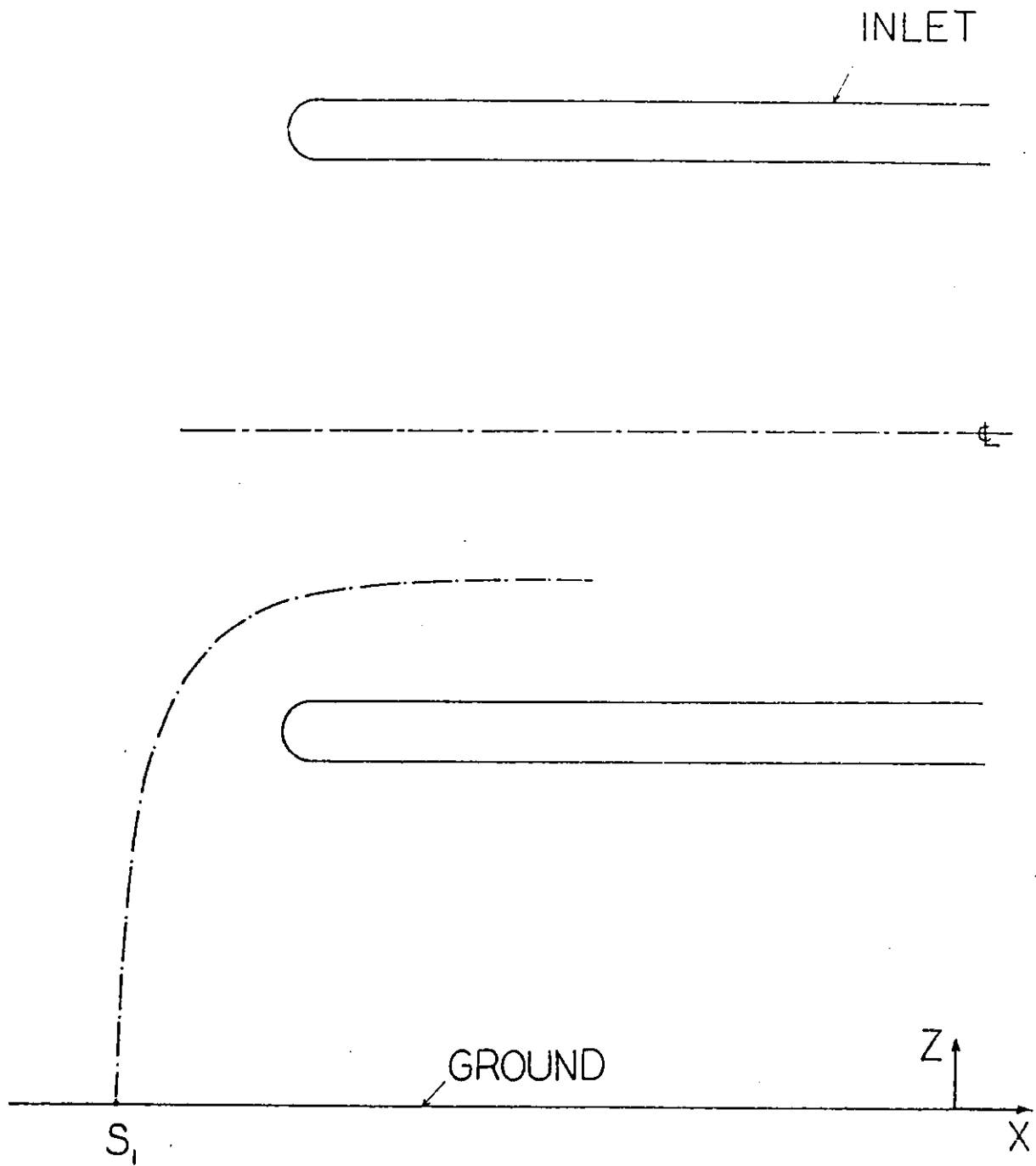
FIGURE 16: Projection of Forward Stagnation Streamline on the x, z
Plane, Case 2
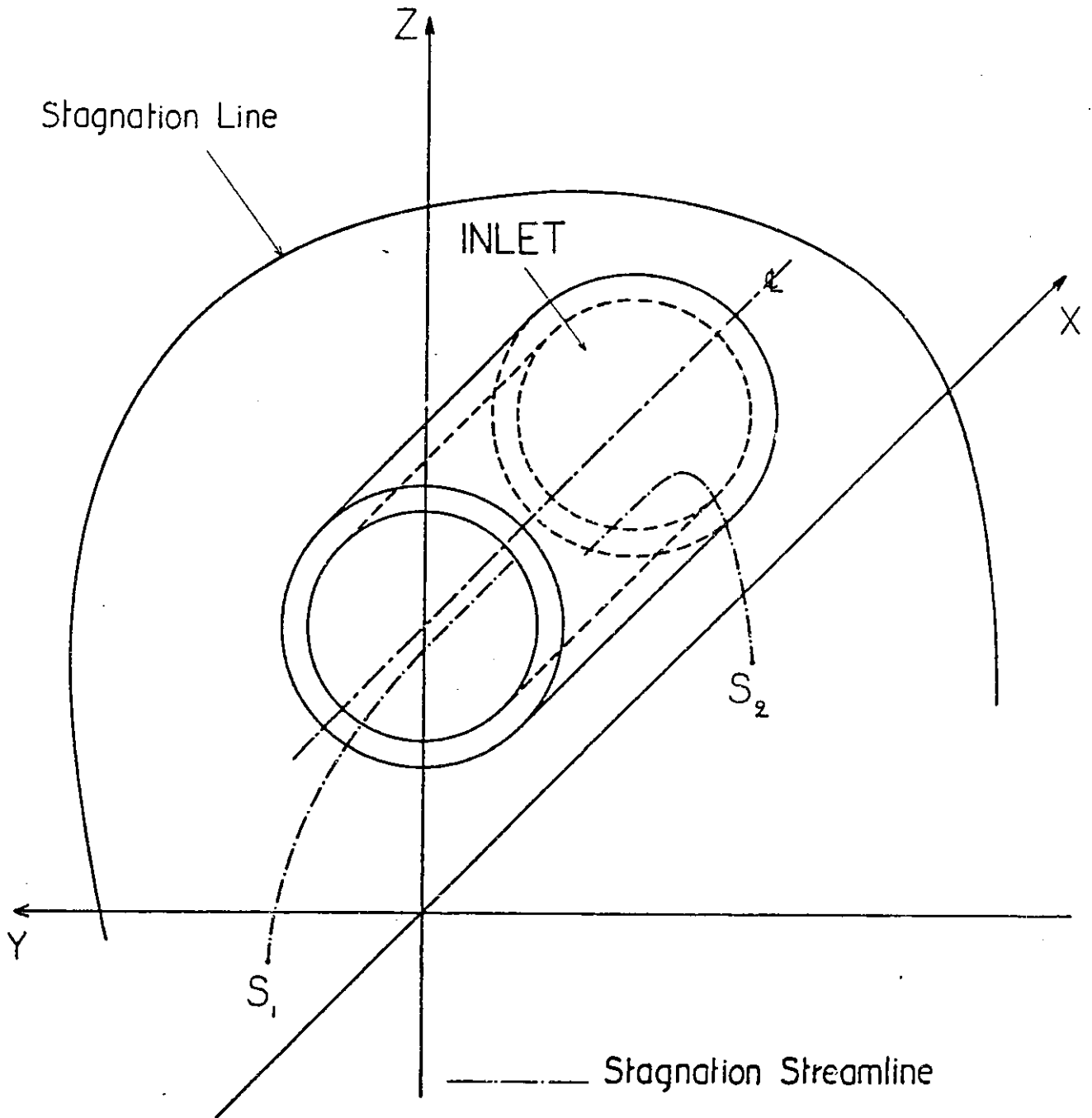
FIGURE 17: Perspective View of Stagnation Locations, Case 2

CAPTURE SURFACE

INLET

S_i

Y

X
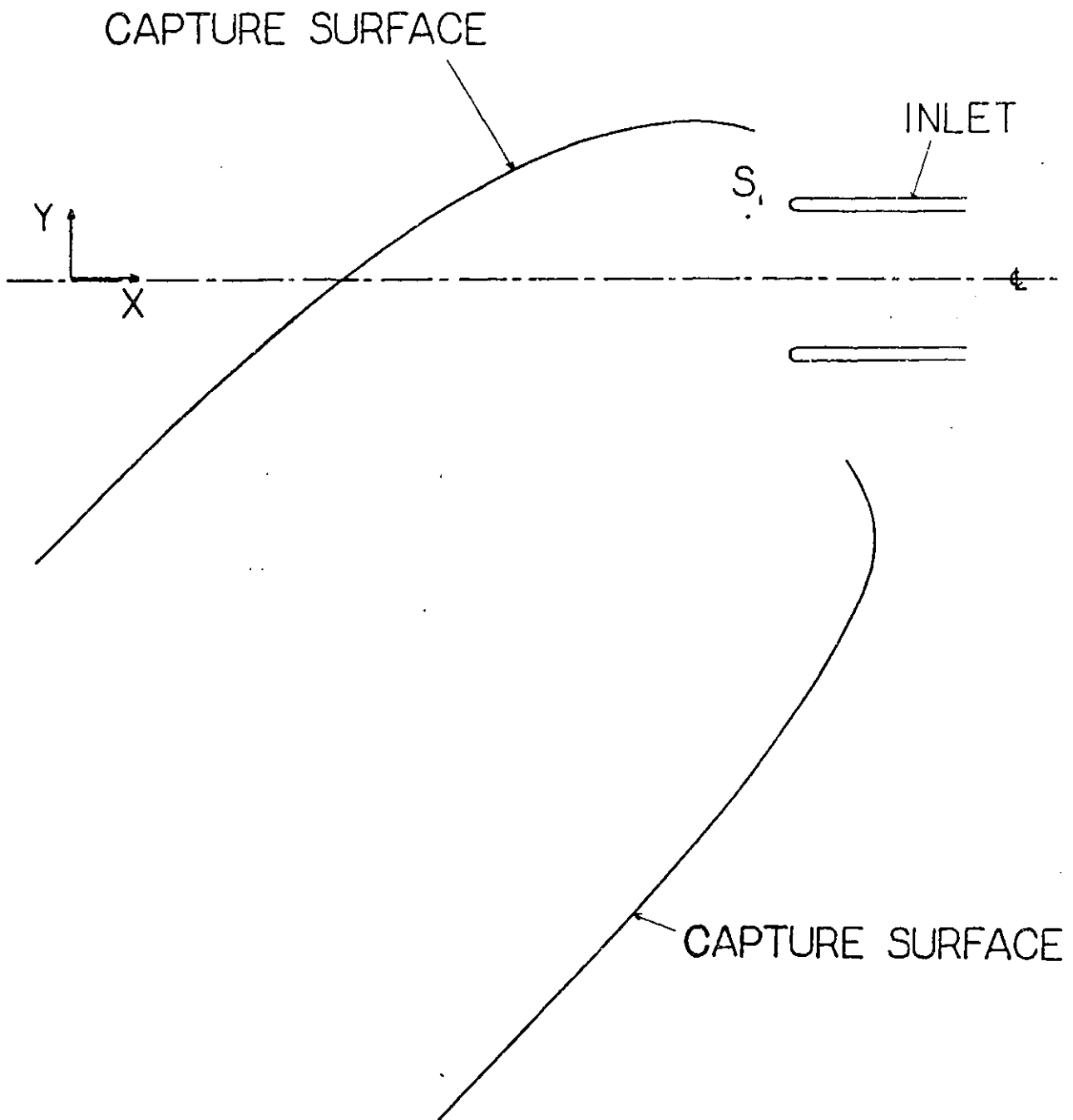
CAPTURE SURFACE

FIGURE 18: Trace of Capture Surface on the x, y Plane, Case 2
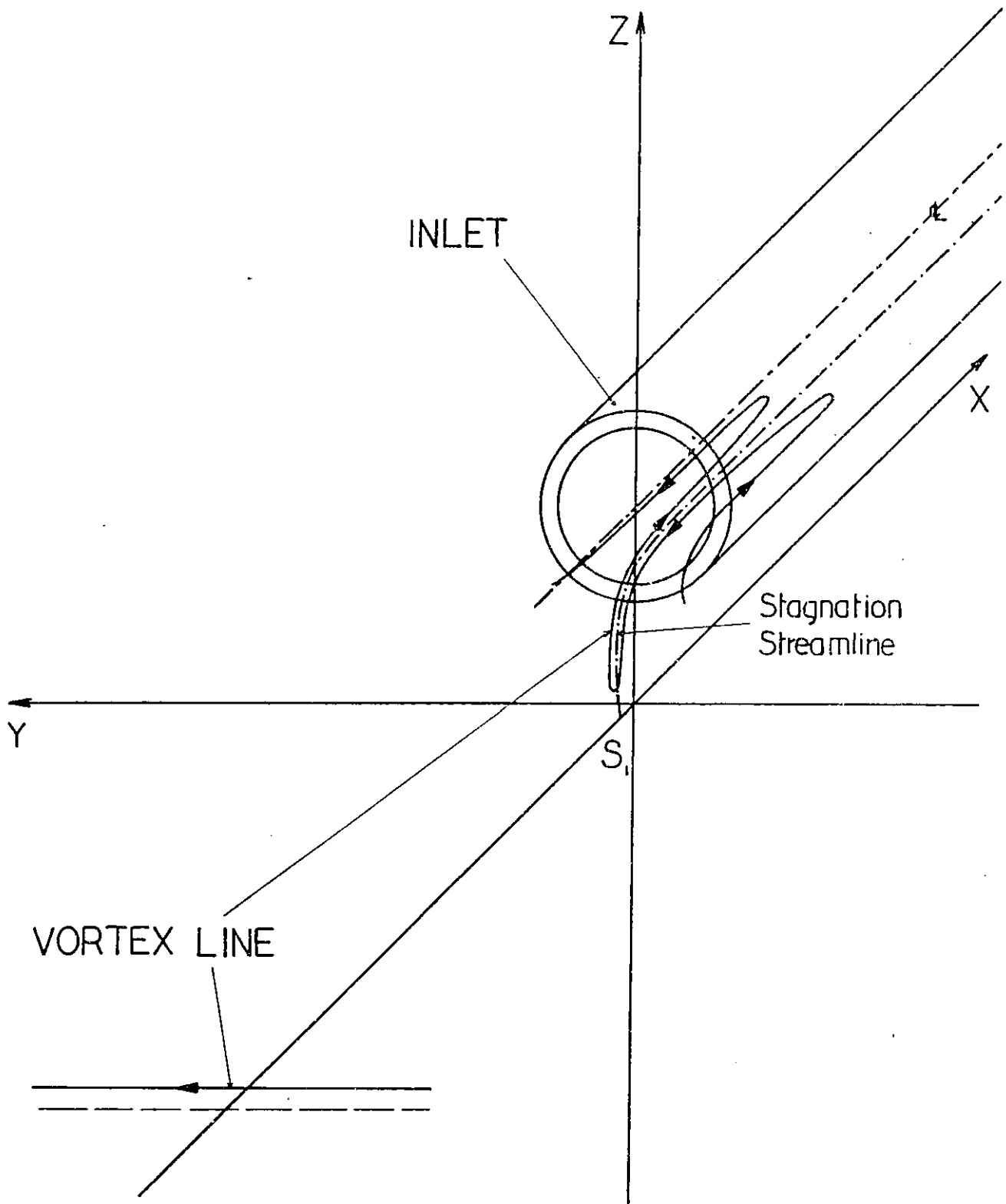
FIGURE 19: Suggested Behavior of a Far Upstream Horizontal Vortex Line,
Case 1

CAPTURE SURFACE

INLET

Stagnation
Streamline

GROUND

Z

X

S_i
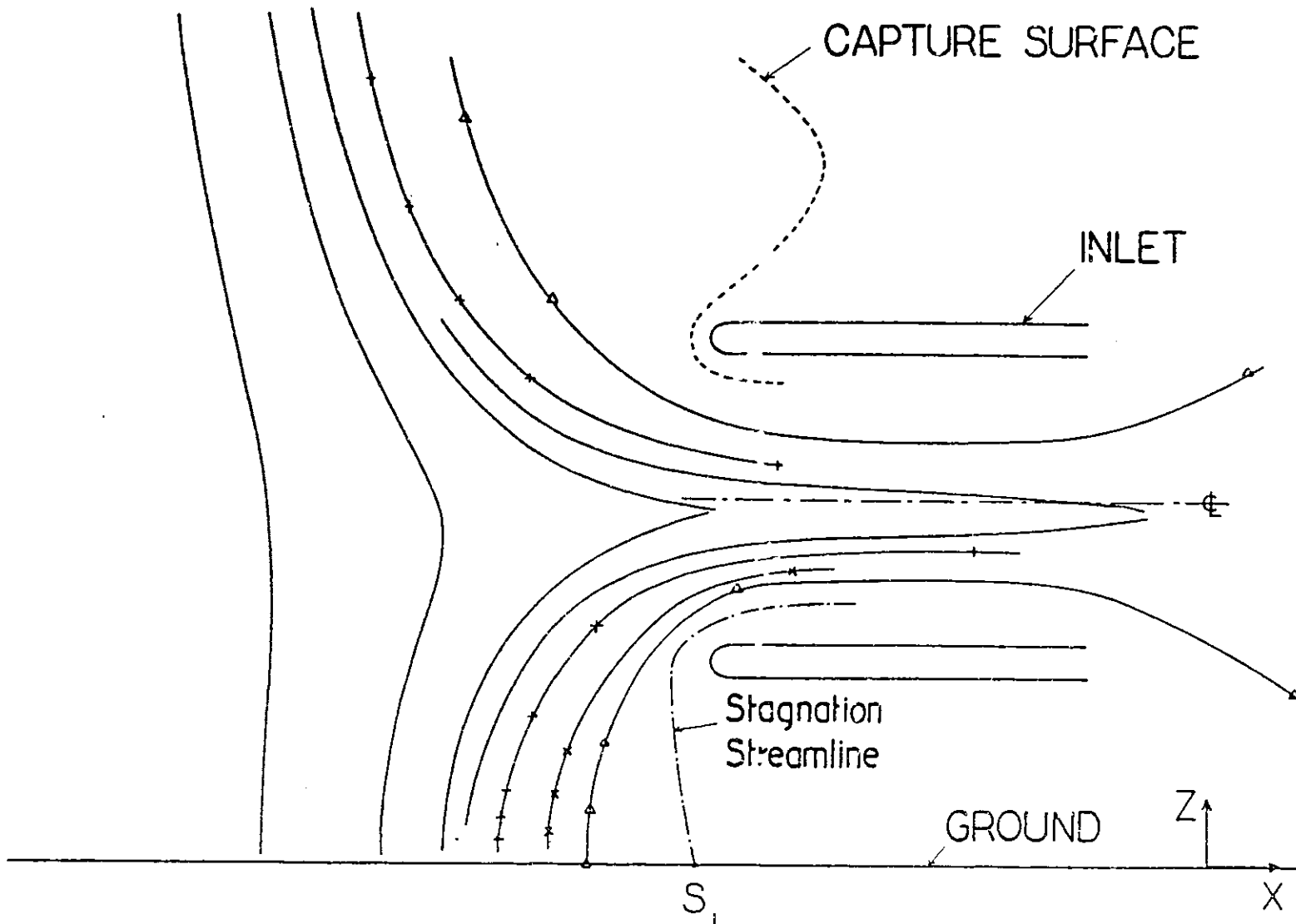
FIGURE 20:   Deformations of a Fluid Line which is Vertical and in the x, z Plane at a Location
Four Inlet Heights Upstream of the Inlet, x, z Plane, Case 1
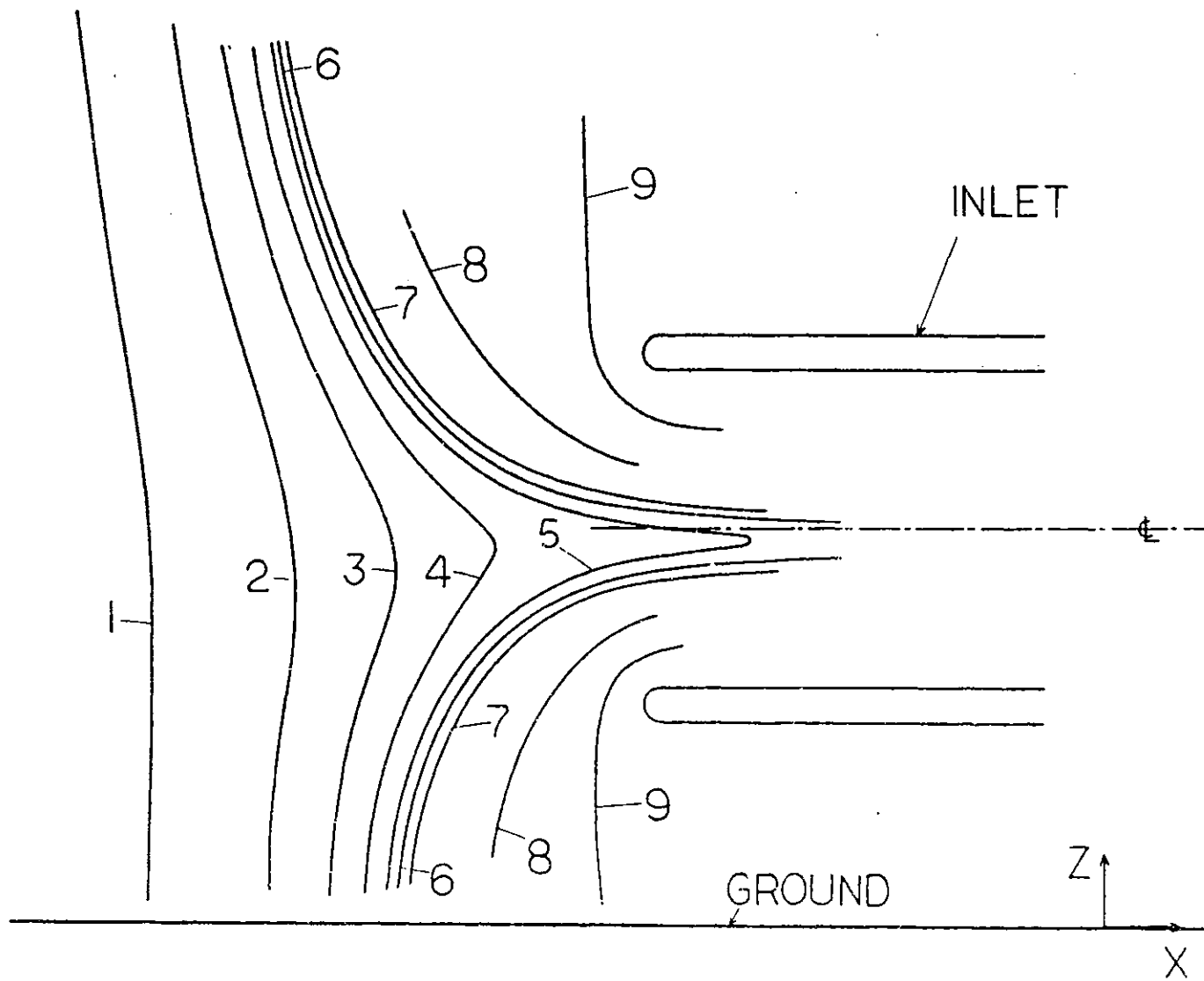
FIGURE 21: Deformations of a Fluid Line which is Vertical and 0.6 Inlet Heights from the x, z Plane at a Location Four Inlet Heights Upstream of the Inlet, Projections on the x, z Plane, Case 1
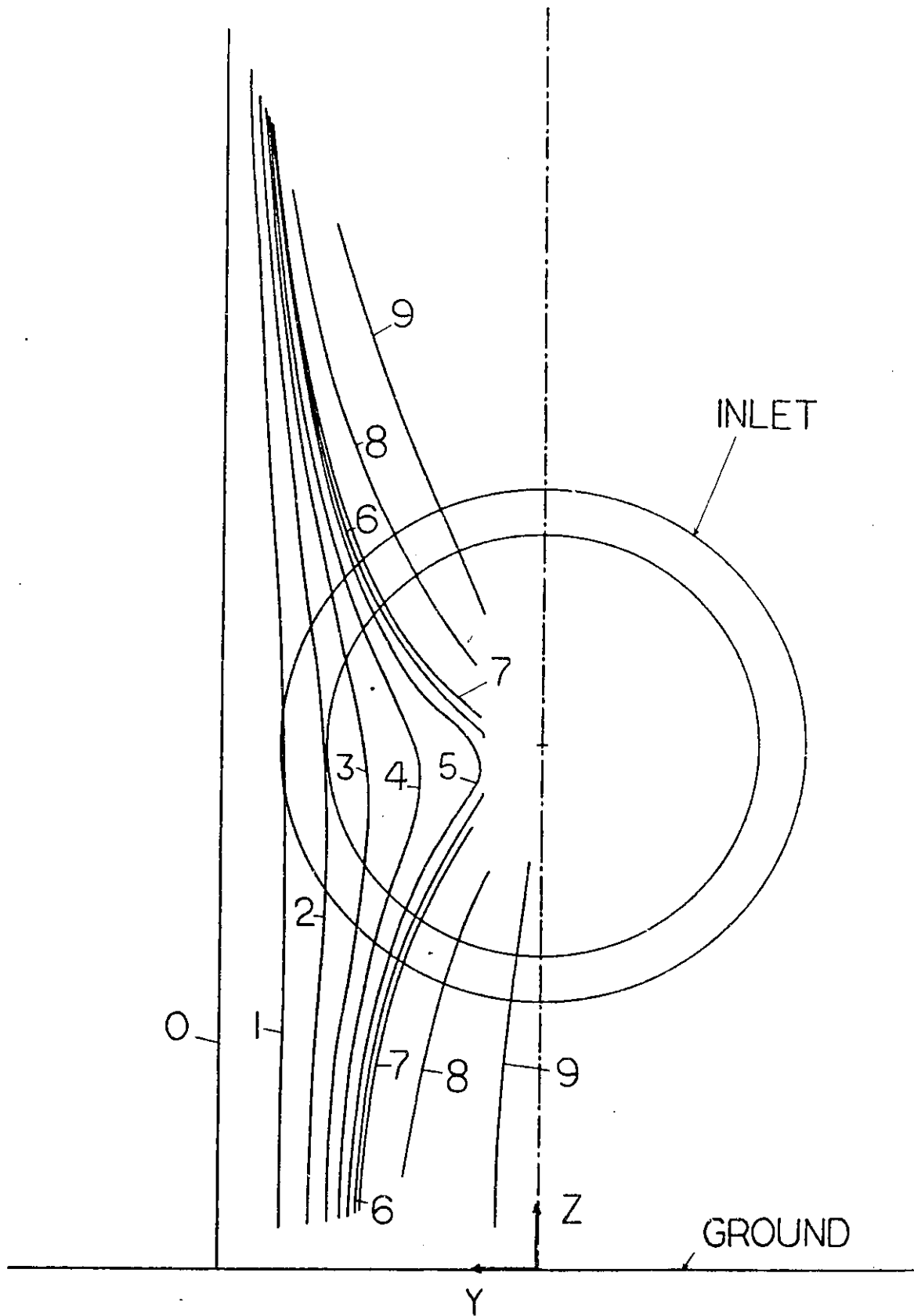
FIGURE 22: Projections of the Material Lines Shown in Figure 21 on the y, z Plane
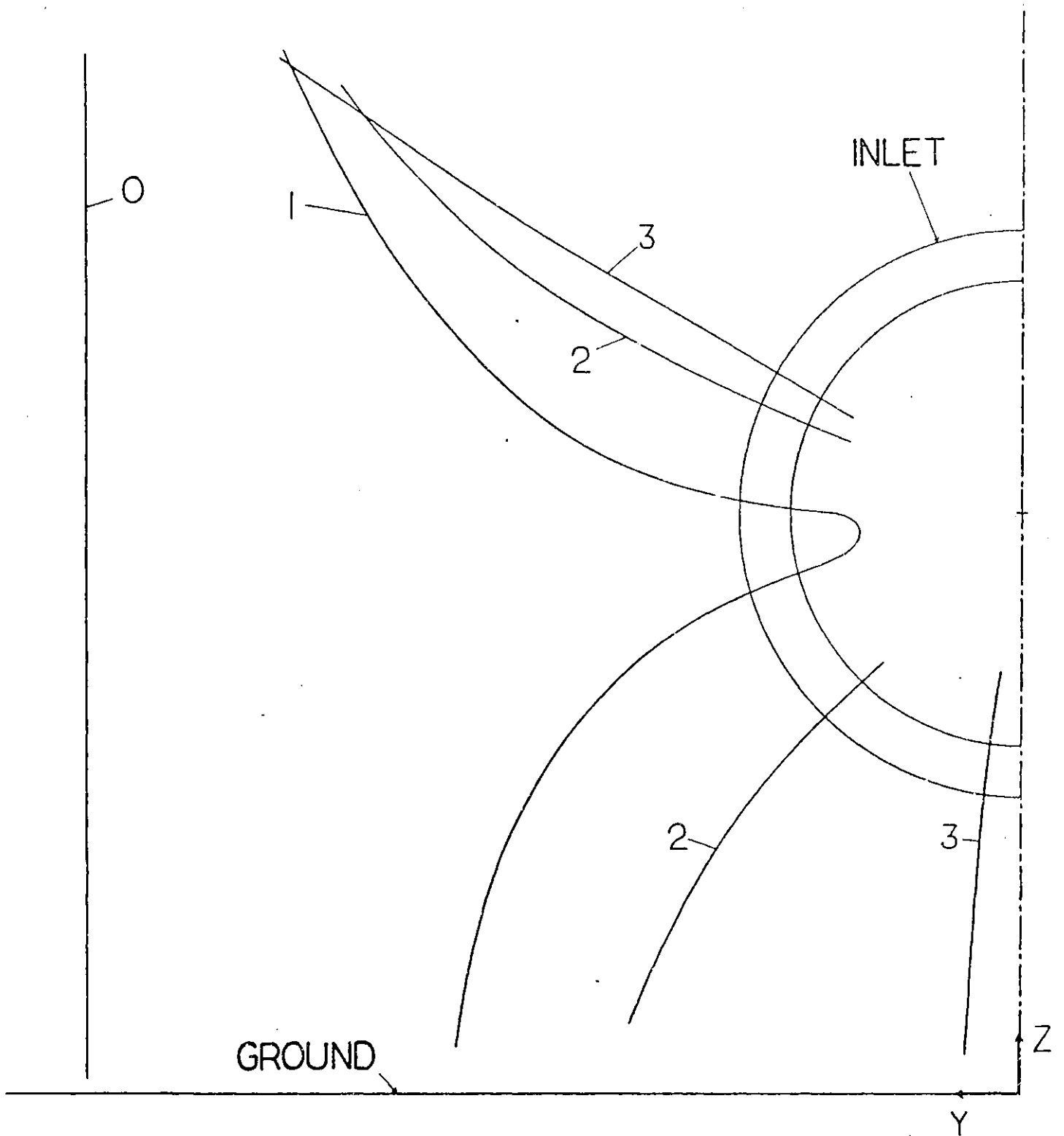
FIGURE 23: Deformations of a Fluid Line which is Vertical and 1.6 Inlet Heights from the x, z Plane at a Location Four Inlet Heights Upstream of the Inlet, Projections on the y, z Plane, Case 1
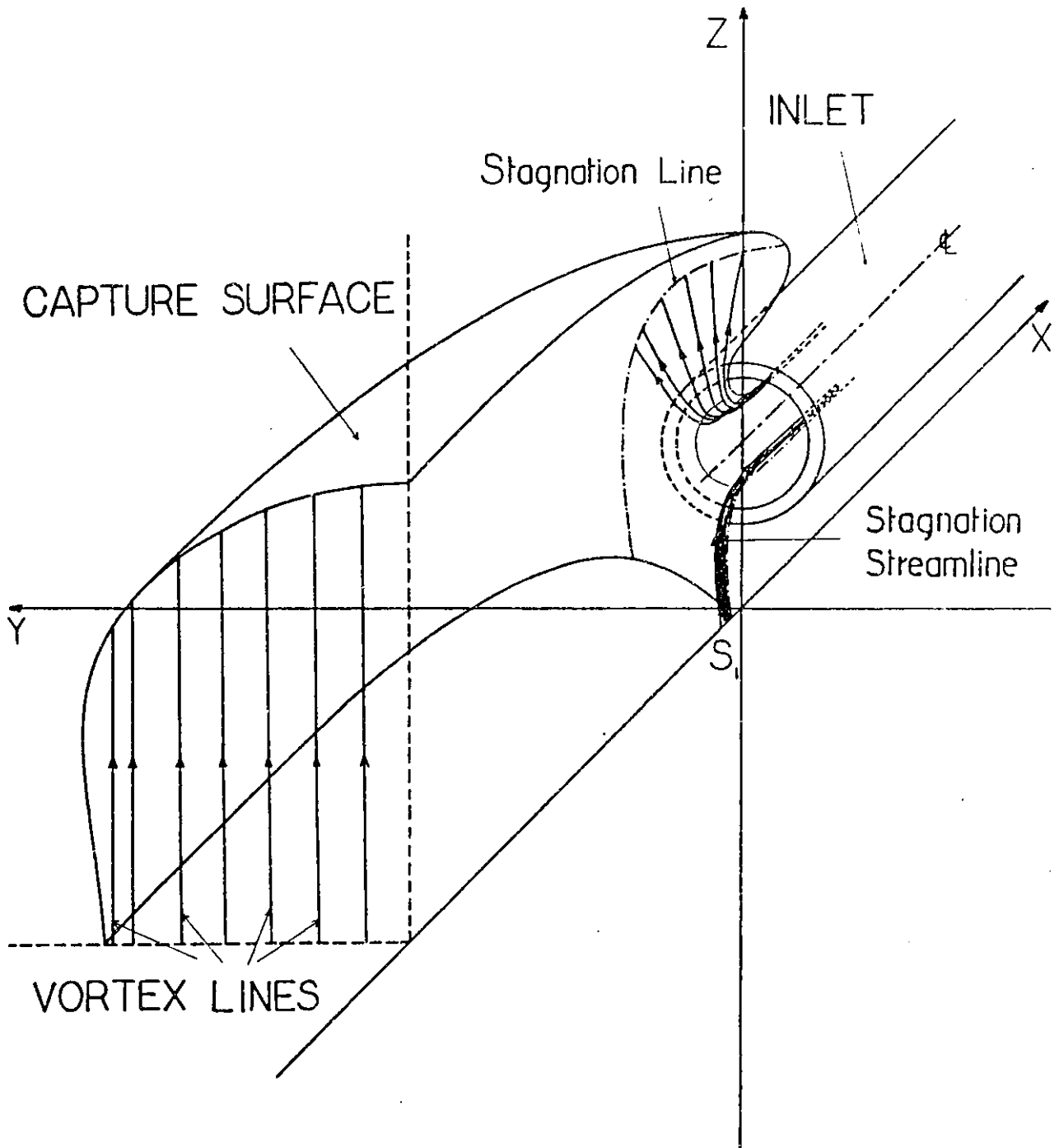
FIGURE 24: Suggested Deformation of a Far Upstream Uniform Distribution of Vertical Vortex Lines, Case 1
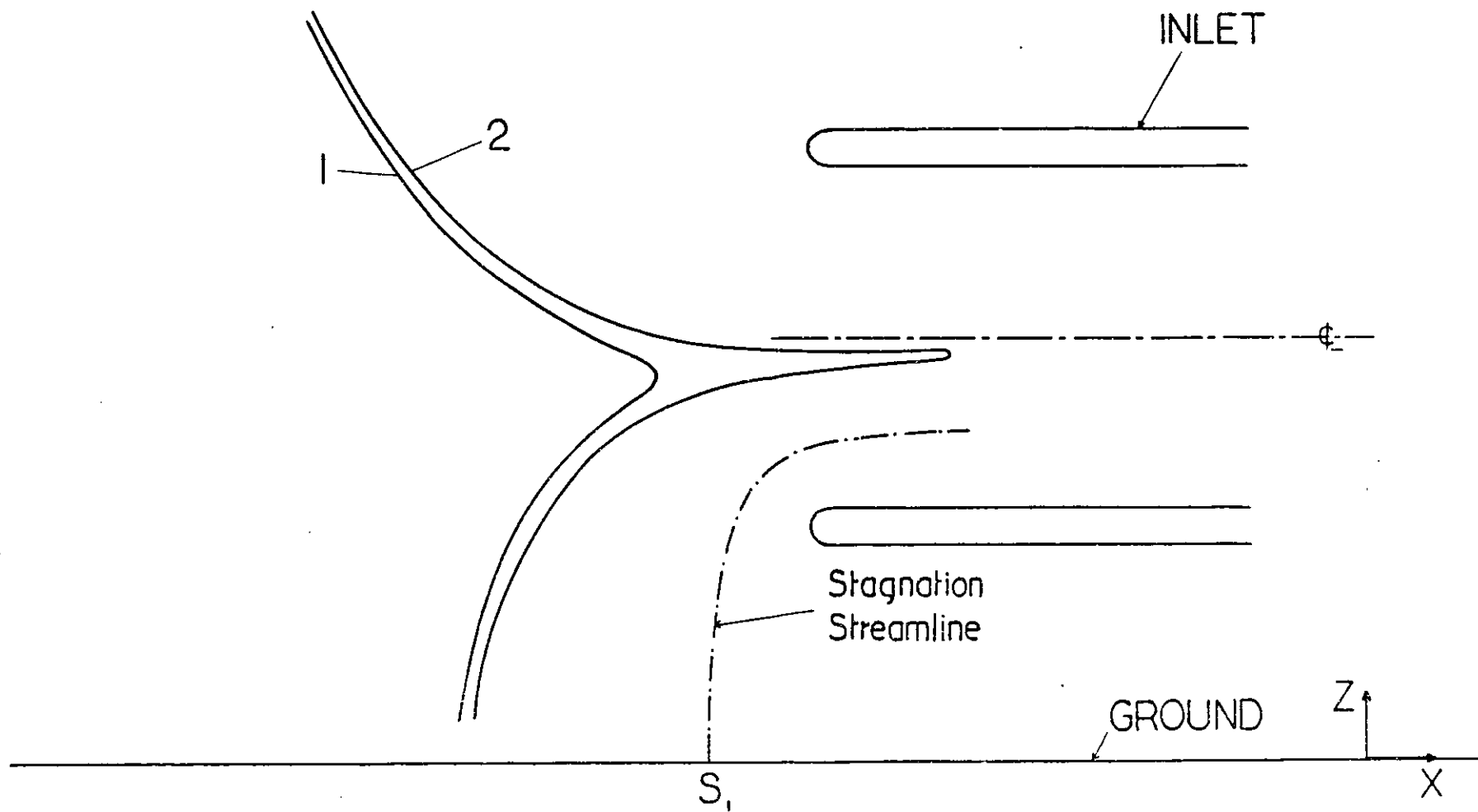
FIGURE 25: Deformations of a Far Upstream Vertical Material Line, Projections on the x, z Plane, Case 2
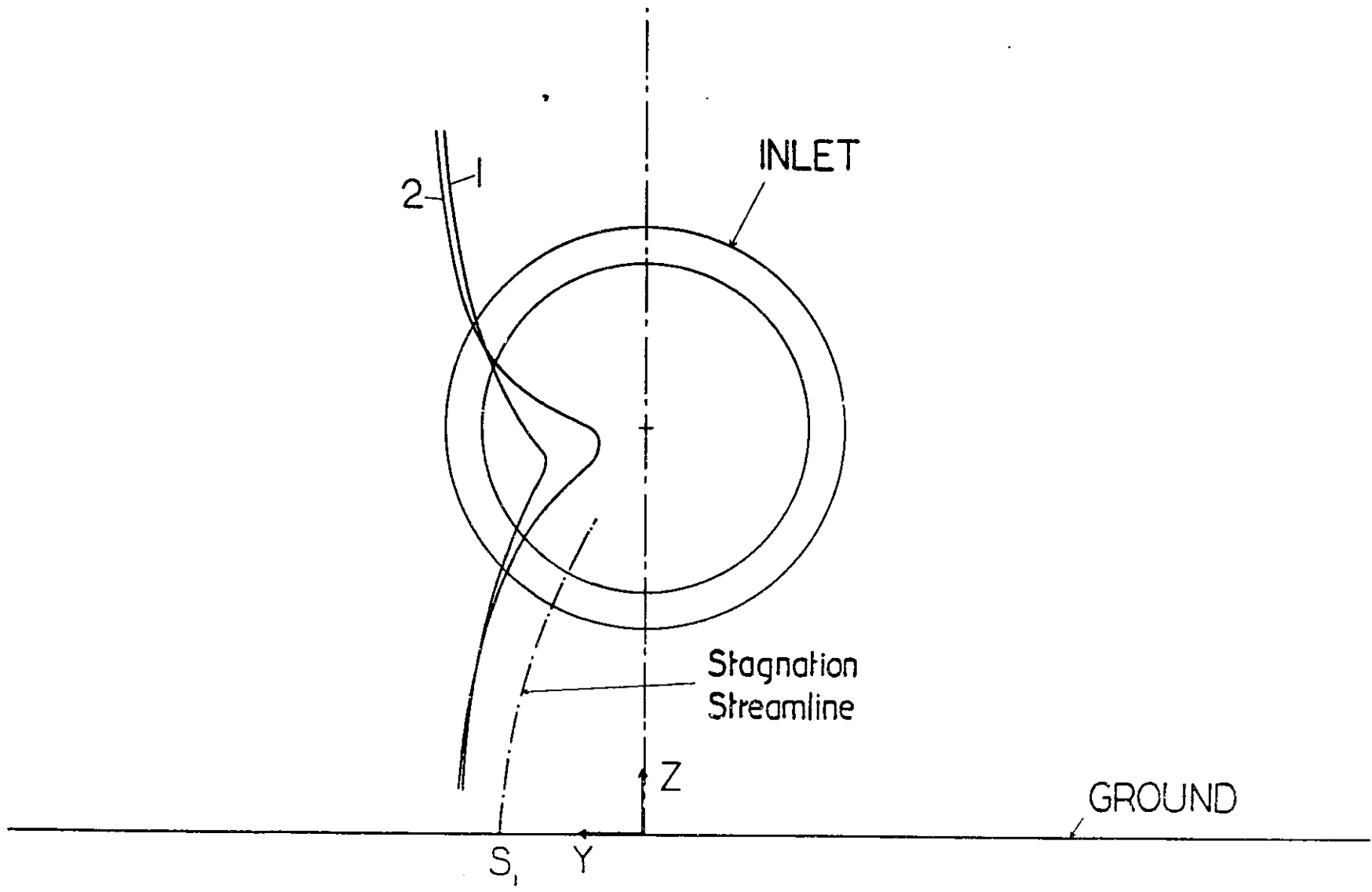
FIGURE 26: Projections of the Material Lines Shown in Figure 25 on the y, z Plane
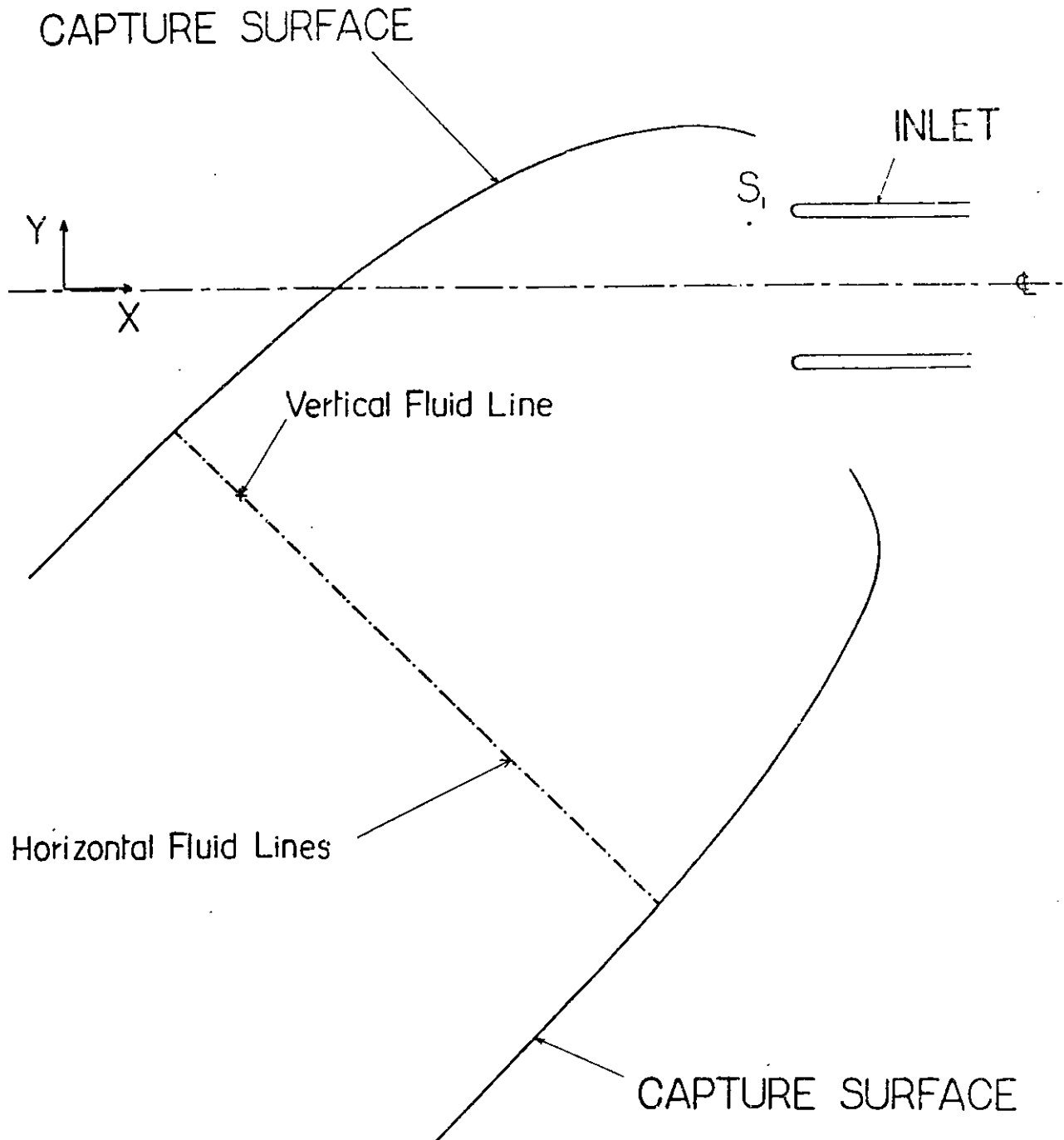
FIGURE 27: "Far Upstream" Location of the Vertical Fluid Line Tracked
in Figures 25 and 26, Common "Far Upstream" Projection of
the Horizontal Material Lines Tracked in Figures 28 through
33, x, y Plane, Case 2
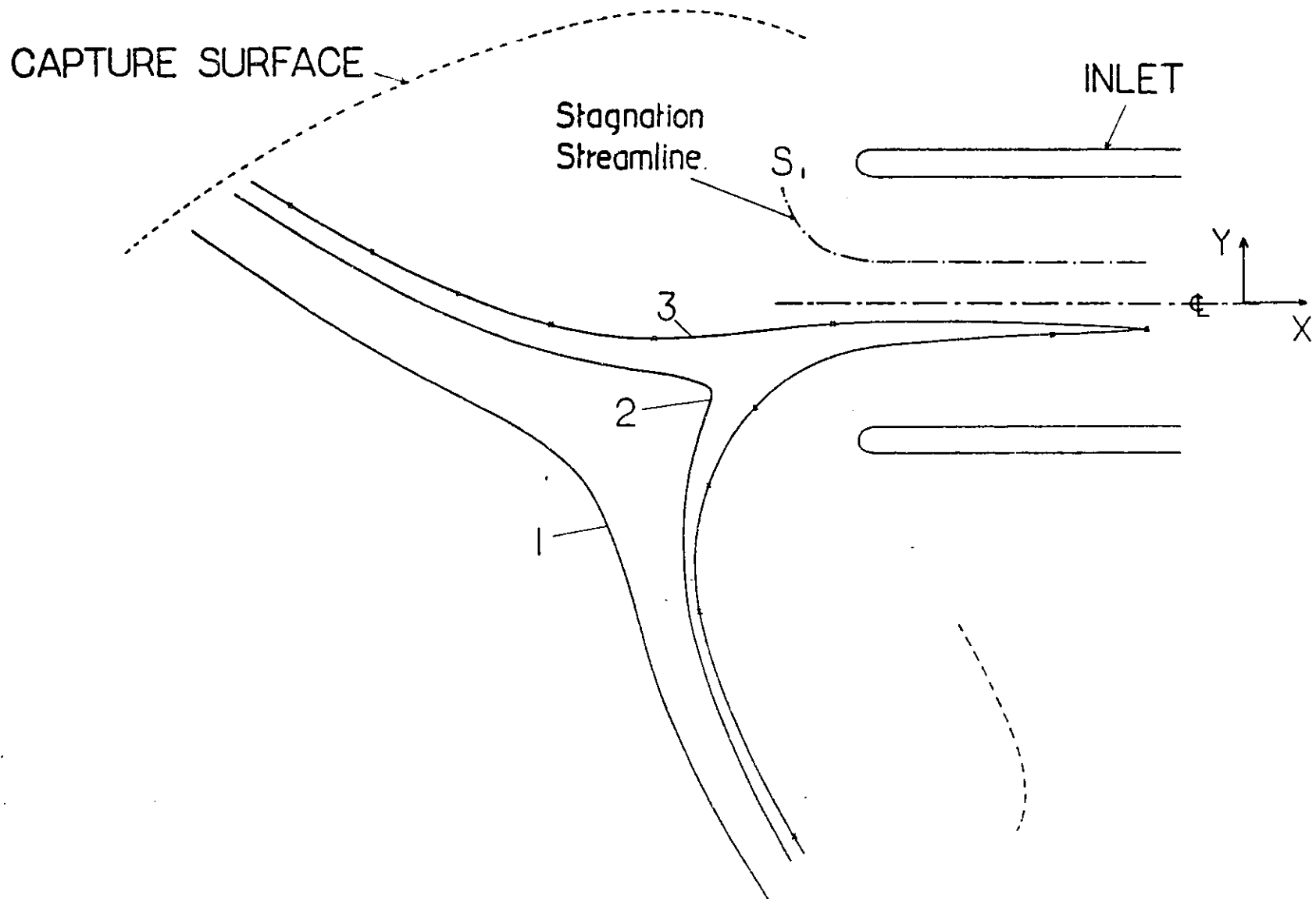
FIGURE 28: Deformations of a Fluid Line which is Initially Horizontal and 0.8 Inlet Heights from the Ground Plane, Projections on the x, y Plane, Case 2
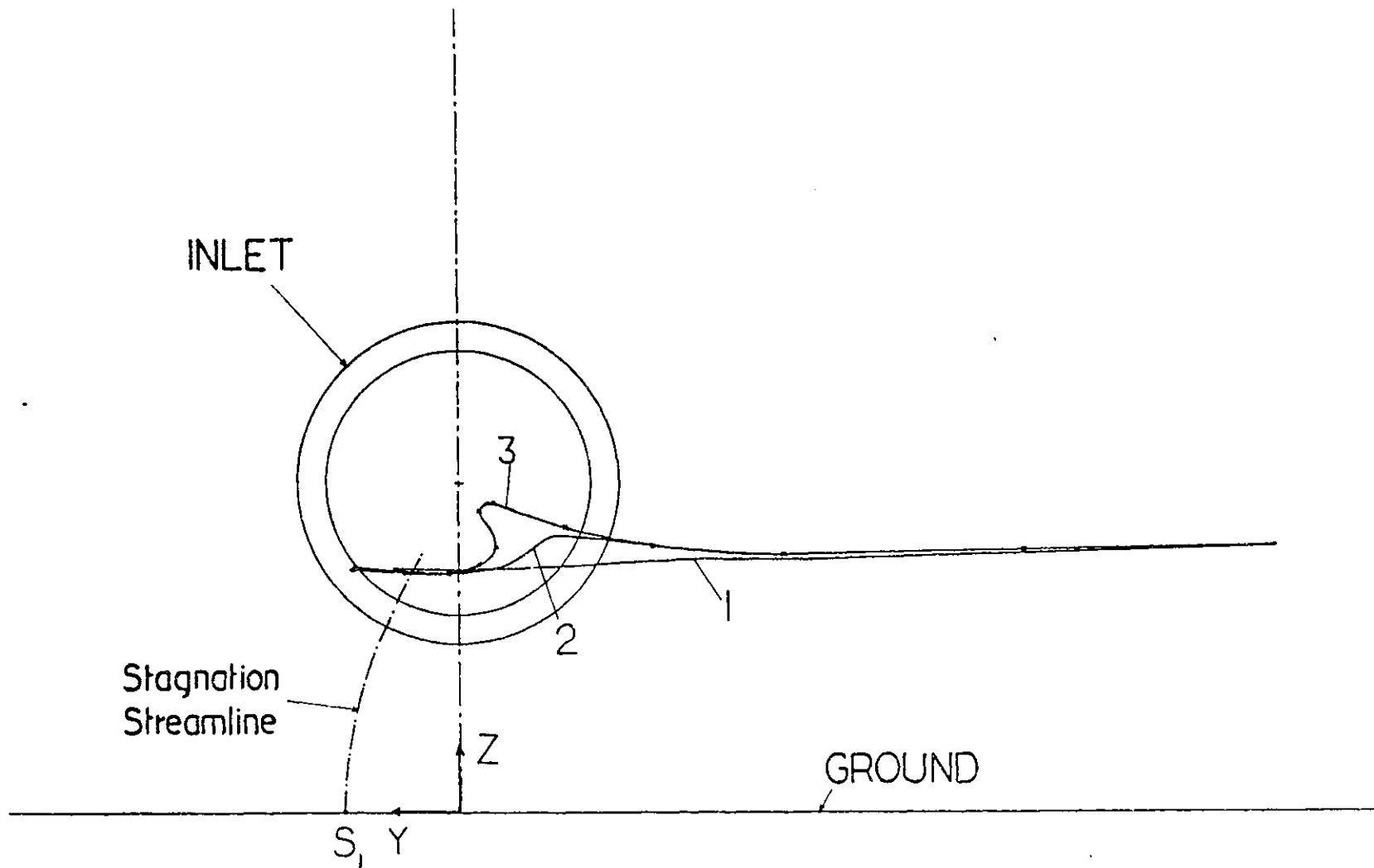
FIGURE 29: Projections of the Material Lines Shown in Figure 28 on the y, z Plane

CAPTURE SURFACE

Stagnation Streamline

S_1

5

4

3

2

1

3

5

4

INLET

Y

X

¢
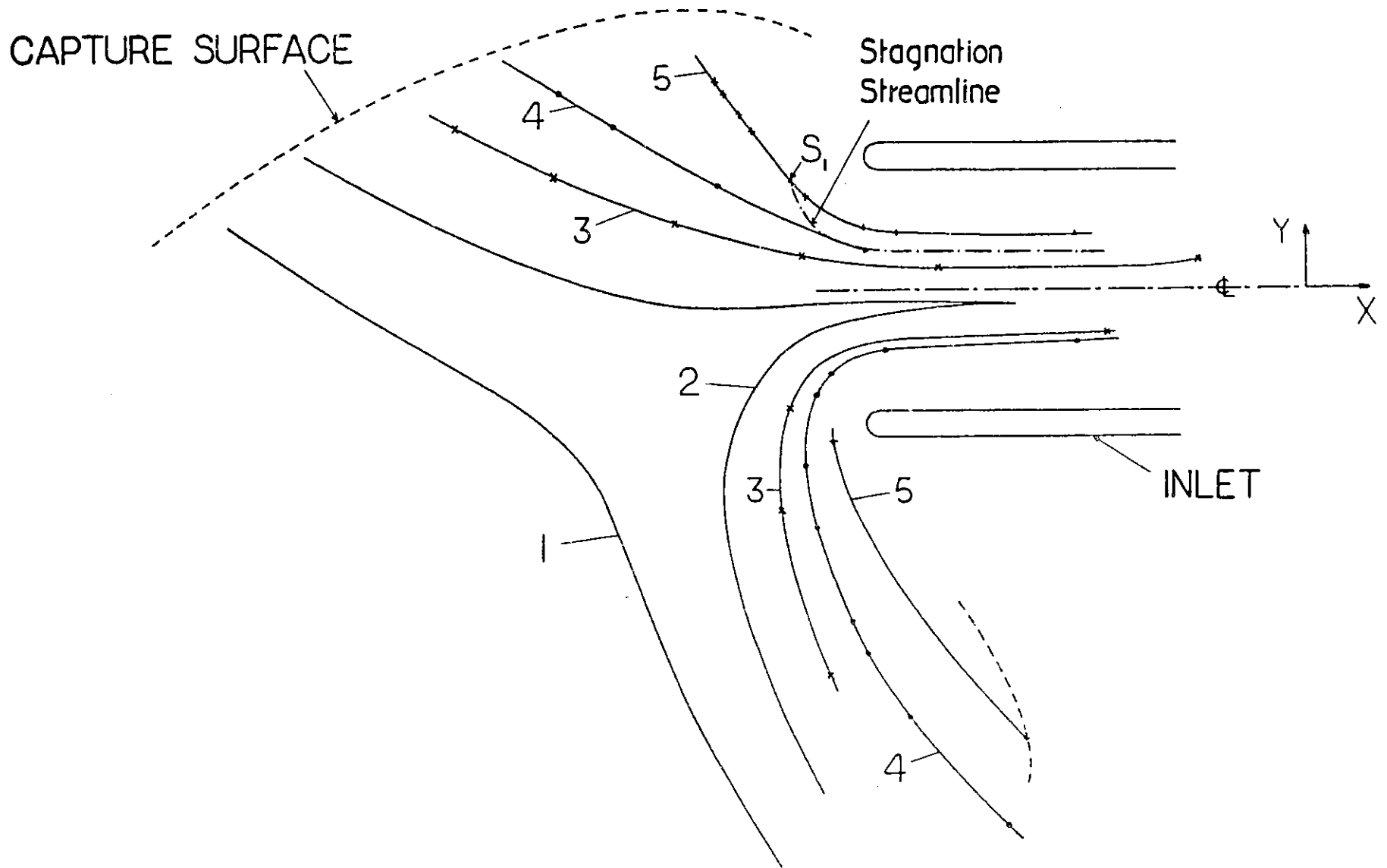
FIGURE 30: Deformations of a Fluid Line which is Initially Horizontal and 0.4 Inlet Heights from the Ground Plane, Projections on the x, y Plane, Case 2
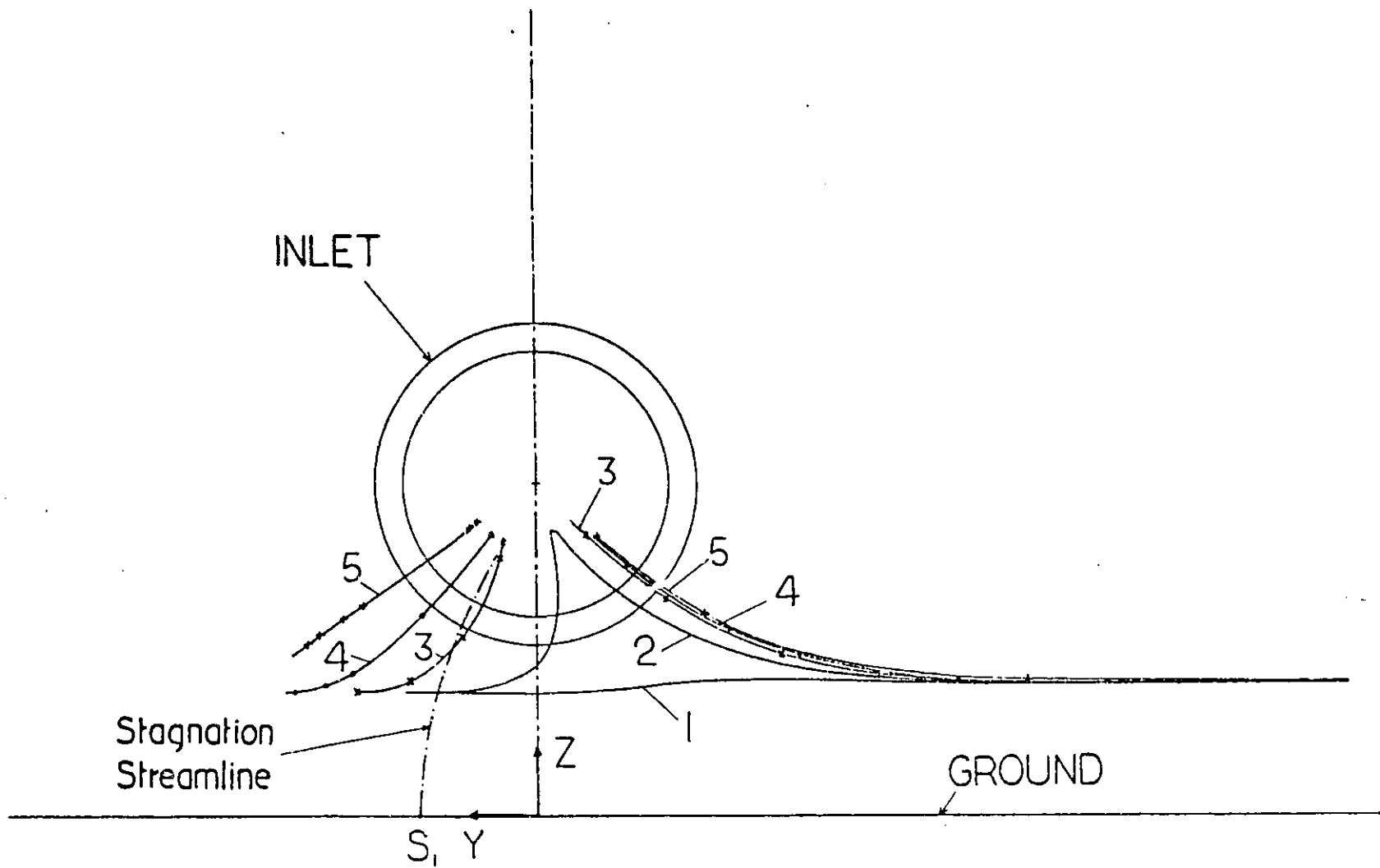
FIGURE 31: Projections of the Material Lines Shown in Figure 30 on the y, z Plane

CAPTURE SURFACE

Stagnation
Streamline

5

S₁

4

3

2

1

5

Y

X

¢
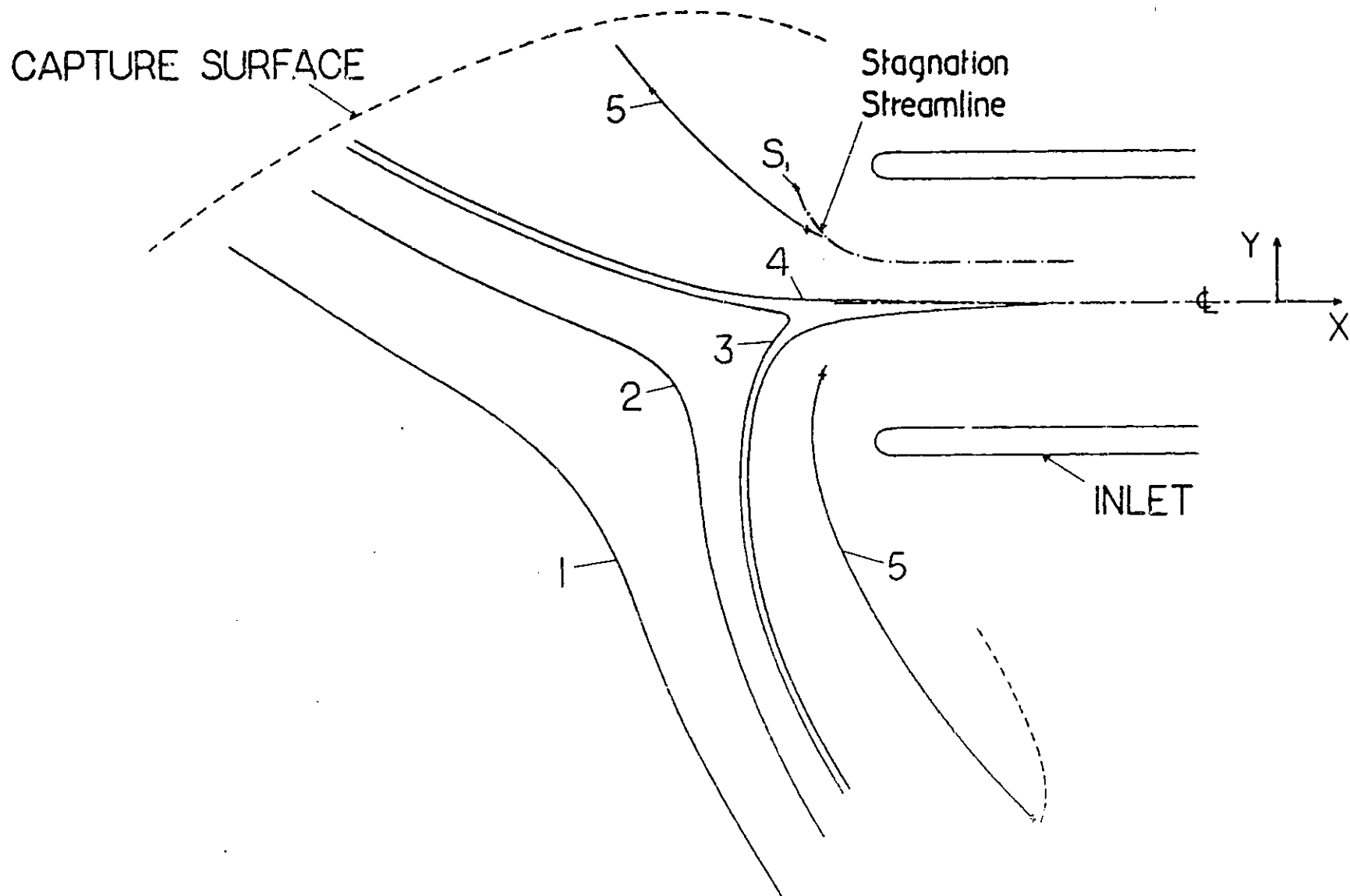
INLET

FIGURE 32:   Deformations of a Fluid Line which is Initially Horizontal and 0.16 Inlet Heights
from the Ground Plane, Projections on the x, y Plane, Case 2
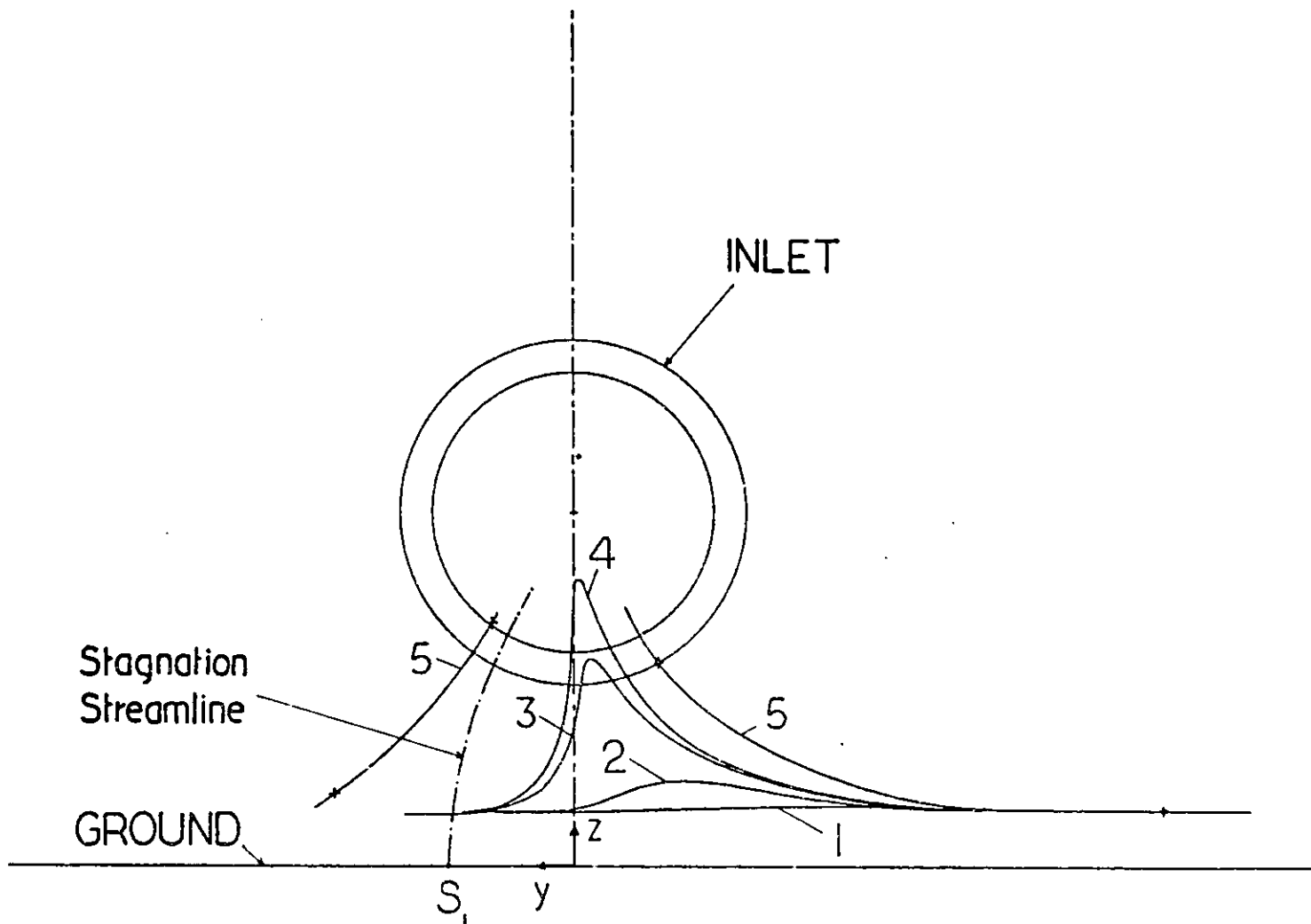
FIGURE 33: Projections of the Material Lines Shown in Figure 32 on the y, z Plane
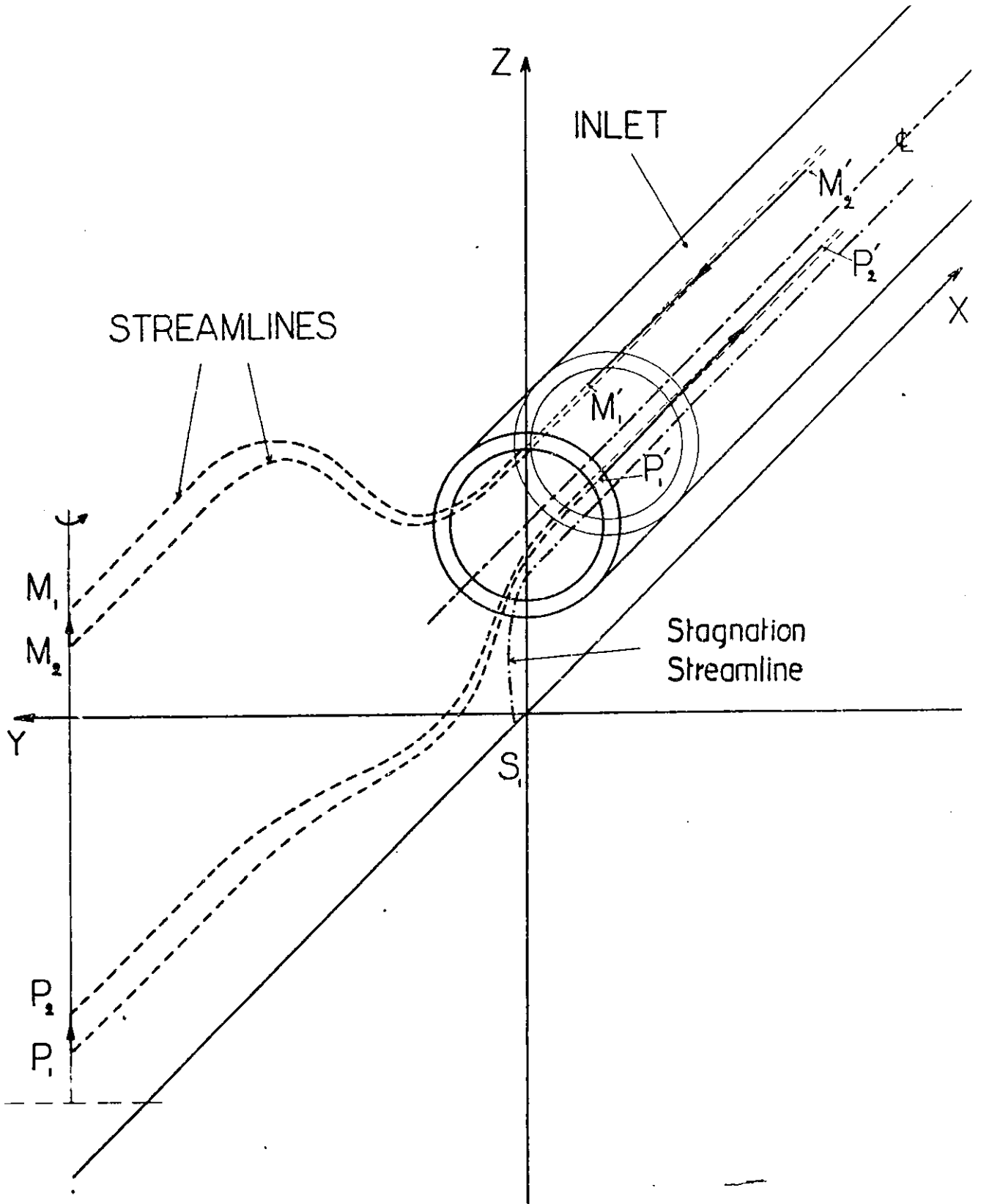
FIGURE 34: Behavior of Fluid Lines Connecting Neighbouring Particles

CAPTURE SURFACE

GRID

INLET

GROUND
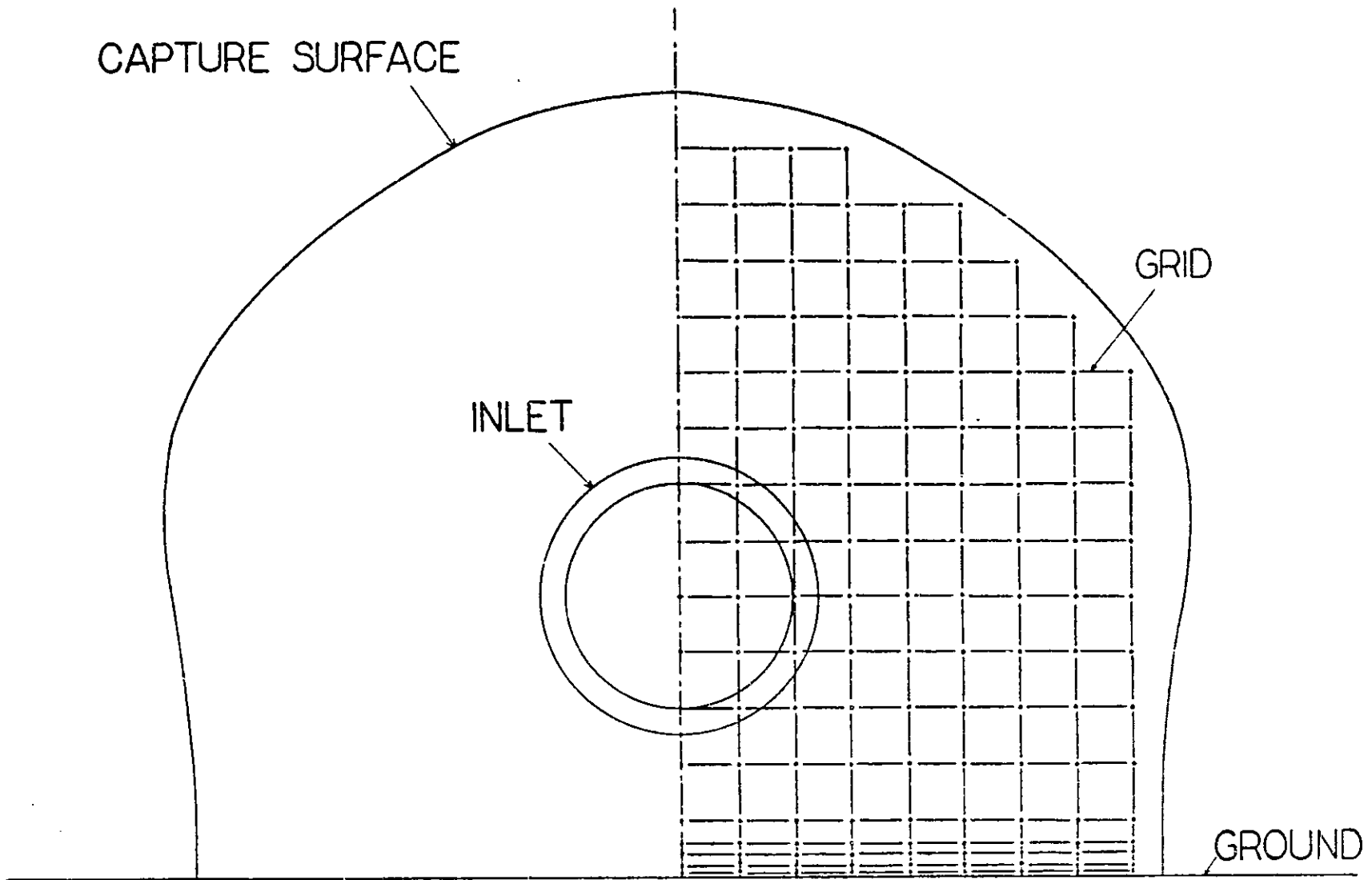
FIGURE 35: Front View of Grid Tracked at a "Far Upstream" Location, Case 1

GRID

Inlet Internal
Surface

S
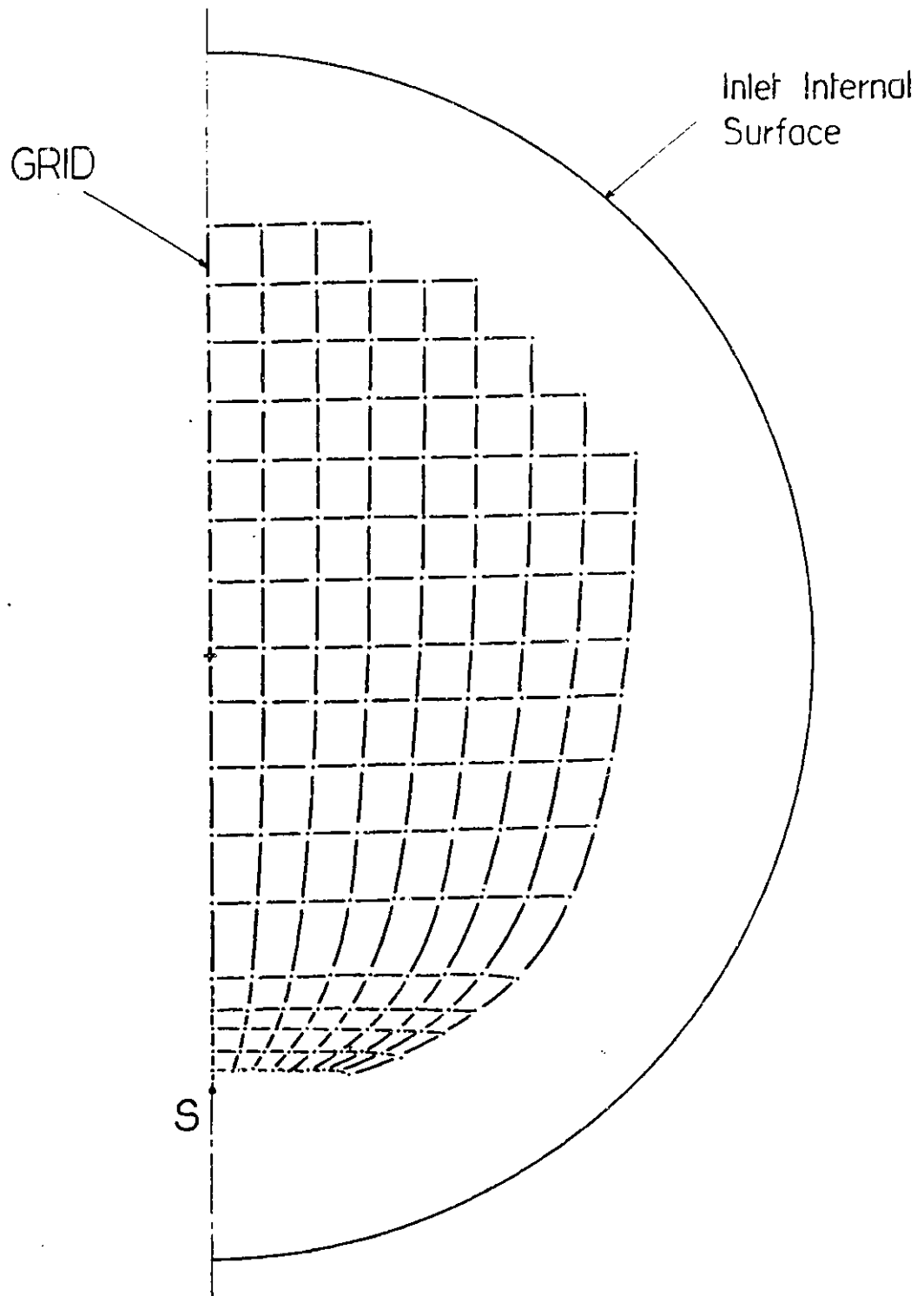
FIGURE 36: Deformation of Grid Shown in Figure 35 at "Engine Face"
Location, Projection on the y, z Plane
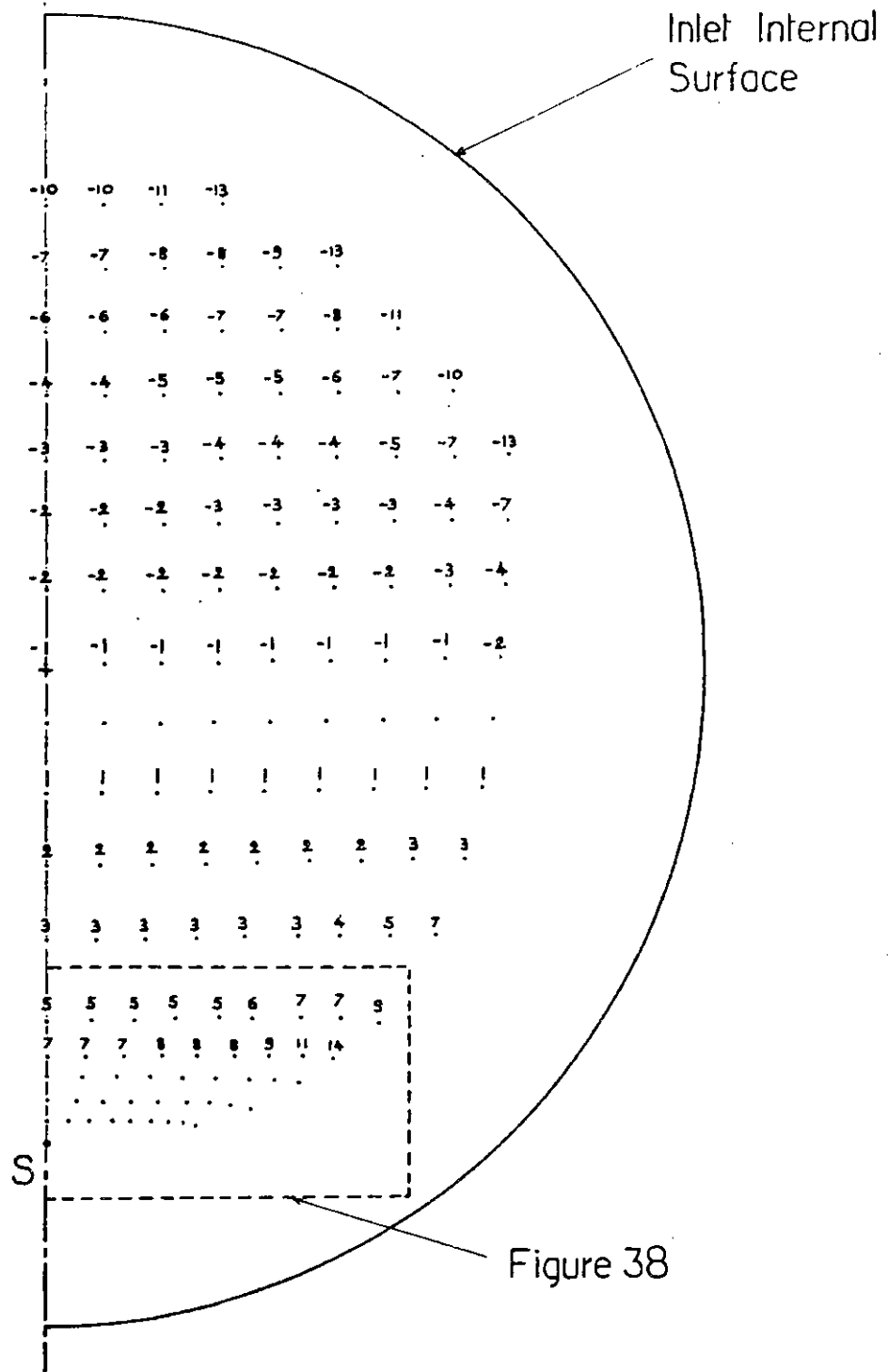
FIGURE 37: Vorticity Distribution at the Engine Face Location Due to
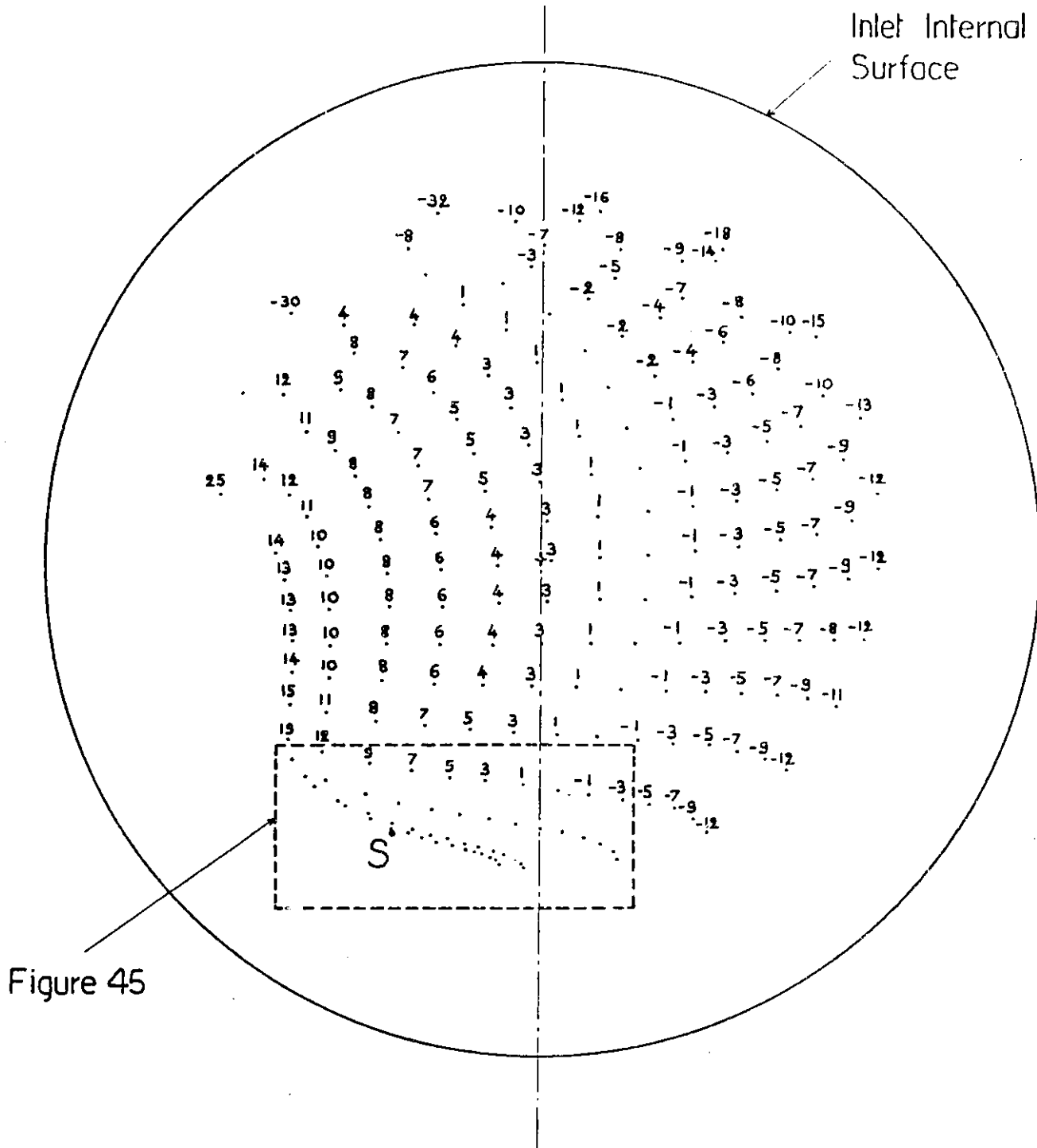a Far Upstream Distribution of Vertical Vorticity, Case 1
(See Key Table 1 p 99)
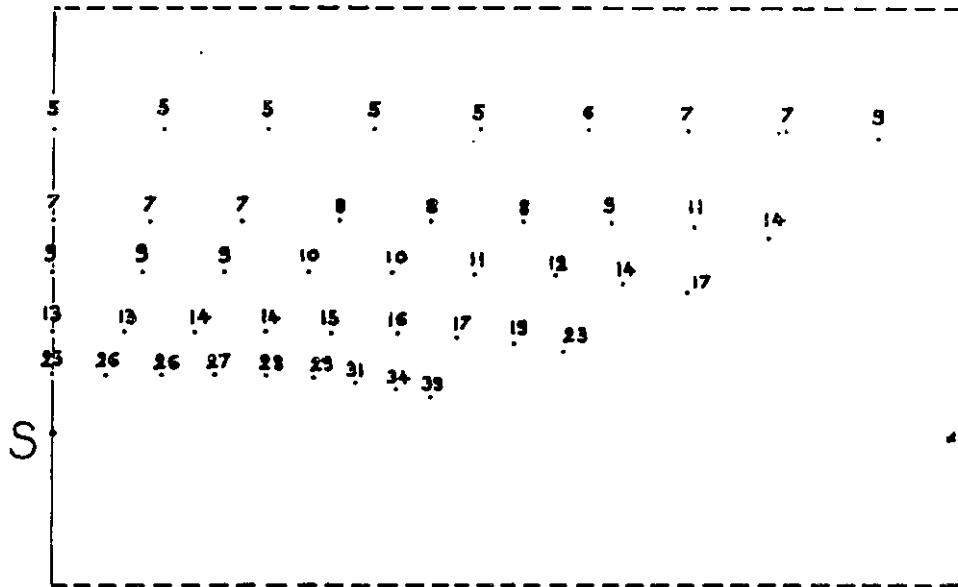
FIGURE 38: Enlarged View of a Portion of Figure 37 (See Key Table 1
p 99)
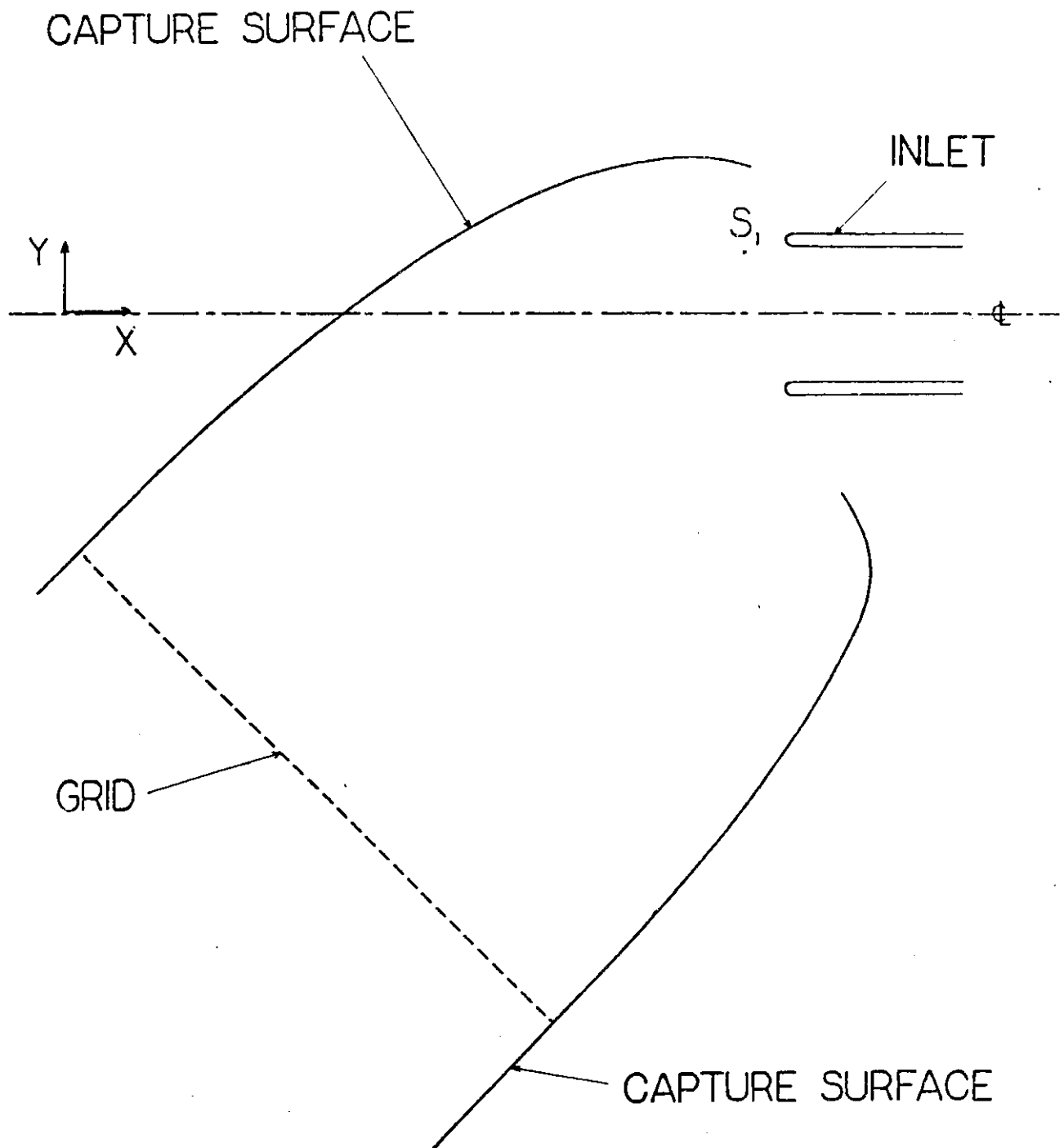
FIGURE 39:   Initial (Far Upstream) Location of Grid Tracked, Projection
on the Ground Plane, Case 2
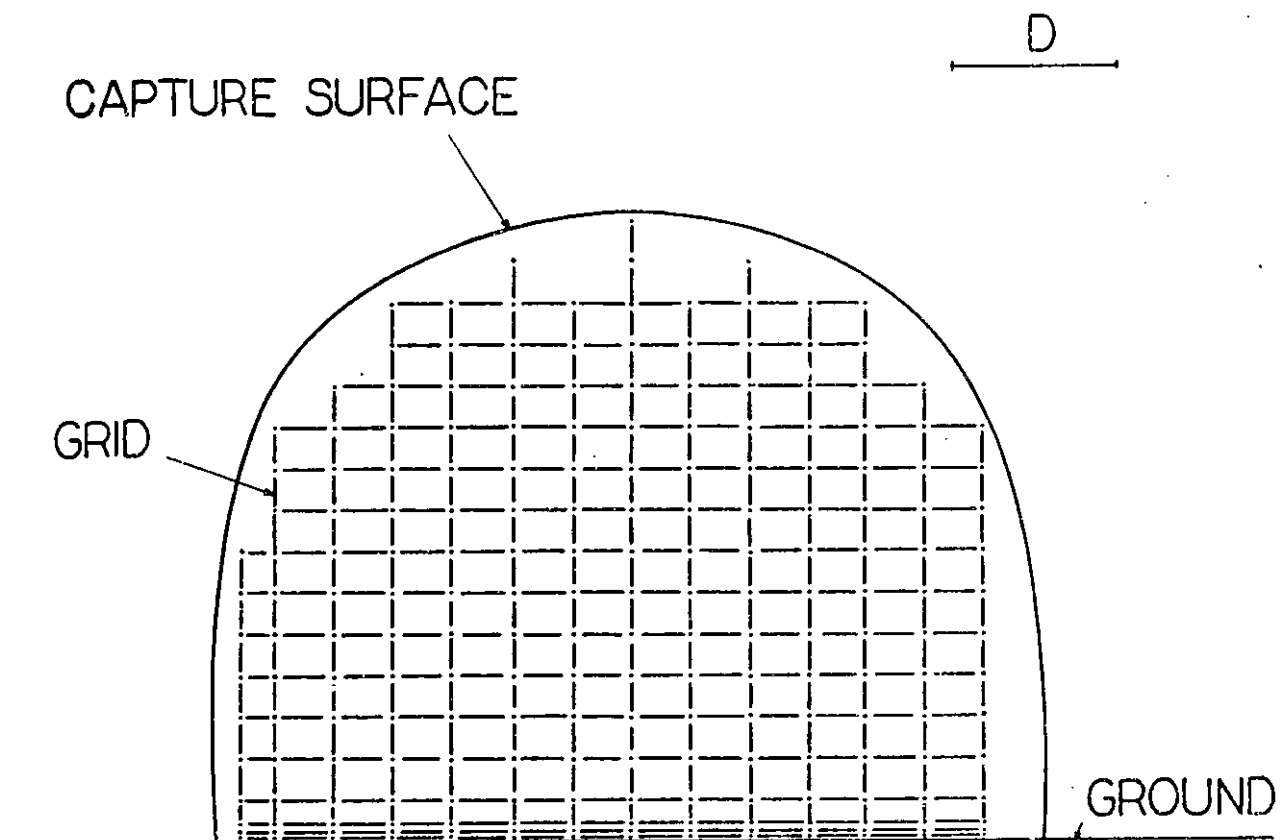
FIGURE 40: Front View of Grid Tracked at a "Far Upstream" Location,
            Case 2
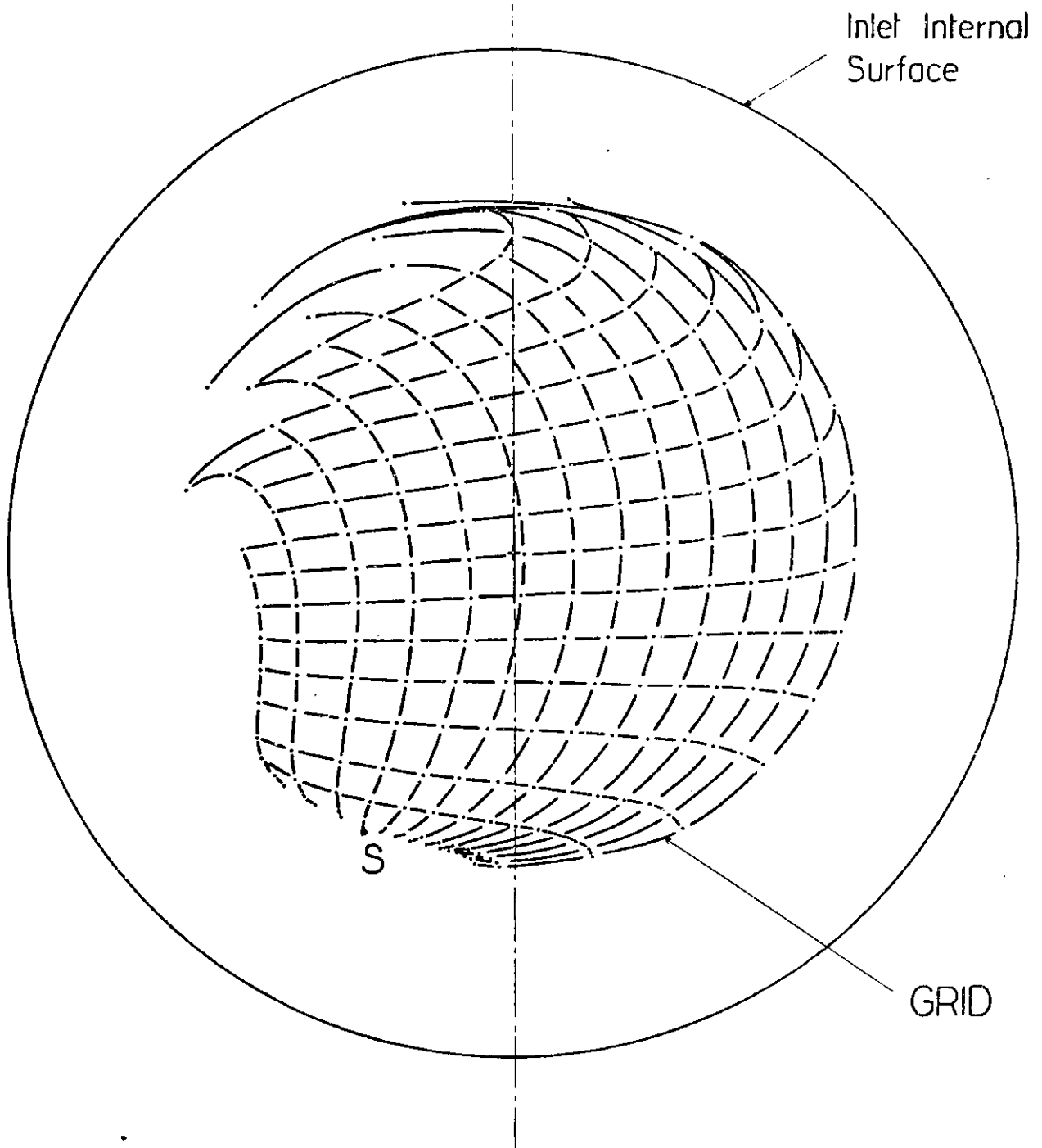
FIGURE 41:   Deformation of Grid Shown in Figure 40 at "Engine Face"
Location, Projection on the y, z Plane
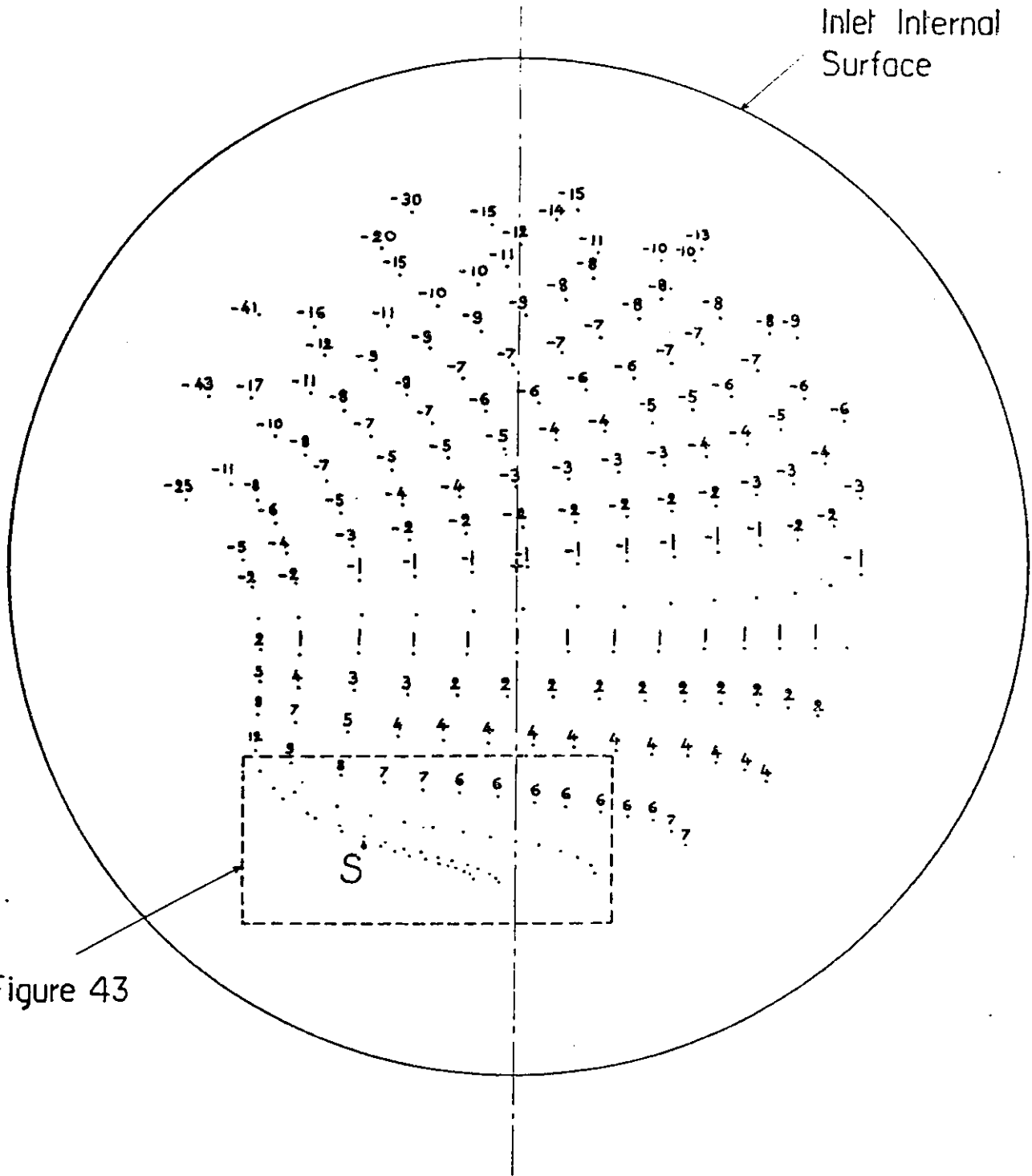
FIGURE 42: Vorticity Distribution at the Engine Face Location Due to a Far Upstream Distribution of Vertical Vorticity, Case 2 (See Key Table 1 p 99)

O.ID

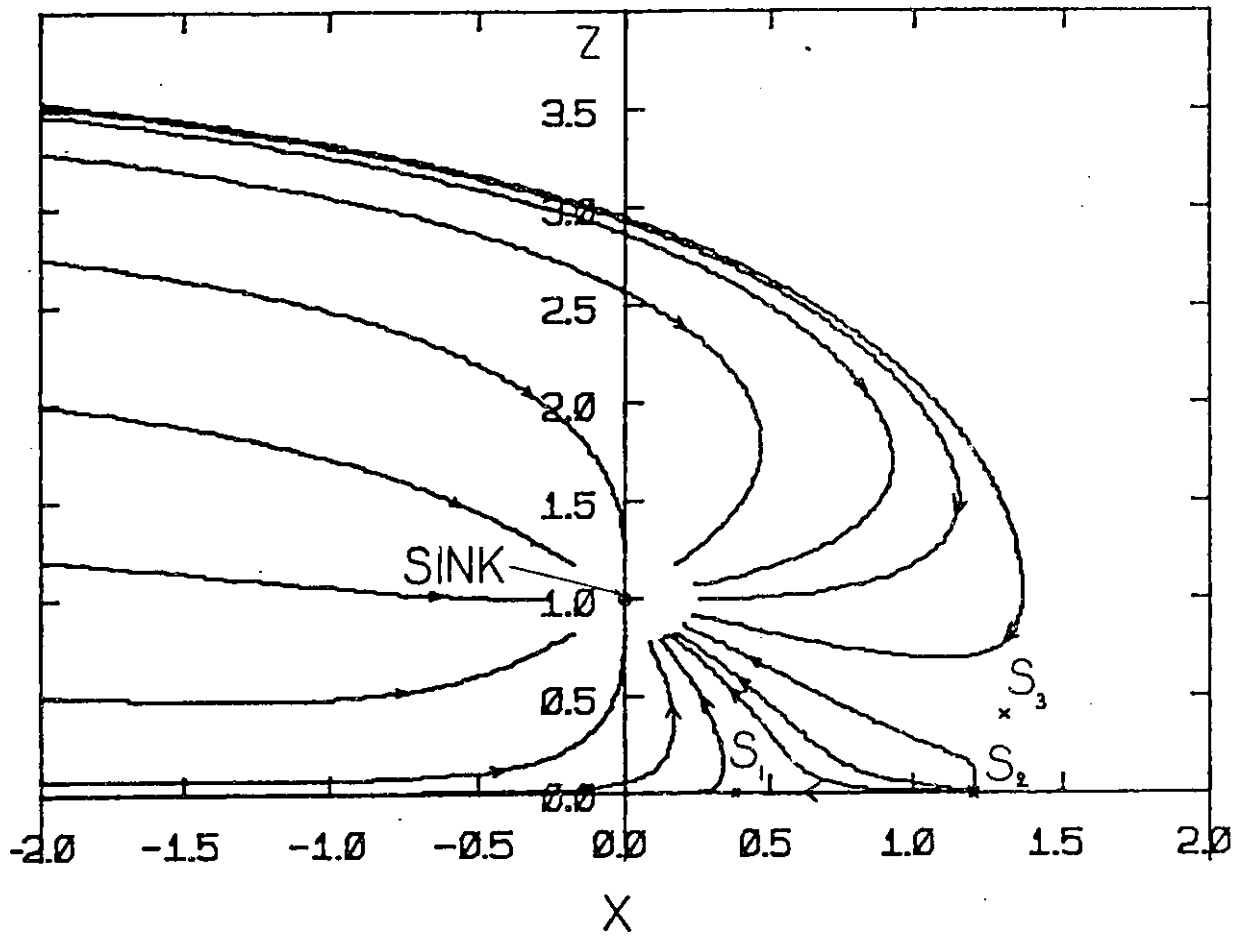FIGURE 43: Enlarged View of a Portion of Figure 42 (See Key Table 1
p 99)

FIGURE 44: Vorticity Distribution at the Engine Face Location Due to
a Far Upstream Distribution of Horizontal Vorticity, Case 2
(See Key Table 1 p 99)
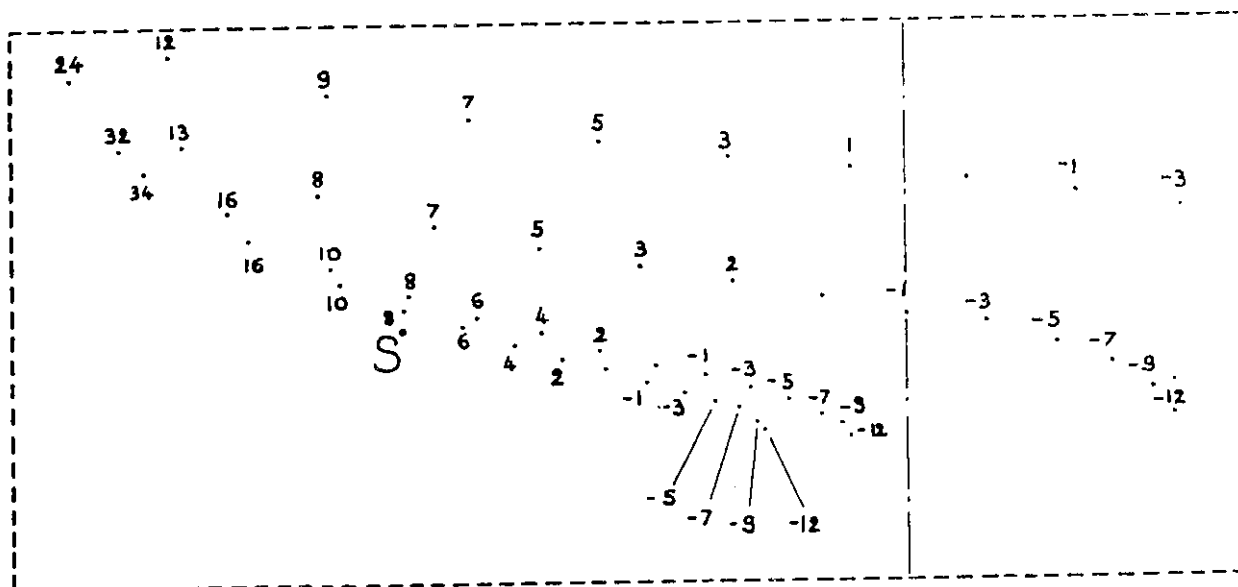
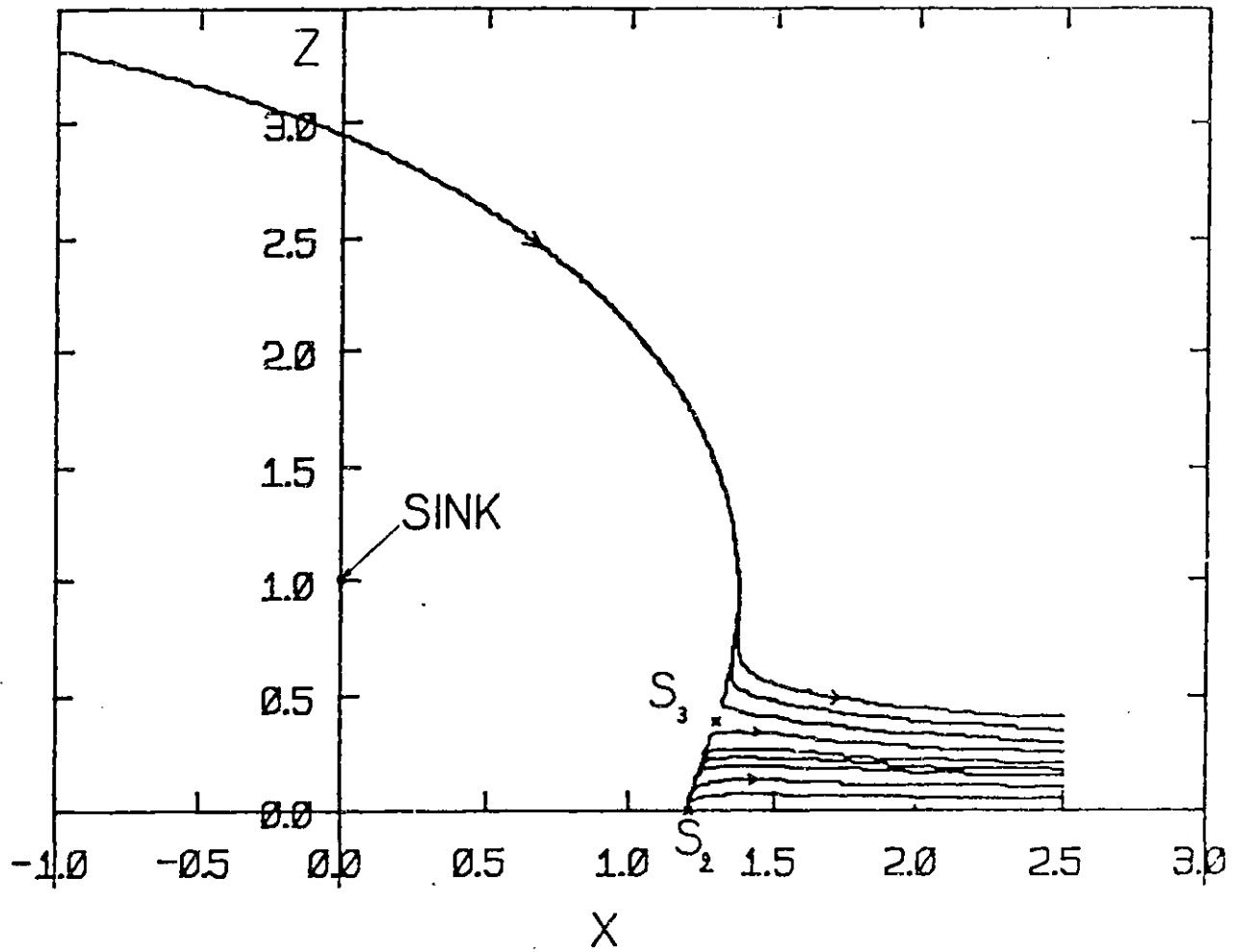FIGURE 45: Enlarged View of a Portion of Figure 44 (See Key Table 1
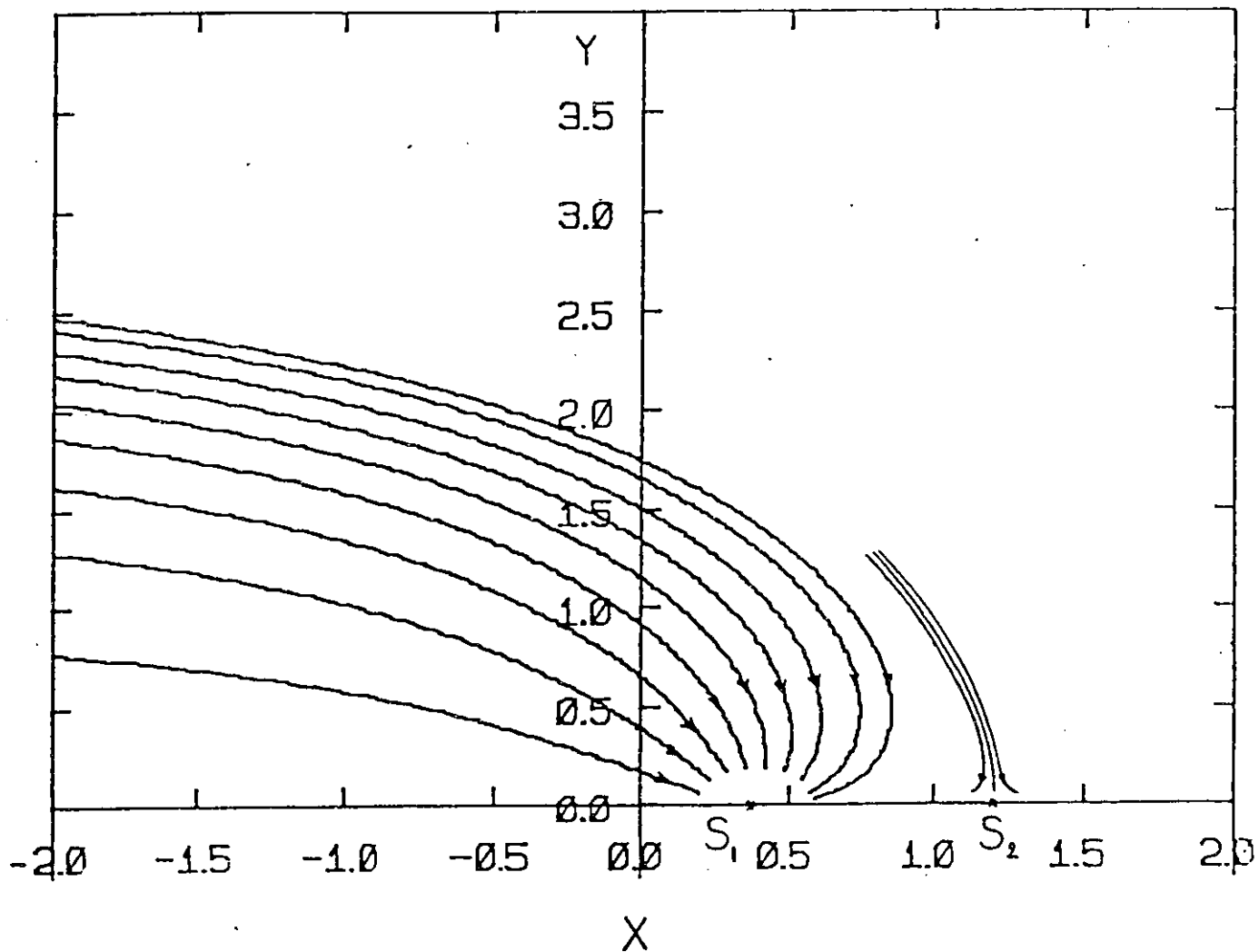p 99)
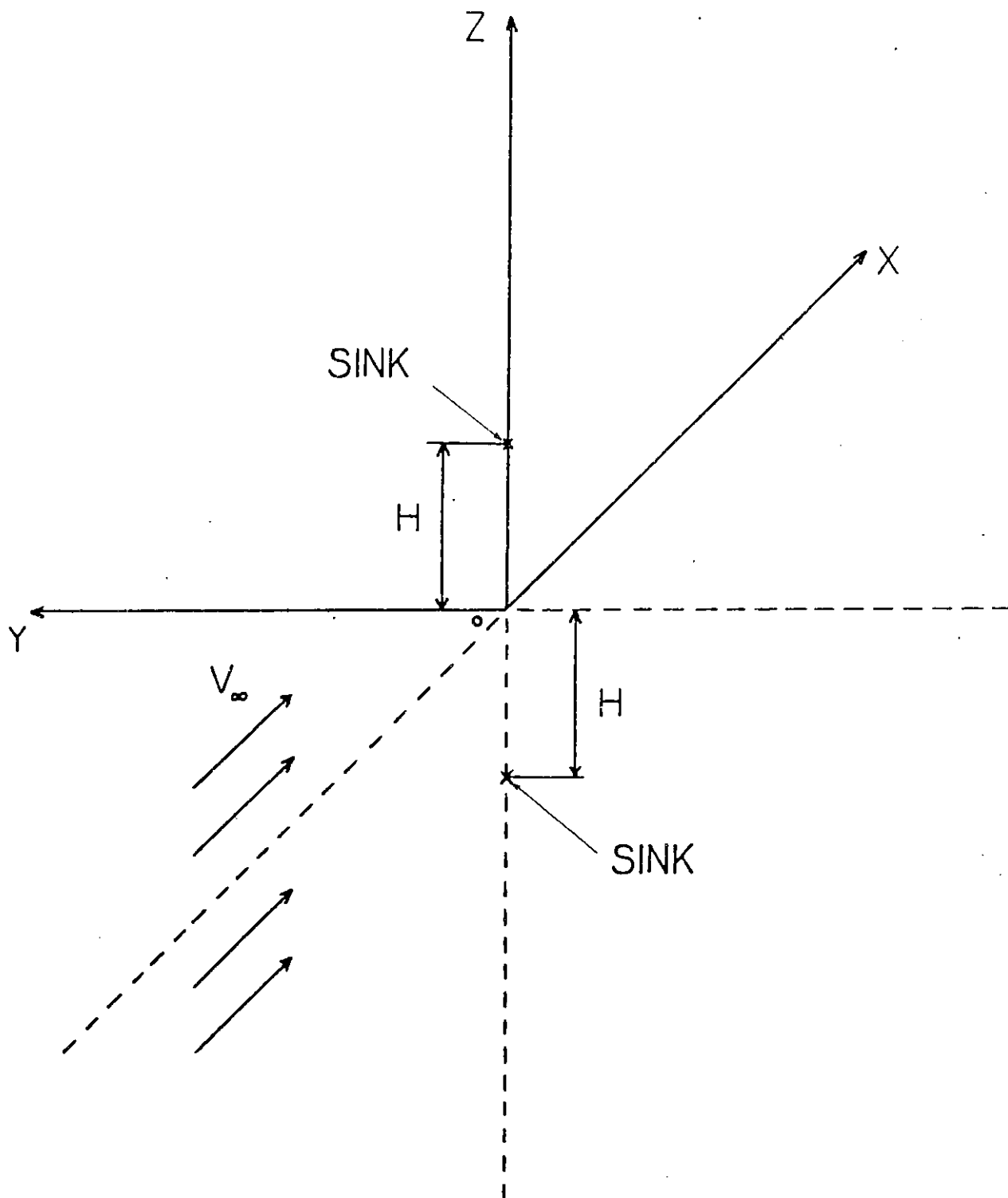
FIGURE B-1:   Basic Two-Sink Model

FIGURE B-2:   Streamlines in the x, z Plane

FIGURE B-3:   Streamlines in the x, z Plane
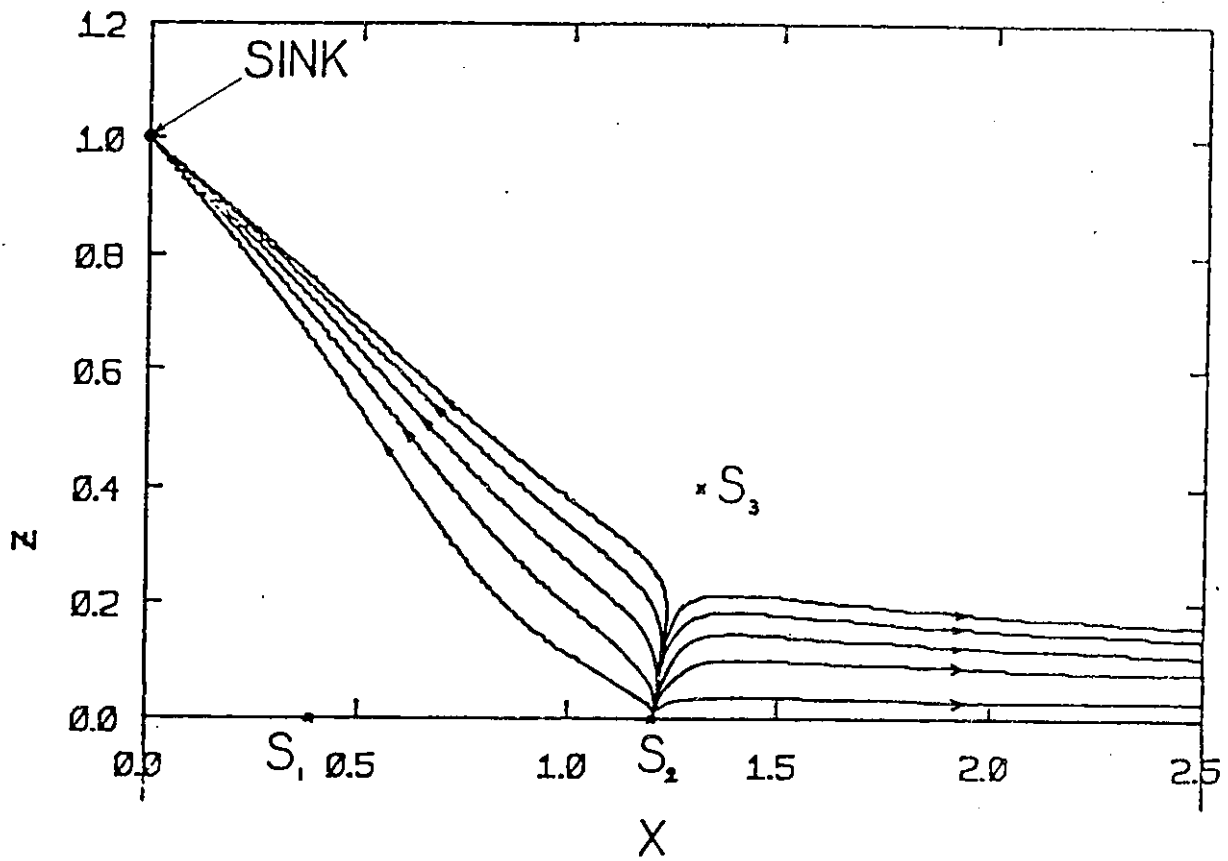
FIGURE B-4: Streamlines in the x, y Plane

FIGURE B-5: Streamlines in the Neighborhood of Stagnation
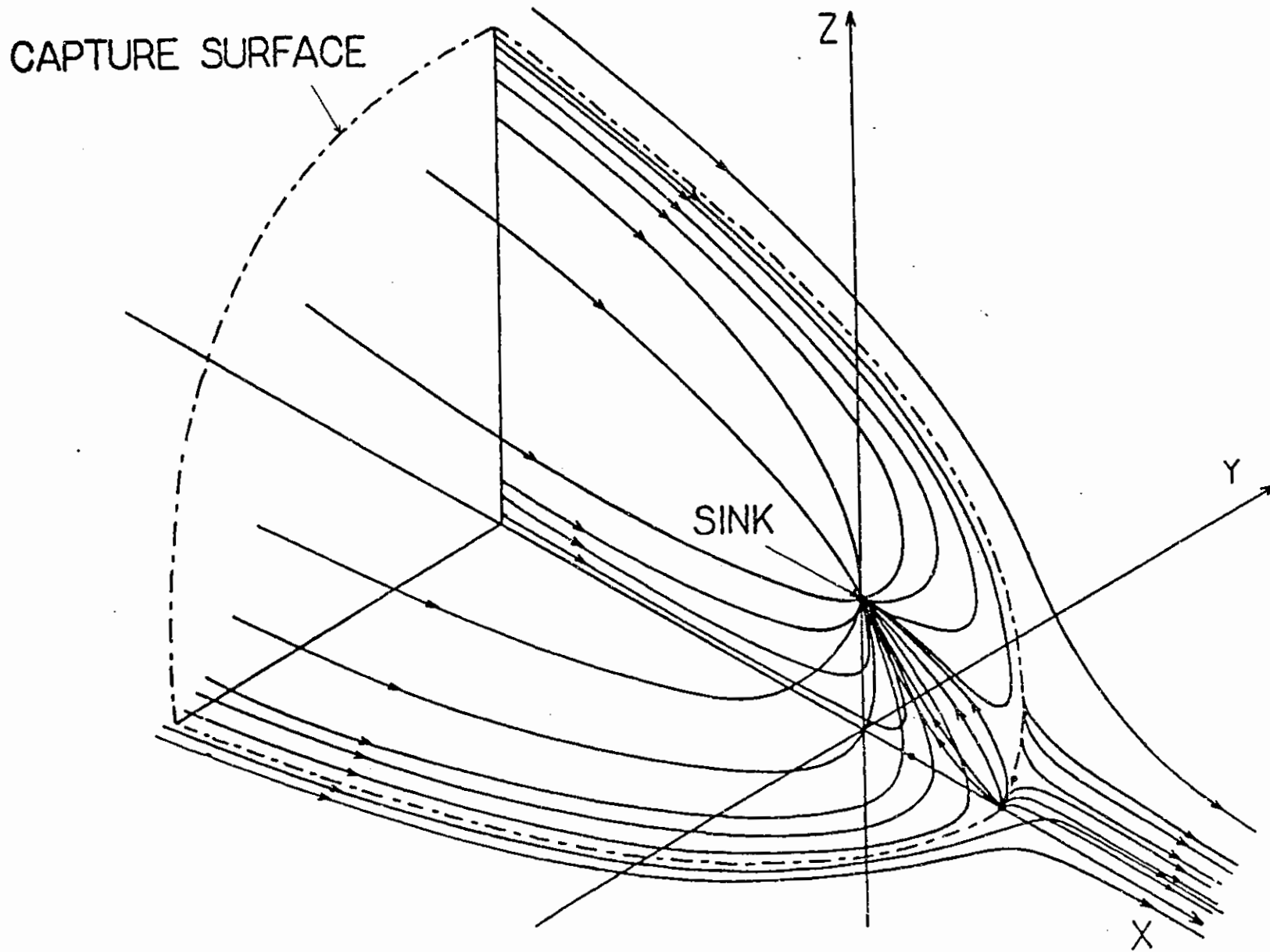   Point S_2, x, z Plane

FIGURE B-6:   Perspective View of Flow Field (Because of Symmetry, Only Half the Flow Field is Shown.)

REFERENCES

1. Rodert, L. A., and Garrett, F. B., "Ingestion of Foreign Objects into Turbine Engines by Vortices", NACA TN3330, February 1955.

2. Klein, H., "Small Scale Tests on Jet Engine Pebble Aspiration", Douglas Aircraft Company Report SM-14885, August 1953.

3. Klein, H., "An Aerodynamic Screen for Jet Engines", Institute of the Aeronautical Sciences, Preprint No. 676, presented at the 25th Annual Meeting, January 28-31, 1957.

4. Glenny, D. E., "Ingestion of Debris into Intakes by Vortex Action", Ministry of Technology, Aeronautical Research Council CP No. 1114, London; 1970.

5. Colehour, J. L., and Farquhar, B. W., "Inlet Vortex", Journal of Aircraft, Vol. 8, No. 1, January 1971, pp 39-43.

6. Motycka, D. L., Walter, W. A., and Muller, G. L., "An Analytical and Experimental Study of Inlet Ground Vortices", AIAA paper No. 73-1313, November 1973.

7. Motycka, D. L., "Ground Vortex - Limit to Engine/Reverser Operation", ASME paper No. 75-GT-3, March 1975.

8. Motycka, D. L., and Walter, W. A., "An Experimental Investigation of Ground Vortex Formation during Reverse Engine Operation", AIAA paper No. 75-1322, 1975.

9. Bissinger, N. C., and Braun, G. W., "On the Inlet Vortex System", Nasa CR-140182, September 1974.

10. Newmann, W. H., and Atassi, H., "A Two-Dimensional Potential Flow Model for Ground-Induced Effects on Jet and Fan Inlets", AIAA paper No. 80-0388, January 1980.

11. Prandtl, L., and Tietjens, O. G., "Fundamentals of Hydro - and Aeromechanics", Dover Publications, New York, 1957.

12. Hawthorne, W. R., "On the Theory of Shear Flow", MIT Gas Turbine Laboratory, Report No. 88, 1966.

13. Lighthill, M. J., "Drift", Journal of Fluid Mechanics, Vol. 1, 1956, pp 31-53.

14. Hess, J. L., and Smith, A. M. O., "Calculation of Potential Flow about Arbitrary Bodies", Progress in Aeronautical Sciences, Vol. 8, Pergamon Press, New York, 1966, pp 1-138.

15. Hess, J. L., "Review of Integral-Equation Techniques for Solving Potential Flow Problems with Emphasis on the Surface-Source Method", Computer Methods in Applied Mechanics and Engineering, Vol. 5, 1975, pp 145-196.

16. Hill, V. P., "A Surface Vorticity Theory for Propellers Ducts and Turbofan Engine Cowls in Non-Axisymmetric Incompressible Flow", Journal Mechanical Engineering Science, 1978, Vol. 20, No. 4, pp 201-219.

17. Hess, J. L., "The Problem of Three-Dimensional Lifting Potential Flow and its Solution by Means of Surface Singularity Distribution", Computer Methods in Applied Mechanics and Engineering, Vol. 4, 1974, pp 283-319.

18. Hess, J. L., "Calculation of Potential Flow about Arbitrary Three-Dimensional Lifting Bodies", Final Technical Report, McDonnell Douglas Report No. MDC J5679-01, October 1972.

19. Rubbert, P. E. and Saaris, G. R., "A General Three-Dimensional Potential Flow Method Applied to V/STOL Aerodynamics", SAE paper No. 680304, 1968.

20. Rubbert, P. E., and Saaris, G. R., "Review and Evaluation of a Three-Dimensional Lifting Potential Flow Computational Method for Arbitrary Configurations", AIAA paper No. 72-188.

21. Johnson, F. T., and Rubbert, P. E., "Advanced Panel-Type Influence Coefficients Methods Applied to Subsonic Flows", AIAA paper No. 75-50.

22. Hess, J. L., and Martin, R. P., "Improved Solution for Potential Flow about Arbitrary Axisymmetric Bodies by the Use of a Higher-Order Surface Source Method", McDonnell Douglas Report J6627-01, also NASA CR 134694, July 1974.

23. Hess, J. L., Mack, D., and Stockman, N. O., "An Efficient User-Oriented Method for Calculating Compressible Flow in and about Three-Dimensional Inlets", McDonnell Douglas Report No. MDC J7733, also NASA CR-159578, April 1979.

24. Stockman, N. O., "Potential and Viscous Flow in VTOL, STOL or CTOL Propulsion System Inlets", NASA TMX-71799.

25. Hess, J. L., and Smith, A. M. O., "A General Method for Calculating Low Speed Flow about Inlets", AGARDograph 103, Aerodynamics of Power Plant Installation, October 1965.

26. Carnahan, B., Luther, H. A., and Wilkes, J. O., "Applied Numerical Methods", John Wiley & Sons, New York, 1969, pp 341-404.

27. Ralston, A., "Runge-Kutta Methods with Minimum Error Bounds", MTAC, Vol. 16, 1962, pp 431-437.